Brigham Young University
BYU ScholarsArchive

Theses and Dissertations

2004-07-12

A Numerical Scheme for Mullins-Sekerka Flow in Three Space Dimensions

Sarah Marie Brown
Brigham Young University - Provo

Follow this and additional works at: https://scholarsarchive.byu.edu/etd

 Part of the Mathematics Commons

BYU ScholarsArchive Citation
Brown, Sarah Marie, "A Numerical Scheme for Mullins-Sekerka Flow in Three Space Dimensions" (2004). *Theses and Dissertations*. 136.
https://scholarsarchive.byu.edu/etd/136

This Dissertation is brought to you for free and open access by BYU ScholarsArchive. It has been accepted for inclusion in Theses and Dissertations by an authorized administrator of BYU ScholarsArchive. For more information, please contact scholarsarchive@byu.edu, ellen_amatangelo@byu.edu.

www.manaraa.com

A NUMERICAL SCHEME FOR MULLINS-SEKERKA FLOW IN THREE SPACE DIMENSIONS

by

Sarah M. Brown

A dissertation submitted to the faculty of

Brigham Young University

in partial fulfillment of the requirements for the degree of

Doctor of Philosophy

Department of Mathematics

Brigham Young University

August 2004

www.manaraa.com

Copyright © 2004 Sarah M. Brown

All Rights Reserved

www.manaraa.com

BRIGHAM YOUNG UNIVERSITY

GRADUATE COMMITTEE APPROVAL

of a dissertation submitted by

Sarah Brown

This dissertation has been read by each member of the following graduate committee and by majority vote has been found to be satisfactory.

Date	Peter W. Bates, Chair
Date	S. -Sum Chow
Date	John C. Dallon
Date	Christopher P. Grant
Date	Vianey Villamizar

www.manaraa.com

BRIGHAM YOUNG UNIVERSITY

As chair of the candidate's graduate committee, I have read the dissertation of Sarah M. Brown in its final form and have found that (1) its format, citations, and bibliographical style are consistent and acceptable and fulfill university and department style requirements; (2) its illustrative materials including figures, tables, and charts are in place; and (3) the final manuscript is satisfactory to the graduate committee and is ready for submission to the university library.

Date

Peter W. Bates
Chair, Graduate Committee

Accepted for the Department

Tyler J. Jarvis
Graduate Coordinator

Accepted for the College

G. Rex Bryce, Associate Dean
College of Physical and Mathematical Sciences

www.manaraa.com

ABSTRACT

A NUMERICAL SCHEME FOR MULLINS-SEKERKA FLOW
IN THREE SPACE DIMENSIONS

Sarah M. Brown

Department of Mathematics

Doctor of Philosophy

The Mullins-Sekerka problem, also called two-sided Hele-Shaw flow, arises in modeling a binary material with two stable concentration phases. A coarsening process occurs, and large particles grow while smaller particles eventually dissolve. Single particles become spherical. This process is described by evolving harmonic functions within the two phases with the moving interface driven by the jump in the normal derivatives of the harmonic functions at the interface. The harmonic functions are continuous across the interface, taking on values equal to the mean curvature of the interface. This dissertation reformulates the three-dimensional problem as one on the two-dimensional interface by using boundary integrals.

A semi-implicit scheme to solve the free boundary problem numerically is implemented. Numerical analysis tasks include discretizing surfaces, overcoming node bunching, and dealing with topology change in a toroidal particle. A particle (node)-cluster technique is developed with the aim of alleviating excessive run time caused by filling the dense matrix used in solving a system of linear equations.

www.manaraa.com

ACKNOWLEDGEMENTS

I am indebted to my advisor, Peter Bates. One could not ask for a better advisor, not just because of his expertise, but also his willingness to give of his time. My committee members Sum Chow, John Dallon, Chris Grant, and Vianey Villamizar were always more than willing to discuss my various mathematical dilemmas. Other faculty members of the Brigham Young University Mathematics Department who were extremely helpful are Michael Dorff, David Clark, Wayne Barrett, and Steve McKay. Fellow graduate student Zhifu Xie spent many lunch hours brainstorming with me. I owe a big thanks for moral support from Daniel and Jacob Brown, two of my brothers. I would like to acknowledge Ira Fulton, who donated the super computer *marylou* to Brigham Young University. Finally, Lonette Stoddard, our intrepid math department secretary, typed some of the dissertation and also answered my many LaTeX questions.

www.manaraa.com

Contents

www.manaraa.com

www.manaraa.com

www.manaraa.com

www.manaraa.com

Chapter 1

Introduction

The Mullins-Sekerka problem arises in modeling a binary material with two stable concentration phases. A coarsening process occurs, and large particles grow while the smaller particles eventually dissolve. Single particles become spherical. This process is described by evolving harmonic functions within the two phases (quasi-static approximation) with the moving interface driven by the jump in the normal derivatives of the harmonic functions at the interface. The field (harmonic functions) is continuous across the interface, taking on values equal to the mean curvature of the interface. This dissertation begins by reformulating the three-dimensional problem as one on the two-dimensional interface by using boundary integrals. The result includes a Fredholm integral equation of the 1^{st} kind, which are usually considered ill-conditioned because solutions are sensitive to small perturbations of, in our case, the mean curvature. Fortunately, for a singular kernel, as occurs in our formulation, the ill-conditioning is quite controllable [4]. We develop a stable algorithm to solve the problem numerically.

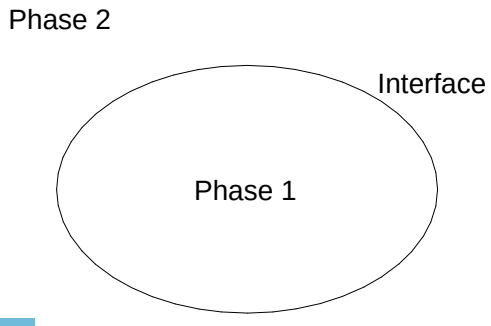

www.manaraa.com

The numerical analysis is the major challenge with tasks that include discretizing two-dimensional surfaces in three-dimensional space, overcoming node bunching, and dealing with topology changes in particles. Instability necessitates small time-stepping and hence extremely long computational run-time, and this problem is addressed by developing and implementing a semi-implicit scheme. Another cause of excessive run time is filling the large matrix required in solving the discretized system of boundary integrals. A particle (node)-cluster technique is developed with the aim of alleviating this problem.

Simulating the evolution process confirms that larger objects absorb smaller particles while overall volume remains constant, consistence with conservation of species. Surface area decreases until the particles reach equilibrium, after which it remains constant.

1.1 Background

In 1963, W. W. Mullins and R. F. Sekerka published the article *Morphological stability of a particle growing by diffusion and heat flow* [36] which proposed a model to describe phase transitions governed by the diffusion of material or heat. The two examples discussed in the paper were a precipitate particle in a supersaturated solution undergoing diffusion-controlled growth and a solid sphere in a supercooled melt whose growth is regulated by the flow of heat.

Key assumptions were threefold. First, crystallographic factors like elastic strain energy or anisotropy of interface properties are negligible. Secondly, the thermal or diffusion fields satisfy Laplace's equation. Lastly, at each element of interface there is local equilibrium.

Mullins and Sekerka studied the stability of a spherical phase boundary by using spherical harmonics to analyze the effects of infinitesimal perturbations. They found that for diffusion controlled growth, the sphere loses its stability at a certain radius being seven times the critical radius of nucleation theory. Analogous results were obtained for the solidification case [36].

The Mullins-Sekerka problem is the following free boundary problem:

www.manaraa.com

Let Ω denote a bounded and simply connected domain in $\mathbb{R}^3$. Let Γ_0 denote a finite collection of smooth, simple closed surfaces in the domain. Find a function $u(x,t)$ and a free boundary $\Gamma(t)$ which for all $x \in \Omega$ and $t \geq 0$ satisfy

$$\begin{aligned}
&\text{i)} \quad \Delta u(\cdot,t) = 0 && \text{in } \Omega \backslash \Gamma(t) \\
&\text{ii)} \quad \frac{\partial u}{\partial n} = 0 && \text{on } \partial\Omega \\
&\text{iii)} \quad u = \kappa && \text{on } \Gamma(t) \\
&\text{iv)} \quad \left[\frac{\partial u}{\partial n}\right]_{\Gamma(t)} = V && \text{on } \Gamma(t) \\
&\text{v)} \quad \Gamma(0) = \Gamma_0
\end{aligned}$$

where n is the outward unit normal, $\left[\frac{\partial u}{\partial n}\right]_{\Gamma(t)}$ is the sum of the outward normal derivatives of u from each side of $\Gamma(t)$ or the jump of the normal derivative of u across $\Gamma(t)$, κ is the mean curvature of $\Gamma(t)$, and V is the normal velocity of $\Gamma(t)$. We follow the convention that $\kappa < 0$ for spheres and that $V > 0$ if the surface is expanding.

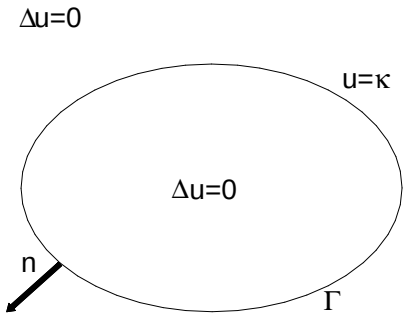

See [31] for physical interpretations of the above conditions in the case that u represents a solute field.

Thus Mullins and Sekerka's model is quasi-static: latent heat is accounted for explicitly on Γ while heat diffusion is instantaneous [10]. It is a Stefan problem with surface tension for which Laplace's equation replaces the diffusion equation. This assumption is valid when the speed of the interface is slow compared to the speed of diffusion, which occurs for materials of negligible specific heat. For further discussion of this see [46].

The Mullins-Sekerka problem is the sharp interface model corresponding to a diffuse interface model introduced by J. Cahn and J. Hilliard [11, 12]. The Cahn-Hilliard equation,

www.manaraa.com

$$\phi_t = \Delta\left(-\eta\Delta\phi + \tfrac{1}{\eta}\left(\phi - \phi^3\right)\right)$$

with boundary condition

$$\frac{\partial\phi}{\partial n} = \frac{\partial\Delta\phi}{\partial n} = 0,$$

models a binary alloy as it undergoes phase separation and a coarsening process. R. Pego formally derived Mullins-Sekerka flow as the asymptotic limit of the Cahn-Hilliard equation as $\eta \to 0$ [38]. N. Alikakos, P. Bates, and X. Chen later rigorously proved this result under the assumption that the Mullins-Sekerka problem has a smooth classical solution by using asymptotic expansions and spectral analysis [1]. B. Stoth proved convergence with less restrictive assumptions but had the additional assumption of radially symmetric solutions [42]. In [15], X. Chen gave a definition for a weak solution to the Mullins-Sekerka problem and showed that the asymptotic limit of solutions to the Cahn-Hilliard equation gives rise to weak solutions of the Mullins-Sekerka problem, assuming the initial energy is bounded independent of η.

Many other results have been produced. Milic used underlying conservation laws to obtain global growth conditions for interfacial area and phase volumes [34]. Existence of solutions locally in time was proved by X. Chen in [13], as was global existence for curves close to a circle in $\mathbb{R}^2$. Well-posedness is proved in arbitrary dimensions by X. Chen, J. Hong, and F. Yi in [14]. J. Escher and G. Simonett proved existence and regularity of classical solutions using a center manifold analysis [17]. The two-dimensional case where the interface meets the boundary orthogonally in exactly two places was studied in [2] by N. Alikakos, P. Bates, X. Chen, and G. Fusco under the assumptions that the curvature of the almost spherical droplet moving along the boundary is large compared to the curvature of the boundary. U. Mayer showed that convexity is not preserved for a bounded domain in $\mathbb{R}^2$ or for the entire plane [29]. In [10], G. Caginalp related the Mullins-Sekerka problem and similar models to an asymptotic limit of a conserved phase field system.

Other numerical schemes to model Mullins-Sekerka evolution have been given. P. Bates, X. Chen, and X. Deng reformulated the Mullins-Sekerka problem as a system of boundary

www.manaraa.com

integral equations and developed a quasi-implicit numerical algorithm which included node redistribution [5, 16]. In [46], J. Zhu, X. Chen, and T. Hou used a tangent angle and arclength formulation and implemented an implicit numerical scheme that simulated interface evolution until particles underwent topological change. Both of these schemes were in two space-dimensions.

The above evolution has various names, including the *two-phase Mullins-Sekerka problem* [5, 17], and *two-sided Mullins-Sekerka flow* [29]. The Mullins-Sekerka problem is similar to the Hele-Shaw problem and has been labelled the *Hele-Shaw problem* [1, 13], the *two-phase Hele-Shaw problem* [16], or the *two-phase Hele-Shaw problem with surface tension* [19]. (One-phase) Hele-Shaw flow usually refers to the above evolution with the additional requirement that u be constant on one side of the interface [14].

We also make mention of the work of G. McFadden, P. Voorthees, R. Boisvert, and D. Meiron [31, 44], who applied boundary integral techniques to Ostwald ripening in two-dimensions and developed a numerical scheme to find the solution. Ostwald ripening, or late stage phase transformation [44], arises in modeling crystal growth [7], and the mathematical description differs from the Mullins-Sekerka problem only in a more general condition for far field behavior and the restriction to multiply-connected, exterior domains [31, 44]. While the reformulation of the Mullins-Sekerka problem presented in this dissertation uses a single layer potential, the reformulation for Ostwald ripening uses a double layer potential. The double layer potential is also used in a very general setting by A. Greenbaum, L. Greengard, and G. McFadden in [22], where the solution to the Dirichlet problem in two-dimensional multiply-connected domains is given and a numerical algorithm using a fast multipole method is set forth.

1.2 Contributions of Dissertation

The main contribution of this dissertation is the design and implementation of a numerical scheme for the Mullins-Sekerka flow in three-dimensional space, as nearly all of the previous

www.manaraa.com

work has been in two space-dimensions.

Within this numerical scheme is a gridding of the sphere which has nearly equally spaced nodes and also makes it possible to catalog each node's eight nearest neighbors. This is then mapped onto particles that are topologically equivalent to spheres. A combination of a particle-particle method and a particle-cluster method helps reduce computation when the number of nodes is large.

As a toroidal particle evolves, nodes tend to bunch along its outer perimeter, leading to erroneous results. A redistribution scheme alleviates this problem. A particle starting with a toroidal interface undergoes a topology change as its center shrinks and the particle tends towards a spherical shape. By projecting the partly evolved torus onto a nearly pinched sphere, the evolution passes beyond the critical point of topology change. We also utilize the symmetry of the torus.

Convergence of various estimations is analyzed with respect to mesh size or time step, as applicable. Comparing numerical results to the predictions given by the mathematical model helps validate the scheme.

1.3 Outline of Dissertation

Chapter 2 reformulates the Mullins-Sekerka problem as a system of boundary integral equations and gives a proof of the equivalence of the formulations. Uniqueness of solutions is also proved under certain existence assumptions.

Chapter 3 describes the numerical scheme, including how surfaces are modeled discretely, how surface area and volume are estimated, what method is used to determine mean curvature and surface normals, and how the system of surface integral equations is solved.

The validation of the scheme is contained in Chapter 4 and includes comparing the behavior of volume and surface area predicted by the mathematical model to behavior demonstrated numerically. Evolution of single spheres, multiple spheres of equal radii, and concentric spheres can be found analytically as well as numerically, and we compare the two

www.manaraa.com

methods.

In Chapter 5 the numerical results are given for various particles. We present an example that suggests pinching off may occur.

Chapter 6 has the concluding remarks and includes further areas of study.

The numerical algorithm was implemented in C. The graphics were created using Maple® and the charts were created using Microsoft Excel®.

www.manaraa.com

www.manaraa.com

Chapter 2

Mathematical Formulation

In this chapter we reformulate the Mullins-Sekerka problem as system of boundary integral equations. By so doing, the dimension of the problem is reduced effectively by one since instead of dealing with all of $\mathbb{R}^3$, we concern ourselves only with the surface Γ. We show the reformulation is equivalent and prove uniqueness of solutions under certain existence assumptions. The arguments are an adaptation of those found in [5, 16], where the two-dimensional problem is reformulated to one along curves. See also [6, 8].

2.1 Description of Problem

We first establish some definitions as found in [21]. Let Ω denote a domain in three-dimensional space. Let $\Gamma \in C^2$ be a finite collection of simple, closed surfaces in the domain. Denote the domain enclosed by Γ as Ω^- and denote $\Omega \backslash \overline{\Omega^-}$ as Ω^+. Let $n(x)$ be the outward unit normal to Γ at $x \in \Gamma$. Note that $n \in C^1(\Gamma)$ [21].

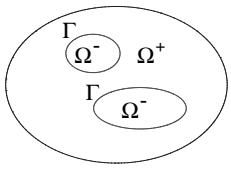

Recall that $C(\overline{\Omega^{\pm}})$ is the space of functions $u \in C(\Omega^{\pm})$ such that u extends continuously to $\overline{\Omega^{\pm}}$. We define $C_n(\Omega^-)$ as the space of functions $u \in C^1(\Omega^-) \cap C(\overline{\Omega^-})$ such that for every $x \in \Gamma$,

$\partial_{n^-} u(x) = \lim_{t<0, t\to 0} n(x) \cdot \nabla u(x + tn(x))$

www.manaraa.com

exists and the convergence is uniform on Γ. Likewise, $C_n(\Omega^+)$ is the space of functions $u \in C^1(\Omega^+) \cap C(\overline{\Omega^+})$ such that

$\partial_{n^+} u(x) = \lim_{t>0, t\to 0} n(x) \cdot \nabla u(x + tn(x))$,

exists for each $x \in \Gamma$, again with the convergence uniform on Γ. The interior and exterior normal derivatives on Γ are defined to be the operators ∂_{n^-} and ∂_{n^+}, respectively. Note that since convergence is uniform, $\partial_{n^\pm} u$ is continuous on Γ.

We now define the Mullins-Sekerka problem. Let Ω denote a bounded, smooth, and simply connected domain in $\mathbb{R}^3$. Let Γ_0 denote a finite collection of simple closed surfaces in the domain. We want to find a free boundary $\Gamma(t)$ and a function $u(x,t)$ which for all $x \in \Omega$ and $0 \le t \le T$ for some finite T satisfy

i)	$\Delta u(\cdot, t) = 0$	in $\Omega \backslash \Gamma(t)$,
ii)	$\dfrac{\partial u}{\partial n} = 0$	on $\partial\Omega$,
iii)	$u = \kappa$	on $\Gamma(t)$,
iv)	$\left[\dfrac{\partial u}{\partial n}\right]_{\Gamma(t)} = V$	on $\Gamma(t)$,
v)	$\Gamma(0) = \Gamma_0$,	

where n is the outward unit normal to Ω and Ω^-, $\left[\dfrac{\partial u}{\partial n}\right]_{\Gamma(t)} \equiv \partial_{n^-} u - \partial_{n^+} u$ is the sum of the outward normal derivatives of u from each side of $\Gamma(t)$ or the jump of the normal derivative of u across $\Gamma(t)$, κ is the mean curvature of $\Gamma(t)$, and V is the normal velocity of $\Gamma(t)$. We follow the convention that $\kappa < 0$ for spheres and that $V > 0$ if the surface of the sphere is expanding.

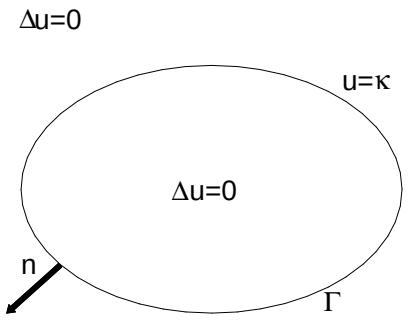

www.manaraa.com

We consider only $\Omega = \mathbb{R}^3$, and therefore replace ii) with

$$\nabla u(\cdot, t) = \mathcal{O}\left(\frac{1}{|x|^3}\right) \qquad \text{as } |x| \to \infty.$$

Note that the condition $\nabla u(\cdot, t) = \mathcal{O}\left(\frac{1}{|x|^3}\right)$ as $|x| \to \infty$ insures that the net flux through a large sphere of radius R goes to zero, i.e., $\int_{\partial B_R} \frac{\partial u}{\partial n} \to 0$ as $R \to \infty$. We label this system on $\mathbb{R}^3$ as (2.1). We write $\Omega = \mathbb{R}^3$ as the disjoint union $\Omega = \Omega^-(t) \cup \Gamma(t) \cup \Omega^+(t)$, where $\Gamma(t)$ encloses $\Omega^-(t)$.

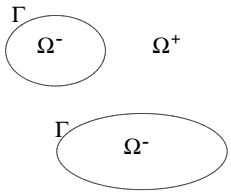

Observe that for iv) to make sense, we need $u(\cdot, t) \in C_n(\Omega^-(t)) \cap C_n(\Omega^+(t))$ and $\Gamma(t) \in C^2$. Also note that i) requires $u \in C^2(\mathbb{R}^3 \backslash \Gamma)$. However, we can relax this since every distribution solution of $\triangle u = 0$ satisfies $u \in C^\infty(\mathbb{R}^3 \backslash \Gamma)$ [21]. Note that $\Gamma(t) \in C^2$ gives that $\kappa(\cdot, t) \in C(\Gamma)$. Finally, for $\Gamma(0)$ sufficiently smooth, there exists a T such that $\Gamma(t)$ is also smooth for $t \in [0, T]$ [13].

2.2 Reformulation of Problem

We now show there exists an integral representation of the solution to system (2.1) via a single layer potential. For a similar reformulation in two dimensions using a double layer potential as applied to Ostwald ripening, see [31, 44].

Lemma 2.2.1 *Let Γ be the union of finitely many disjoint simple, closed, C^2 surfaces such that Γ separates $\mathbb{R}^3$ into finitely many bounded regions, collectively denoted as Ω^-, and one unbounded region Ω^+. Let n denote the outward unit normal to Γ. For each $g \in C(\Gamma)$ define $W_g : \mathbb{R}^3 \to \mathbb{R}^3$ by*

$$W_g(x) = -\frac{1}{4\pi} \int_\Gamma \frac{1}{|x - y|} g(y) dS_y$$

Then the following hold:

www.manaraa.com

1. *W_g is well-defined and continuous on $\mathbb{R}^3$.*

2. *$\Delta W_g = 0$ in $\mathbb{R}^3 \backslash \Gamma$.*

3. *$W_g \in C_n(\Omega^-) \cap C_n(\Omega^+)$ and $-\left[\frac{\partial W_g}{\partial n}\right]_\Gamma \equiv -(\partial_{n^-} W_g - \partial_{n^+} W_g) = g$ on Γ.*

4. *$W_g = \mathcal{O}\left(\frac{1}{|x|}\right)$ as $|x| \to \infty$.*

5. *If we also assume that $\int_\Gamma g(y) dS_y = 0$, then $\nabla W_g = \mathcal{O}\left(\frac{1}{|x|^3}\right)$.*

Proof. Since $\frac{1}{|y|} \in L^1(\Gamma)$ and g is bounded, W_g is well-defined. To prove continuity, we show that given $x \in \mathbb{R}^3$, for every $\epsilon > 0$ there exists δ such that $|x - v| < \delta$ implies $|W_g(x) - W_g(v)| < \epsilon$. In the arguments that follow, C will absorb constants as necessary. For $x \notin \Gamma$, let α be the distance from x to Γ and assume $|x - v| < \frac{\alpha}{2}$. Then

$$\begin{aligned} |W_g(x) - W_g(v)| &= |-\frac{1}{4\pi} \int_\Gamma \left(\frac{1}{|x-y|} - \frac{1}{|v-y|}\right) g(y) dS_y| \\ &\leq C \int_\Gamma \frac{|x-v|}{|x-y||v-y|} dS_y \\ &\leq C \frac{|x-v|}{\alpha^2}. \end{aligned}$$

Choose δ small enough so that $C\frac{|x-v|}{\alpha^2} < \epsilon$.

Now consider $x \in \Gamma$. Since $\Gamma \in C^2$, Γ is locally diffeomorphic to the plane and we can consider the integral

$$W_g(x) = -\frac{1}{4\pi}\left(\int_{\Gamma \backslash \phi^{-1}(B_R)} \frac{1}{|x-y|} g(y) dS_y + \int_{\phi^{-1}(B_R)} \frac{1}{|x-y|} g(y) dS_y\right)$$

where B_R is a ball of radius R centered at the origin in $\mathbb{R}^2$ and ϕ is a C^2 embedding of a neighborhood of x in $\mathbb{R}^3$ into $\mathbb{R}^3$ mapping x to the origin and a neighborhood of x in Γ into the xy-plane. We may assume that $\phi^{-1}(B_{2R})$ lies in this neighborhood. We also assume $|x - v| < R$. We denote $\phi(v)$ as v'. Then

$$\begin{aligned} |W_g(x) - W_g(v)| &= \left|-\frac{1}{4\pi} \int_\Gamma \left(\frac{1}{|x-y|} - \frac{1}{|v-y|}\right) g(y) dS_y\right| \\ &\leq C\left(\int_{\Gamma \backslash \phi^{-1}(B_R)} \frac{|x-v|}{|x-y||v-y|} dS_y + \int_{B_R} \frac{1}{|y|} dS_y + \int_{B_R} \frac{1}{|v'-y|} dS_y\right). \end{aligned}$$

www.manaraa.com

Since $\frac{1}{|y|} \in L^1(\Gamma)$, we can choose R sufficiently small so that $C\int_{B_R} \frac{1}{|y|} dS_y < \frac{\epsilon}{3}$. We next bound $\int_{B_R} \frac{1}{|v'-y|} dS_y$ by $\int_{B_{2R}} \frac{1}{|y|} dS_y$. First we take the simple case that v' lies on the z-axis. Then $|v'-y|^2 = |v'|^2 + |y|^2$, so $\frac{1}{|v'-y|} \leq \frac{1}{|y|}$. Therefore $\int_{B_R} \frac{1}{|v'-y|} dS_y \leq \int_{B_R} \frac{1}{|y|} dS_y$. If $v' = (v_1', v_2', v_3')$ is not on the z-axis, we make the change of variables $u = y - (v_1', v_2', 0)$. Then

$$\int_{B_R} \frac{1}{|v'-y|} dS_y \leq \int_{B_{2R}} \frac{1}{|(0,0,v_3')-u|} dS_u \leq \int_{B_{2R}} \frac{1}{|u|} dS_u.$$

Choose R small enough so that $C\int_{B_{2R}} \frac{1}{|u|} dS_u < \frac{\epsilon}{3}$.

Having fixed R, we now consider $\int_{\Gamma\backslash\phi^{-1}(B_R)} \frac{|x-v|}{|x-y||v-y|} dS_y$. Denote by α the distance from x to $\Gamma\backslash\phi^{-1}(B_R)$ and assume $|x-v| < \frac{\alpha}{2}$. Then

$$\int_{\Gamma\backslash\phi^{-1}(B_R)} \frac{|x-v|}{|x-y||v-y|} dS_y \leq |x-v| \frac{1}{\alpha^2}$$

Choose δ small enough so that $C\frac{|x-v|}{\alpha^2} < \frac{\epsilon}{3}$. This completes the proof of Statement 1.

We note that $g \in L^p$ with $p > 2$ is sufficient to prove Statement 1. The proof uses Holder's inequality and is similar to the one given. However, continuity of g is required for Statement 3. The above proof of continuity is essentially the same as that given in [21] although there continuity is shown only on Γ. Continuity on Γ with g bounded is also proved for a more general kernel. In [33], continuity of W_g is proved for g measurable and bounded and Γ a closed Lyapunov surface.

Statement 2 holds since we can differentiate under the integral sign by Lebesgue's dominated convergence theorem and $\Delta_x \left(\frac{1}{|x-y|} \right) = 0$ for $x \notin \Gamma$.

Statement 3 is in [21] as Theorem 3.28 and Corollary 3.29.

Statement 4 follows from $\frac{1}{|x-y|} = \mathcal{O}\left(\frac{1}{|x|}\right)$ and the boundedness of Γ.

To show Statement 5 we note that if $\int_\Gamma g(y) dS_y = 0$

$$\begin{aligned} \nabla W_g(x) &= \frac{1}{4\pi} \int_\Gamma \frac{x-y}{|x-y|^3} \, g(y) dS_y \\ &= \frac{1}{4\pi} \int_\Gamma \left(\frac{x-y}{|x-y|^3} - \frac{x}{|x|^3} \right) g(y) dS_y. \end{aligned}$$

www.manaraa.com

Utilizing the Triangle Inequality, we have

$$\begin{aligned}\left|\frac{x-y}{|x-y|^3}-\frac{x}{|x|^3}\right| &= \left|\frac{|x|^3-|x-y|^3}{|x-y|^3\cdot|x|^3}\,x-\frac{y}{|x-y|^3}\right| \\ &\le \left|\frac{|x|^3-(|x|-|y|)^3}{|x-y|^3|x|^3}\,x-\frac{y}{|x-y|^3}\right| \\ &= \left|\frac{3|x|^2|y|-3|x||y|^2+|y|^3}{|x-y|^3|x|^3}\,x-\frac{y}{|x-y|^3}\right| \\ &= \mathcal{O}\left(\frac{1}{|x|^3}\right).\end{aligned}$$

Therefore $\nabla W_g(x)=\mathcal{O}\left(\frac{1}{|x|^3}\right)$. □

2.3 Equivalency of Formulations

We have just found a function which is harmonic on $\mathbb{R}^3\backslash\Gamma$. This function plus any constant is also harmonic on $\mathbb{R}^3\backslash\Gamma$. We now show that the trace of a harmonic function is realized by the harmonic function found previously from the jump in the normal derivative, up to a constant.

We will use the following version of Green's First Identity, which is almost exactly the one stated without detailed proof in [21], differing only in the smoothness requirement of the boundary. It differs from most statements of the identity in its relaxing of the hypothesis $u\in C^2(\overline{U})$. Thanks to Peter Bates and David Clark for their help with this proof.

Lemma 2.3.1 *Let U be a bounded domain with C^1 boundary. Let $u,v\in C^1(\overline{U})$. Then*

$$\int_{\partial U} v\partial_n u dS=\int_U (v\triangle u+\nabla v\cdot\nabla u)dx$$

Proof. First we point out that $C^2(\overline{U})$ is dense in $C^1(\overline{U})$. This can be shown by modifying the constructive proof of the Weierstrass Approximation Theorem found in [21] to include the first partial derivatives of the approximating polynomials. Let $\{u_k\}$ be a sequence of functions in $C^2(\overline{U})$ such that $u_k\to u$ in the $C^1(\overline{\Omega})$ norm, i.e., $\sum_{|\alpha|\le 1}\sup_{x\in U}\left|\frac{\partial^\alpha u_k}{\partial x^\alpha}(x)-\frac{\partial^\alpha u}{\partial x^\alpha}(x)\right|\to 0$ as $k\to\infty$. Since $\triangle u$ may not exist, we view u as the distribution defined by $<u,\phi>\equiv\int_\Gamma u\phi$ and

www.manaraa.com

note that the sequence of distributions $\left\{\frac{\partial^\alpha u_k}{\partial x^\alpha}\right\}$ converges to the distribution $\frac{\partial^\alpha u}{\partial x^\alpha}$, where $|\alpha| \geq 0$ [35]. Convergence of a sequence $\{u_k\}$ of distributions to a distribution u means that $<u_k, \phi> \to <u, \phi>$ for every test function $\phi \in C_c^\infty(\Gamma)$.

By the usual Green's first identity,

$$\int_{\partial U} v \partial_\nu u_k dS = \int_U (v \triangle u_k + \nabla v \cdot \nabla u_k) dx.$$

We let $k \to \infty$ to get our desired result. □

We also need the following technical lemma.

Lemma 2.3.2 *Let u be continuous on $\mathbb{R}^3$ or continuous on the compliment of a bounded open set whose boundary is a finite collection of simple closed surfaces. Let u be continuously differentiable for $|\vec{x}|$ sufficiently large. Also let $\nabla u = \mathcal{O}\left(\frac{1}{|\vec{x}|^3}\right)$. Then u tends to a constant limit as $|\vec{x}| \to \infty$. In particular, u is bounded.*

Proof. We show that u tends to a constant limit in the first octant. The proofs for other octants are similar and by the continuity of u, u tends to the same limit in all octants. Let $\{\vec{x}_n\} = \{(x_n, y_n, z_n)\}$ be any sequence such that $|\vec{x}_n| \to \infty$ as $n \to \infty$ and $x_n, y_n, z_n \geq 0$. We will show $\{u(\vec{x}_n)\}$ is a Cauchy sequence and hence has a limit. We have the following for m, n sufficiently large:

$$\begin{aligned}
\left|u(\vec{x}_n) - u(\vec{x}_m)\right| &= \left|\int_0^1 \nabla u(\vec{x}_m + s(\vec{x}_n - \vec{x}_m)) \cdot (\vec{x}_n - \vec{x}_m) ds\right| \\
&\leq \left|\vec{x}_n - \vec{x}_m\right| \int_0^1 \left|\nabla u(\vec{x}_m + s(\vec{x}_n - \vec{x}_m))\right| ds \\
&\leq C \left|\vec{x}_n - \vec{x}_m\right| \int_0^1 \frac{1}{|\vec{x}_m + s(\vec{x}_n - \vec{x}_m)|^3} ds \\
&= C \left|\vec{x}_n - \vec{x}_m\right| \int_0^1 \frac{1}{|(a,0) + s((b,c) - (a,0))|^3} ds
\end{aligned}$$

where we rotate the triangle having vertices $\vec{x}_m, \vec{x}_m$, and $(0,0,0)$ so it lies on the xy-plane, where it has vertices $(a,0), (b,c)$, and $(0,0)$ with $a = |\vec{x}_m|$. Note that $b, c \geq 0$ and $|\vec{x}_n| = \sqrt{b^2 + c^2}$.

www.manaraa.com

To evaluate $\int_0^1 \frac{1}{|(a,0)+s((b,c)-(a,0))|^3}ds$, we consider two cases. If $c=0$, then $\int_0^1 \frac{1}{|(a,0)+s((b,c)-(a,0))|^3}ds = \frac{a+b}{2a^2b^2} = \frac{|\vec{x}_m|+|\vec{x}_n|}{2|\vec{x}_m|^2|\vec{x}_n|^2}$.

Thus $\left|u(\vec{x}_n)-u(\vec{x}_m)\right| \le C\left|\vec{x}_n-\vec{x}_m\right| \frac{|\vec{x}_m|+|\vec{x}_n|}{2|\vec{x}_m|^2|\vec{x}_n|^2} \le C\frac{(|\vec{x}_m|+|\vec{x}_n|)^2}{2|\vec{x}_m|^2|\vec{x}_n|^2}$, which we can make as small as desired by choosing n,m large.

In the case that $c\neq 0$ we have with the aid of Maple®,

$$\begin{aligned}\int_0^1 \frac{1}{|(a,0)+s((b,c)-(a,0))|^3}ds &= \frac{-b\sqrt{b^2+c^2}+a\sqrt{b^2+c^2}+b^2+c^2-ab}{a^2c^2\sqrt{b^2+c^2}} \\ &= \frac{(|\vec{x}_m|+|\vec{x}_n|)(|\vec{x}_n|-b)}{|\vec{x}_m|^2|\vec{x}_n|c^2} \\ &= \frac{|\vec{x}_m|+|\vec{x}_n|}{|\vec{x}_m|^2|\vec{x}_n|(|\vec{x}_n|+b)} \\ &\le \frac{|\vec{x}_m|+|\vec{x}_n|}{|\vec{x}_m|^2|\vec{x}_n|^2}.\end{aligned}$$

We have $\left|u(\vec{x}_n)-u(\vec{x}_m)\right| \le C\left|\vec{x}_n-\vec{x}_m\right| \frac{|\vec{x}_m|+|\vec{x}_n|}{|\vec{x}_m|^2|\vec{x}_n|^2} \le C\frac{(|\vec{x}_m|+|\vec{x}_n|)^2}{|\vec{x}_m|^2|\vec{x}_n|^2} \to 0$ as $n,m\to\infty$.

Thus $\{u(\vec{x}_n)\}$ is a Cauchy sequence and has a limit. □

The lemma is also true for $\nabla u = \mathcal{O}\left(\frac{1}{|\vec{x}|^2}\right)$, and we conjecture that it holds for $\nabla u = \mathcal{O}\left(\frac{1}{|\vec{x}|^p}\right)$ with $p>1$. We now return to proving equivalency of formulations.

Lemma 2.3.3 *Let Γ be the union of finitely many disjoint simple closed C^2 surfaces such that Γ separates $\mathbb{R}^3$ into finitely many bounded regions, collectively denoted as Ω^-, and one unbounded region Ω^+. Let n denote the outward unit normal to Γ. Suppose $u\in C_n(\Omega^+)\cap C_n(\Omega^-)$ and $g\in C(\Gamma)$ satisfy*

i) $\Delta u = 0$ *in* $\mathbb{R}^3\backslash\Gamma$

ii) $\nabla u = \mathcal{O}\left(\frac{1}{|x|^3}\right)$ *as* $|x|\to\infty$.

iii) $-\left[\frac{\partial u}{\partial n}\right]_\Gamma = g$ *on* Γ.

www.manaraa.com

Then $\int_\Gamma g(y)dS_y = 0$. *Furthermore, if* $f \equiv u|_\Gamma$, *there exists a constant* c *such that for* $x \in \Gamma$, $f(x) = -\frac{1}{4\pi}\int_\Gamma \frac{1}{|x-y|}\ g(y)dS_y + c$.

Proof. To show $\int_\Gamma g(y)dS_y = 0$, we let B_R be a ball of radius R in $\mathbb{R}^3$ centered at the origin, where R is large enough so that $\Gamma \subset B_R$. Denote the region between ∂B_R and Γ as Ω_0, i.e., $\Omega_0 = B_R \backslash \overline{\Omega^-}$.

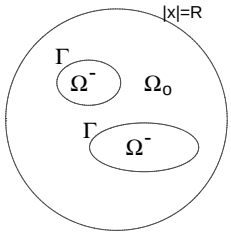

Then we have

$$\begin{aligned}
\int_\Gamma g &= -\int_\Gamma \left[\frac{\partial u}{\partial n}\right] \\
&= -\left(-\int_\Gamma \partial_{n^+} u + \int_{\partial B_R} \partial_n u\right) - \int_\Gamma \partial_{n^-} u + \int_{\partial B_R} \partial_n u \\
&= -\int_{\Omega_0} \triangle u - \int_{\Omega^-} \triangle u + \int_{\partial B_R} \partial_n u \\
&= \int_{\partial B_R} n \cdot \nabla u \\
&= 4\pi R^2 \cdot \mathcal{O}\left(\frac{1}{R^3}\right) \\
&= \mathcal{O}\left(\frac{1}{R}\right).
\end{aligned}$$

Let $R \to \infty$ to get $\int_\Gamma g(y)dS_y = 0$.

We must justify our use of Green's first identity. Here we give details of the explanation in [21]. With regard to Ω^-, Green's first identity requires $u \in C^1(\overline{\Omega^-})$, but we have only $u \in C^1(\Omega^-) \cap C(\overline{\Omega^-})$. However, we can replace Ω^- with Ω_s^-, where the boundary of Ω_s^- is $\Gamma_s \equiv \{x + sn(x) | x \in \Gamma\}$ and $s < 0$ is sufficiently close to 0 to for Γ_s to be C^1. Note that the normal to Γ_s is also n. Then $\int_{\Gamma_s} \partial_n u = \int_{\Omega_s^-} \triangle u = 0$. We take the limit of $\int_{\Gamma_s} \partial_n u$ as $s \to 0^-$. Since $n(x) \cdot \nabla u(x + sn(x))$ converges uniformly on Γ by the definition of $C_n(\Omega^-)$, we can apply Lebesgue's Dominated Convergence Theorem:

www.manaraa.com

$$\begin{aligned}\lim_{s\to 0^-}\int_{\Gamma_s}\partial_n u(y)dS_y &= \lim_{s\to 0^-}\int_{\Gamma} n(x+sn(x))\cdot\nabla u(x+sn(x))dS_x \\ &= \int_{\Gamma}\lim_{s\to 0^-} n(x)\cdot\nabla u(x+sn(x))dS_x \\ &= \int_{\Gamma}\partial_{n^-}u.\end{aligned}$$

The case for Ω_0 is similar.

Let W_g be defined as in 2.3.1. Define

$$c(x) = u(x) - W_g(x).$$

We will show c is constant. Since u and W_g belong to $C_n(\Omega^+)\cap C_n(\Omega^-)$, we have $f\in C(\Gamma)$, c is continuous on $\mathbb{R}^3$, and ∇c is continuous on $\mathbb{R}^3\backslash\Gamma$. We also have $\Delta c = 0$ in $\mathbb{R}^3\backslash\Gamma$ and $\left[\frac{\partial c}{\partial n}\right]_\Gamma = -g-(-g) = 0$. Finally, $\nabla c = \mathcal{O}\left(\frac{1}{|x|^3}\right)$ as $|x|\to\infty$, which implies that c is bounded by Lemma 2.3.2. We now apply Green's first identity to Ω^- and $\Omega_0 = B_R\backslash\overline{\Omega^-}$ where R is large enough so that $\overline{\Omega^-}\subset B_R$. We have

$\int_\Gamma c\partial_{n^-}c = \int_{\Omega^-}(c\triangle c + |\nabla c|^2)$ and $\int_{\partial B_R} c\partial_n c - \int_\Gamma c\partial_{n^+}c = \int_{\Omega_0}(c\triangle c + |\nabla c|^2)$ Since $\Delta c = 0$ on $B_R\backslash\Gamma = \Omega^-\cup\Omega_0$ and $\left[\frac{\partial c}{\partial n}\right]_\Gamma = 0$, we can combine these to get

$$\int_{\partial B_R} c\partial_n c = \int_{B_R\backslash\Gamma}|\nabla c|^2.$$

Since $\partial_n c = \mathcal{O}\left(\frac{1}{R^3}\right)$ and c is bounded,

$$\int_{B_R\backslash\Gamma}|\nabla c|^2 = 4\pi R^2\mathcal{O}\left(\frac{1}{R^3}\right) = \mathcal{O}\left(\frac{1}{R}\right) \text{ as } R\to\infty.$$

Thus $\nabla c = 0$ and c is constant. Then $u(x) = W_g(x) + c$ and for $x\in\Gamma$, $f(x) = W_g(x) + c$. Thus we've shown

$$f(x) = -\frac{1}{4\pi}\int_\Gamma \frac{1}{|x-y|}\, g(y)dS_y + c \qquad \text{for } x\in\Gamma. \qquad \square$$

We now combine Lemmas 2.2.1 and 2.3.3 and let $f=\kappa$ and $g=-V$, the mean curvature and normal velocity of Γ, respectively. We show this system is equivalent to (2.1). We impose the requirement that $\Gamma_0\in C^{2+\alpha}$ in order to use the uniqueness results found in [17, 18].

www.manaraa.com

Theorem 2.3.1 *Let $\alpha \in (0,1)$ and suppose there exists some finite time T and $c \in C([0,T])$ such that $\cup_{0\le t\le T}\Gamma(t)$ is a family of surfaces with $\Gamma_0 \in C^{2+\alpha}$ that satisfies*

i) $\kappa(x,t) = \dfrac{1}{4\pi}\displaystyle\int_{\Gamma(t)} \frac{1}{|x-y|} V(y,t)dS_y + c(t) \qquad$ *for* $x \in \Gamma(t)$.

ii) $\displaystyle\int_{\Gamma(t)} V(y,t)dS_y = 0.$

where $V(\cdot,t) \in C(\Gamma(t))$ is the normal velocity of $\Gamma(t)$ and $\kappa(x,t)$ is the mean curvature of $\Gamma(t)$. Then $\Gamma(t)$ is the interface associated with the solution of (2.1).

Conversely, if $(u,\Gamma(t))$ is a solution to (2.1) with $\Gamma_0 \in C^2$ and $V(\cdot,t) \in C(\Gamma(t))$, then i) and ii) hold.

Proof. Suppose $\cup_{0\le t\le T}\Gamma(t)$ is a family of surfaces with $\Gamma_0 \in C^{2+\alpha}$ that satisfies

i) $\kappa(x,t) = \dfrac{1}{4\pi}\displaystyle\int_{\Gamma(t)} \frac{1}{|x-y|} V(y,t)dS_y + c(t) \qquad$ for $x \in \Gamma(t)$.

ii) $\displaystyle\int_{\Gamma(t)} V(y,t)dS_y = 0.$

By Lemma 2.2.1, $u(\cdot,t)$ defined on $\mathbb{R}^3$ by

$$u(x,t) = \frac{1}{4\pi}\int_{\Gamma} \frac{1}{|x-y|} V(y,t)dS_y + c(t)$$

is a solution of (2.1). By [17, 18], solutions to (2.1) are unique given $\Gamma_0 \in C^{2+\alpha}$. Hence $\Gamma(t)$ is that solution.

To prove the converse we simply apply Lemma 2.3.3 with $g = -V$ and $f = \kappa$. □

2.4 Existence and Uniqueness

We now show that the mean curvature uniquely determines the normal velocity for a simple closed surface $\Gamma \in C^3$ assuming the existence of a sufficiently smooth solution to an exterior Dirichlet problem. The more stringent smoothness condition on Γ is needed for the existence of a sufficiently smooth solution, namely $u \in C_n(\Omega^-)$, to the interior Dirichlet problem, where as done previously, we denote the portion of $\mathbb{R}^3$ enclosed by Γ as Ω^- and the unbounded portion outside Γ as Ω^+. We have the following interior and exterior Dirichlet problem:

www.manaraa.com

$$\begin{aligned} \Delta u &= 0 && \text{on } \mathbb{R}^3 \backslash \Gamma, \\ u &= \kappa && \text{on } \Gamma, \\ \nabla u &= \mathcal{O}\left(\frac{1}{|x|^3}\right) && \text{as } |x| \to \infty. \end{aligned}$$

where $\kappa \in C^1(\Gamma)$ is the mean curvature of Γ. Since for a surface locally represented as $(u, v, f(u, v))$ the mean curvature is $\kappa = \dfrac{f_{uu}(1+f_v^2) - 2f_u f_v f_{uv} + f_{vv}(1+f_u^2)}{2(1+f_u^2+f_v^2)^{\frac{3}{2}}}$, we need $f \in C^3$ for $\kappa \in C^1(\Gamma)$, i.e., we need $\Gamma \in C^3$.

Previous results for existence (and uniqueness) for the interior Dirichlet problem give $u \in C^\infty(\Omega^-) \cap C(\overline{\Omega^-})$ if $\kappa \in C(\Gamma)$ [32]. Since $\kappa \in C^1(\Gamma)$, we have $u \in C^\infty(\Omega^-) \cap C^1(\overline{\Omega^-})$ and hence $u \in C_n(\Omega^-)$.

The author is not aware of existence or uniqueness results for the above exterior Dirichlet problem. There are other exterior Dirichlet problems for which existence and uniqueness is known. If u is bounded and the limit of u at infinity is specified, the exterior problem is uniquely solvable [30]. Another exterior problem requires u to be harmonic at infinity and has a (unique) solution $u \in C(\overline{\Omega^+})$ [21]. By definition, a function u satisfying the Laplace equation on an exterior domain is harmonic at infinity if its Kelvin transform has a removable singularity at the origin [21].

The difference between the three exterior problems is shown by the case that Γ is the unit sphere centered at the origin and $\kappa \equiv -1$. The function $u(x) = -\dfrac{1}{|x|}$ is the solution that is harmonic at infinity, but it does not satisfy $\nabla u = \mathcal{O}\left(\dfrac{1}{|x|^3}\right)$. However, $u \equiv -1$ does satisfy $\nabla u = \mathcal{O}\left(\dfrac{1}{|x|^3}\right)$. Furthermore, $u \equiv -1$ is not harmonic at infinity, as its Kelvin transform is $\dfrac{-1}{|x|}$ [21, 40]. Both $u \equiv -1$ and $u(x) = -\dfrac{1}{|x|}$ tend to a limit as $|x| \to \infty$. In general, as proved in Lemma 2.3.2, $\nabla u = \mathcal{O}\left(\dfrac{1}{|x|^3}\right)$ implies u has a limit, assuming u exists. We note that for a function u satisfying the Laplace equation on an exterior domain, harmonic at infinity is equivalent to $u = \mathcal{O}\left(\dfrac{1}{|x|}\right)$ and also equivalent to $u(x) \to 0$ as $|x| \to \infty$ [21].

www.manaraa.com

Existence and uniqueness using the condition $u = \mathcal{O}\left(\frac{1}{|x|}\right)$ are proved in [33].

We now prove that the mean curvature κ uniquely determines the normal velocity V, assuming the existence of a sufficiently smooth solution to the above exterior Dirichlet problem.

Theorem 2.4.1 *Let Γ be the union of finitely many disjoint simple closed C^3 surfaces such that Γ separates $\mathbb{R}^3$ into finitely many bounded regions, collectively denoted as Ω^-, and one unbounded region Ω^+. Let n denote the outward unit normal to Γ. Let $f \in C^1(\Gamma)$. Assume there exists a solution $u \in C_n(\Omega^+)$ to the exterior Dirichlet problem*

$$\begin{aligned} \Delta u &= 0 && \text{on } \Omega^+, \\ u &= f && \text{on } \Gamma, \\ \nabla u &= \mathcal{O}\left(\frac{1}{|x|^3}\right) && \text{as } |x| \to \infty. \end{aligned}$$

Then there exists a unique $g \in C(\Gamma)$ and constant c such that

i) $f(x) = -\frac{1}{4\pi}\int_\Gamma \frac{1}{|x-y|} g(y)dS_y + c \qquad$ *for $x \in \Gamma$.*

ii) $\int_\Gamma g(y)dS_y = 0.$

Proof. We first show the existence of g and c. Let $u \in C_n(\Omega^-) \cap C_n(\Omega^+)$ be a solution to the Dirichlet problem below:

$$\begin{aligned} \Delta u &= 0 && \text{on } \mathbb{R}^3\backslash\Gamma, \\ u &= f && \text{on } \Gamma, \\ \nabla u &= \mathcal{O}\left(\frac{1}{|x|^3}\right) && \text{as } |x| \to \infty. \end{aligned}$$

Let $g = -\left[\frac{\partial u}{\partial n}\right]_\Gamma$. Then g is continuous and by Lemma 2.3.3, $\int_\Gamma g = 0$ and $c \equiv u(x) + \frac{1}{4\pi}\int_\Gamma \frac{1}{|x-y|} g(y)dS_y = u(x) - W_g(x)$, $x \in \Gamma$, is constant.

www.manaraa.com

We now show uniqueness. Since i) and ii) is a linear system, we need only show that $f \equiv 0$ implies $g \equiv 0$ and $c = 0$. Let $w(x) \equiv -\frac{1}{4\pi}\int_\Gamma \frac{1}{|x-y|} g(y) dS_y + c = W_g(x) + c$. Utilizing Lemma 2.2.1, we have

1. w is well-defined and continuous on $\mathbb{R}^3$.

2. $\Delta w = 0$ in $\mathbb{R}^3 \backslash \Gamma$.

3. $w \in C_n(\Omega^-) \cap C_n(\Omega^+)$ and $-\left[\frac{\partial w}{\partial n}\right]_\Gamma \equiv -(\partial_{n^-} w - \partial_{n^+} w) = g$ on Γ.

4. $w = c + \mathcal{O}\left(\frac{1}{|x|}\right)$ as $|x| \to \infty$.

5. $\nabla w = \mathcal{O}\left(\frac{1}{|x|^3}\right)$ as $|x| \to \infty$.

Also, $w = f = 0$ on Γ.

We show $w \equiv 0$ using Green's first identity. The relaxed regularity of w can be justified using the technique found in Lemma 2.3.3. First we consider Ω^-. We have

$$\begin{aligned} \int_\Gamma w \partial_{n^-} w &= \int_{\Omega^-} \left(w \triangle w + |\nabla w|^2\right) \\ \implies \qquad 0 &= \int_{\Omega^-} |\nabla w|^2. \end{aligned}$$

Hence w is constant on Ω^-. Since $w = 0$ on Γ and w is continuous on $\mathbb{R}^3$, $w = 0$ on Ω^-.

Now consider $\Omega_0 = B_R \backslash \overline{\Omega^-}$ where R is large enough so that $\overline{\Omega^-} \subset B_R$.

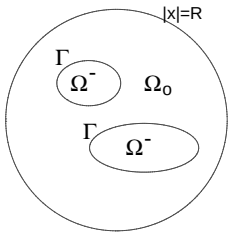

Again by Green's first identity we have

www.manaraa.com

$$
\begin{aligned}
\int_{\partial B_R} w\partial_n w - \int_{\Gamma} w\partial_{n^+} w &= \int_{\Omega_0} \left(w\triangle w + |\nabla w|^2\right) \\
\implies \int_{\partial B_R} w\partial_n w &= \int_{\Omega_0} |\nabla w|^2 \\
\implies 4\pi R^2 \left(c + \mathcal{O}\left(\frac{1}{R}\right)\right) \mathcal{O}\left(\frac{1}{R^3}\right) &= \int_{\Omega_0} |\nabla w|^2 \\
\implies \mathcal{O}\left(\frac{1}{R}\right) &= \int_{\Omega_0} |\nabla w|^2.
\end{aligned}
$$

Then $\nabla w = 0$ and $w = 0$ on $\mathbb{R}^3$.

Since $0 = -\left[\dfrac{\partial w}{\partial n}\right]_{\Gamma} = -\left[\dfrac{\partial W_g}{\partial n}\right]_{\Gamma} = g$, we have $g \equiv 0$ on Γ. Hence, $c = 0$. □

We can now solve (2.1) in the following way: Given $\Gamma(t)$ we calculate $\kappa(x,t)$ on $\Gamma(t)$. We solve the system

$$
\begin{cases}
\kappa(x,t) = \dfrac{1}{4\pi} \displaystyle\int_{\Gamma(t)} \frac{1}{|x-y|} V(y,t) dS_y + c(t) \\
\displaystyle\int_{\Gamma(t)} V(y,t) dS_y = 0
\end{cases}
$$

for $V(\cdot,t)$ and $c(t)$. We then advance the surface to $\Gamma(t+\Delta t)$ by a suitable scheme. In our case we use a semi-implicit method based on the Implicit Trapezoid method [9].

www.manaraa.com

www.manaraa.com

Chapter 3

Numerical Scheme

This chapter describes the numerical scheme. The first component of the scheme is modeling surfaces discretely. Various factors must be taken into account, including ease of cataloging the nodes onto a rectangular grid and having nodes as equidistant as possible.

Surface area must be estimated, both locally for the discretized surface integrals and globally as a validation of the scheme. We use triangular patches and show theoretically and numerically that smaller mesh size leads to convergence of estimated surface area to actual surface area. We also derive estimates of the volume enclosed by the surfaces, which is necessary only for scheme validation.

Speed of evolution of a node, or point, on a surface is governed by the mean curvature, so a good estimate is vital. The node then travels in the direction of the normal to the surface, which must also be found numerically. The method we use, obtained from [45], utilizes an iterative method to fit a node and its neighbors to a quadratic surface. We explain it in detail and show numerical results of convergence.

The system of boundary integral equations must be evaluated over the triangular patches that comprise the surface. We use an average over the vertices to estimate the value of the function $\frac{1}{|x-y|}$ over a patch. This discretization leads to a system of linear equations whose solution gives the normal velocities of the nodes. Solving the system of equations is extremely computationally expensive, so a particle-cluster method is used to reduce the computations involved for large numbers of nodes, or points on the surfaces.

www.manaraa.com

Many choices are available to advance the surface. A semi-implicit scheme is the most advantageous, and we show how the necessary calculations are made.

3.1 Surface Modeling

Our purpose is to discretize any number of simple, smooth closed surfaces. For simplicity we consider only ellipsoids, torii, and distortions thereof.

Several factors come into play as we choose discrete representations of various surfaces. Of course simplicity and flexibility are overriding goals. Since the points on the surface, or nodes, must be stored in computer memory in a way that is easily referred back to, we want the discretization to easily adapt to a rectangular array. A rectangular $N \times M$ array also makes exhaustive algorithms more straightforward. In the C programming language, indices of arrays begin at 0, so visually we have the following:

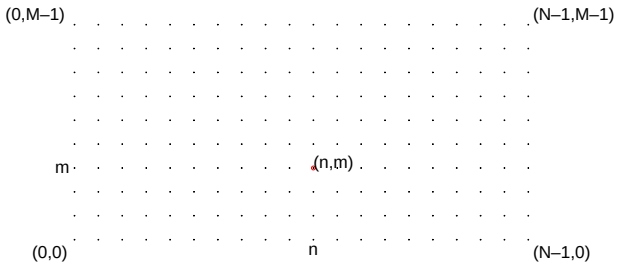

Keeping track of a node's eight nearest neighbors is easier if neighbors spatially are also neighbors on the array.

Another consideration is that when nodes that are fairly equally spaced, we can use a much larger time step than if nodes are clustering in certain areas. For example, below are two different ways to discretize a sphere. The left discretization, based on spherical coordinates, is extremely simple to fit with a rectangular array and the nearest neighbor scheme is straightforward, but the clustering of nodes at the poles quickly leads to "blow-up," or isolated nodes suddenly evolving large distances from the other nodes. The discretization on the below right, which is based on a regular icosahedron, has very evenly distributed nodes, but is quite complicated with regard to record keeping. The latter is what we use.

www.manaraa.com

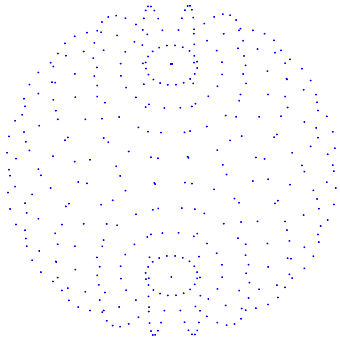

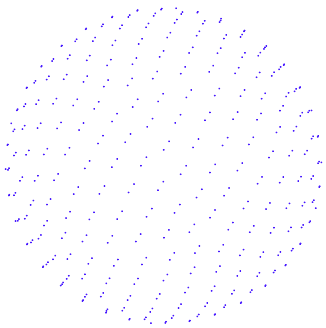

We also want a decrease in mesh size, which is the average of the distance between nodes and their eight neighboring nodes, to lead to greater accuracy in area, volume, outward normal, and mean curvature approximations. We analyze convergence of these estimates.

3.1.1 Torus

The torus is the simplest surface to discretize. The following method was also utilized in [8]. The surface can be given implicitly by $z^2 + (\sqrt{x^2+y^2} - R)^2 = r^2$ where R denotes the large radius of the torus and r the small radius. However, it is simpler to use an angular parametrization. We have

$$x = (R + r\cos\phi)\cos\theta$$

$$y = (R + r\cos\phi)\sin\theta$$

$$z = r\sin\phi$$

where $\theta \in [0, 2\pi)$ is the angle between the positive x axis and the projection of the line from the origin to the node onto the xy-plane. We find ϕ by intersecting the torus with a plane perpendicular to the xy-plane containing the node to get a circle. We let $\phi \in [0, 2\pi)$ be the angle between the line on the xy-plane and the line from the center of the circle.

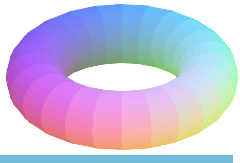

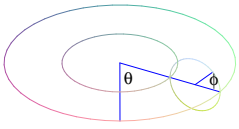

www.manaraa.com

As our array is N by M, we let n vary from 0 to $N-1$ and m vary from 0 to $M-1$ and assign

$$\theta = \frac{2\pi n}{N}$$
$$\phi = \frac{2\pi m}{M}.$$

This, in effect, wraps the grid into a cylinder and then bends the cylinder around to join the ends. Below is the case $N = 20$, $M = 10$, $R = 3$, and $r = 1$.

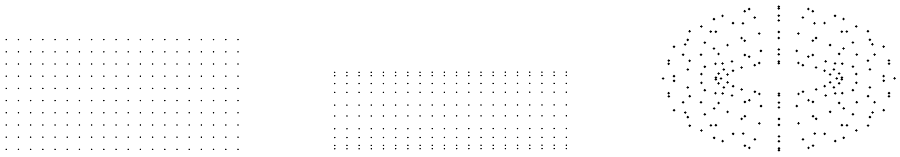

3.1.2 Distorted Torus

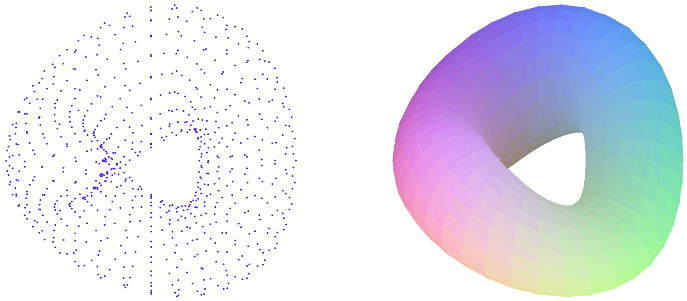

We shall distort the torus by perturbing the radii, cross sections, and the distance from the xy-plane. The objects below are a distortion of a torus with large radius $R = 4$ and small radius $r = 2$. The discretization below is based on a 40×20 array, i.e., $N = 40$ and $M = 20$.

Recall that for a non-distorted torus we have the parametrization

$$x = (R + r\cos\phi)\cos\theta$$
$$y = (R + r\cos\phi)\sin\theta$$
$$z = r\sin\phi$$

The distorted torus will be parameterized by

www.manaraa.com

$$x = (R' + r' \cos\phi) \cos\theta$$

$$y = (R' + r' \cos\phi) \sin\theta$$

$$z = b \sin\phi + h$$

First we distort the radii R and r to find $R'(\theta)$ and $r'(\theta)$. The torus projected onto the xy-plane is an annulus with inner radius $R-r$ and outer radius $R+r$. We perturb this inner radius to $R_I = (R-r)(1+0.1\sin 2\theta)$ and the outer radius to $R_O = (R+r)(1+0.1\sin 2\theta)$, although other functions may be used. Then the small radius r' of the perturbed torus is $\dfrac{R_O - R_I}{2}$ and the large radius R' is $R_I + r'$. Note that at $\theta = 0$ and $\theta = \pi$ we have $R' = R$ and $r' = r$.

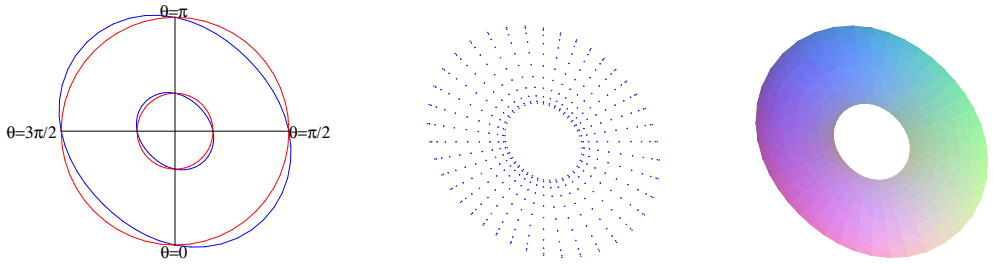

The cross sections are varied from circular to elliptical by specifying $b = r' - \dfrac{r'}{2}\sin\theta$. Again, other functions may be used. At $\theta = 0$ and $\theta = \pi$ the cross sections are circular with radius r while at $\theta = \dfrac{\pi}{2}$ and $\theta = \dfrac{3\pi}{2}$ the cross sections are the ellipses $\dfrac{x^2}{(r')^2} + \dfrac{y^2}{(\frac{r'}{2})^2} = 1$ and $\dfrac{x^2}{(r')^2} + \dfrac{y^2}{(\frac{3r'}{2})^2} = 1$, respectively.

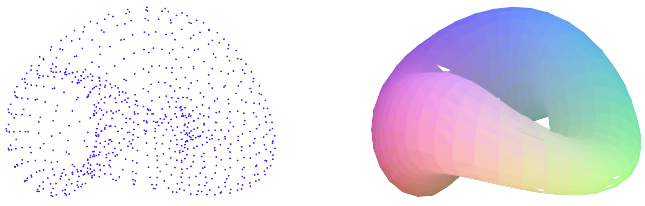

We add $h = \dfrac{r}{2}\cos 2\theta$ to the z value to distort the distance from the xy-plane, again realizing we have many choices of functions.

www.manaraa.com

3.1.3 Ellipsoid

Given a sphere or more generally an ellipsoid, we wish discretize its surface. The model is based on the regular icosahedron. We arrange nodes on each of its 20 equilateral triangles and project the results onto an ellipsoid.

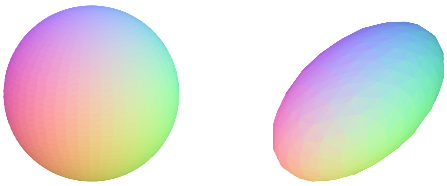

First we find the coordinates of the 12 vertices. The vertices $(\pm 1, \pm\tau, 0)$, $(0, \pm 1, \pm\tau)$, and $(\pm\tau, 0, \pm 1)$, where $\tau = \dfrac{1+\sqrt{5}}{2}$ is the golden ratio, form a regular icosahedron [43]. However, placing two of the vertices on $(1, 0, 0)$ and $(-1, 0, 0)$ simplifies the discretizations of tubes and barbells, which are areas of work in progress. We next show how to find the vertices given this constraint.

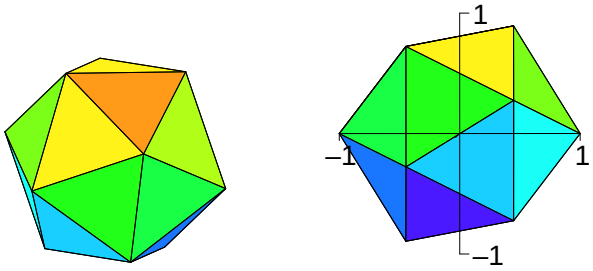

We will use the term 'pole' to refer to $(1, 0, 0)$ or $(-1, 0, 0)$. The five triangles surrounding the pole $(1, 0, 0)$ are the 'right cap'. 'Left cap' is defined similarly. The remaining 10 triangles form what we shall call the 'belt'.

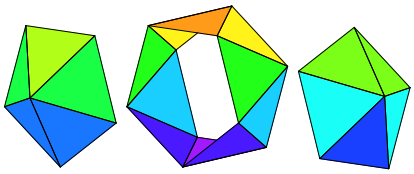

To find the appropriate coordinates of the vertices, we consider the triangle formed by the edge lying on the first quadrant of the xz-plane and by the line segments connecting the vertices of the edge to the origin. Here s denotes the length of an edge. The eventual goal is to calculate $\cos\alpha$ and $\sin\alpha$, where α is as shown below.

www.manaraa.com

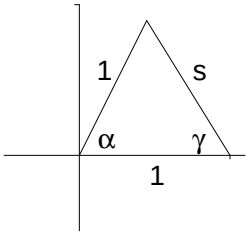

By the law of cosines we have $\cos\gamma = \frac{s}{2}$, so the height of the triangle is $\frac{s}{2}\sqrt{4-s^2}$.

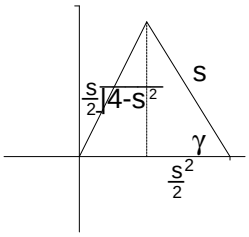

Next we look at the right cap of the icosahedron as projected onto the yz-plane.

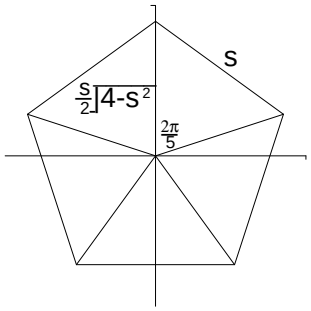

By the law of cosines, $s^2 = 2\left(\frac{s}{2}\sqrt{4-s^2}\right)^2 - 2\left(\frac{s}{2}\sqrt{4-s^2}\right)^2 \cos\frac{2\pi}{5}$, and $s = \sqrt{4 - \frac{2}{1-\cos\frac{2\pi}{5}}}$.

Fortunately $\cos\frac{2\pi}{5}$ can be found algebraically in the following way. Express $\cos 5x$ in terms of $\cos x$ by using sum and double angle formulas along with the relation $\cos^2 x + \sin^2 x = 1$. Let $x = \frac{2\pi}{5}$ and use an algebraic solver such as Maple® to solve the resulting fifth degree polynomial equation $16a^5 - 20a^3 + 5a - 1 = (a-1)(4a^2+2a-1)^2 = 0$ where $a = \cos\frac{2\pi}{5}$. The applicable root is $\cos\frac{2\pi}{5} = \frac{\sqrt{5}-1}{4}$.

We can now calculate $\cos\alpha = 1 - \frac{s^2}{2} = \frac{1}{\sqrt{5}}$. It follows directly that $\sin\alpha = \frac{2}{\sqrt{5}}$. The coordinates of the vertices of the icosahedron other than the poles are as follows: The x-coordinates are $\pm\cos\alpha$. The y-coordinates are $\sin\alpha\cos\beta$ where β is $\frac{\pi}{2}$ plus a multiple of $\frac{2\pi}{5}$ for the right cap and $-\frac{\pi}{2}$ plus a multiple of $\frac{2\pi}{5}$ for the left cap. The z-coordinate is $\sin\alpha\sin\beta$.

www.manaraa.com

The next step is to arrange nodes onto the twenty faces. Since the nodes are to be stored in a rectangular array, it is convenient to section an array into 20 isosceles right triangles and put the same number of nodes in the isosceles triangles onto the triangular faces of the icosahedron, as shown below.

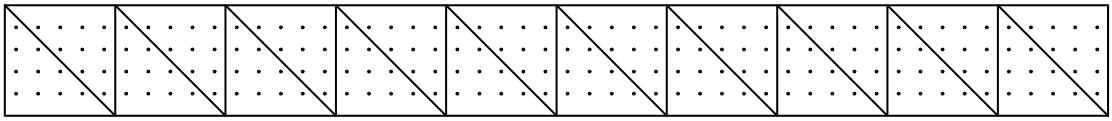

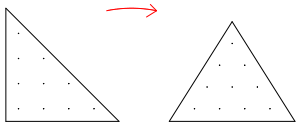

Since there are 20 faces, if there are M nodes in the array vertically, there are $10(M+1)$ nodes along the array horizontally and $10M(M+1)$ nodes total. Below are faces with $M = 5, 7,$ and 10.

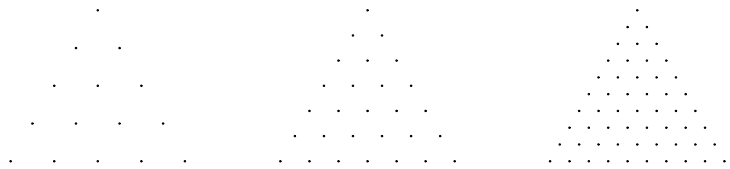

Our method of bookkeeping dictates there be the same number of nodes on each face, so to prevent overlap or omission of nodes when arranging the triangular clusters of nodes on the icosahedron, we don't put nodes on the edges. Instead we create a small buffer zone which is half the horizontal distance between nodes. Below is a face scaled so that the distance between nodes is 1.

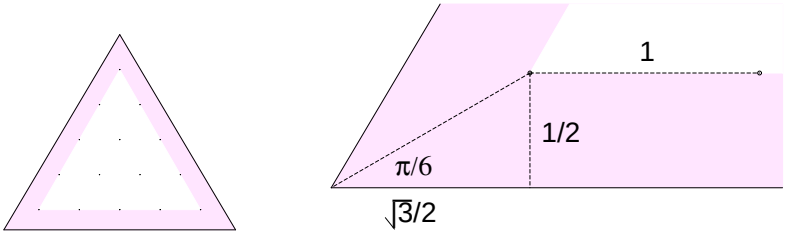

Given the three vertices P, Q, R of a face of the icosahedron, we generate the nodes by first finding the distance, or mesh size m, between nodes given the buffer zone as described above.

www.manaraa.com

Since the length of an edge is $s = \sqrt{4 - \dfrac{2}{1-\cos\frac{2\pi}{5}}} = \sqrt{\dfrac{10-2\sqrt{5}}{5}}$, $m = \dfrac{\sqrt{\frac{10-2\sqrt{5}}{5}}}{M-1+\sqrt{3}}$. We next find the node nearest one of the vertices, say P. We label this node as S, and $S = P + \dfrac{\sqrt{3}}{2} m \dfrac{\overrightarrow{PR}}{\| \overrightarrow{PR} \|} + \dfrac{1}{2} m \dfrac{\overrightarrow{PQ} + \overrightarrow{RQ}}{\| \overrightarrow{PQ} + \overrightarrow{RQ} \|}$ Then we find vectors $\mathbf{u}, \mathbf{v}$ of length m parallel to $\overrightarrow{PQ}$ and $\overrightarrow{PR}$. Adding integer multiples of $\mathbf{u}$ and $\mathbf{v}$ to S generates the nodes on the face.

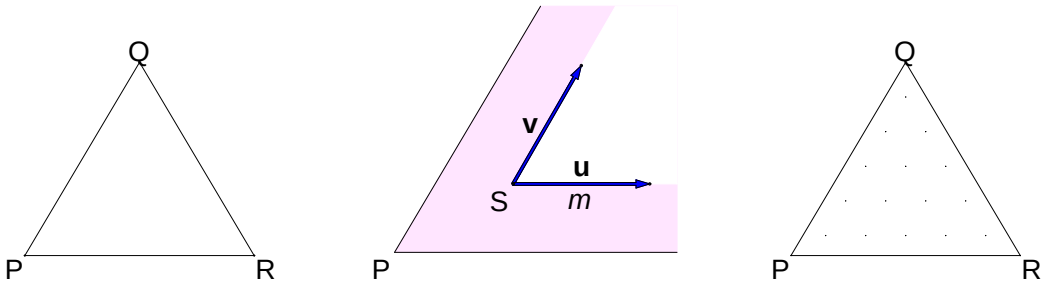

We generate nodes on all the faces of the icosahedron and project the nodes onto an ellipsoid by the following method. Supposing first that the ellipsoid is centered at the origin, we need to find for each node (u, v, w) on the icosahedron the constant k such that the product $k(u, v, w)$ lies on the surface $\dfrac{x^2}{a^2} + \dfrac{y^2}{b^2} + \dfrac{z^2}{c^2} = 1$. Then $\dfrac{(ku)^2}{a^2} + \dfrac{(kv)^2}{b^2} + \dfrac{(kw)^2}{c^2} = 1$ and $k = \dfrac{abc}{\sqrt{u^2b^2c^2 + v^2a^2c^2 + w^2a^2b^2}}$. If the ellipsoid is centered at a node C other than the origin, we simply translate by finding $k(u, v, w) + C$. Below we show the case for a sphere where $M = 5$ is the number of nodes along each edge, for a total of 300 nodes.

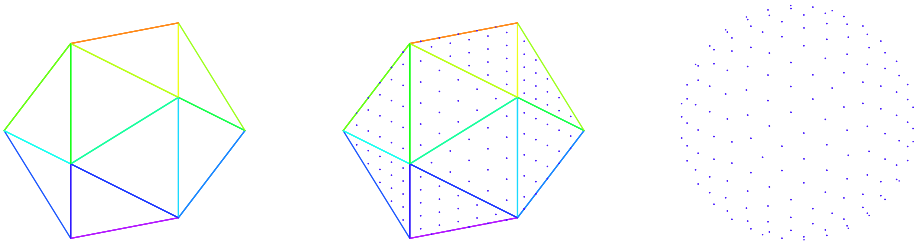

3.1.4 Distorted Ellipsoid

An ellipsoid of radius R is easily distorted by adding perturbations to the radius based on the spherical coordinates θ and ϕ. For example, the radius of the distorted unit sphere shown below is

$$\rho = 1 + 0.2\sin(2\phi) + 0.3\sin(2\phi)\sin\theta + \frac{0.3}{\sqrt{0.25\sin^2\phi\cos^2\theta + 2\sin^2\phi\sin^2\theta + 0.1\cos^2\phi}}$$

www.manaraa.com

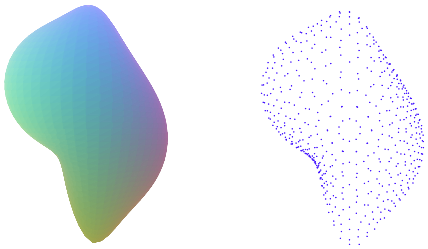

A distorted ellipsoid is discretized similarly to a non-distorted ellipsoid, differing only in the projection step. Given a node (u, v, w) on the discretized icosahedron, we calculate $\phi = \cos^{-1} \frac{w}{\sqrt{u^2+v^2+w^2}}$ and $\theta = \cos^{-1} \frac{u}{u^2+v^2}$ for $v \geq 0$ and $\theta = 2\pi - \cos^{-1} \frac{u}{u^2+v^2}$ for $v < 0$. Then $\rho = f(\phi, \theta)$ is the perturbed radius. Lastly, we find the rectangular coordinates using $x = \rho \sin\phi \cos\theta$, $y = \rho \sin\phi \sin\theta$, and $z = \rho \cos\phi$.

3.2 Nearest Neighbors

For each node on the discretized surface we catalogue 8 neighboring nodes. These neighbors are used in estimating surface area, volume, mean curvature, and outward normals. We choose the neighbors based largely on spacial considerations. Occasionally ease of cataloguing or facilitating the tiling of the surface with triangular patches will dictate that a neighbor may not be one of the nearest eight nodes. However, in most cases the neighbors will be the nearest ones.

3.2.1 Torus

The torus is the simplest surface for which to catalogue the neighbors. The nearest neighbors on the surface correspond to the nearest neighbors on the array. Thus a node indexed by (n, m) will have neighbors indexed by $(n+1, m), (n+1, m+1), (n, m+1), (n-1, m+1), (n-1, m), (n-1, m-1), (n, m-1)$, and $(n+1, m-1)$. However, this is valid only if (n, m) does not lie on the edge of the array, i.e., $n \neq N$ and $m \neq M$. Since the array wraps around, we have the more general formula for the neighbors of (n, m): $((n+1)\,\%N, m)\,, ((n+1)\%N, (m+1)\%M), (n, (m+1)\%M), ((n-1+N)\%N, (m+1)\%M), ((n-1+N)\%N, m), ((n-1+N)\%N, (m-1+M)\%M), (n, (m-1+M)\%M)$, and $((n+1)\%N, (m-1+M)\%M)$, where

www.manaraa.com

we adopt the C programming language's notation % for modular arithmetic.

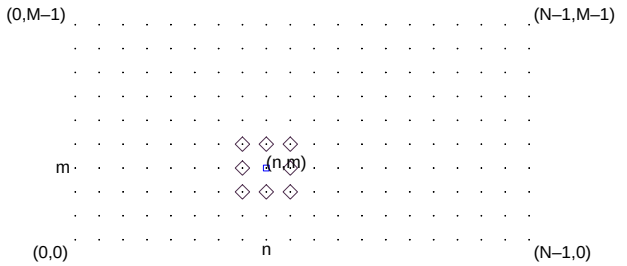

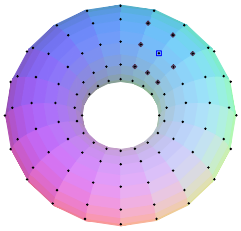

3.2.2 Ellipsoid

The ellipsoid's neighbor scheme is more complex because special cases are needed where triangular faces meet. We omit the details for these special cases. For a node which is interior to a face, the scheme is straightforward. Six of the nodes are obvious choices for neighbors: they form a hexagon around the node. For the other two nodes, we simply make a choice and stick with it. We pick the nodes directly above and below the central node. Below is an example face with an interior node and its neighbors. The left triangle is the node and neighbor as they are catalogued in the rectangular array in which they are stored.

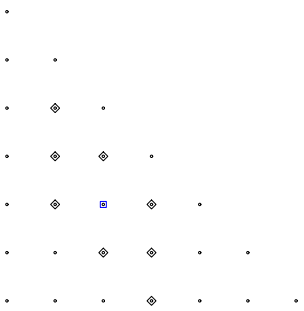

Neighbors on Array

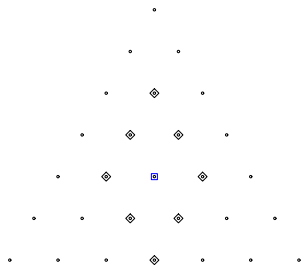

Neighbors on Face

3.3 Surface Area Estimates

Dividing a surface into "patches" serves two purposes. First, we can estimate the total surface area, providing a check that surface area is indeed non-increasing as mathematically predicted (see 4.2). Secondly, the patches are used in approximating surface integrals (see 3.7).

www.manaraa.com

3.3.1 Subdivision Points

We tile surfaces with triangular patches by designating four triangular patches for each node, with the node a vertex of each of the four triangles. The other vertices are found by averaging the node and three of its eight nearest neighbors. We call these vertices subdivision points.

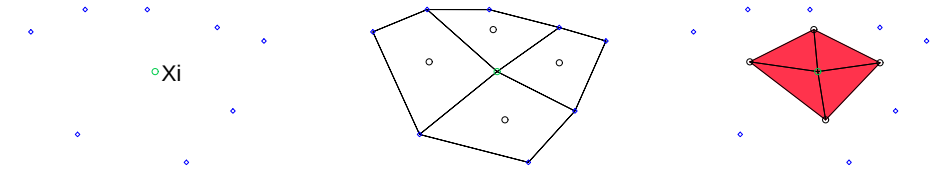

Node and 8 Neighbors Subdivision Points Triangular Patches

We demonstrate with a torus discretized by 256 nodes.

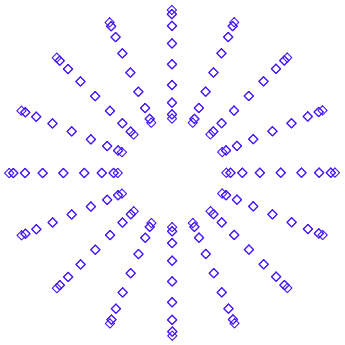

Nodes

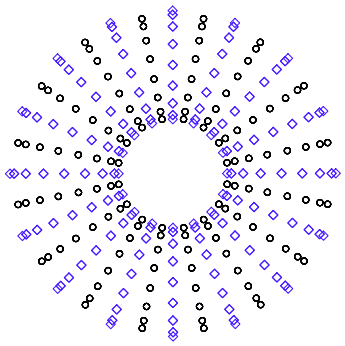

Nodes and Subdivision Points

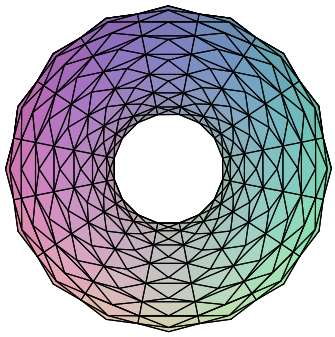

Patches

The patches completely tile the torus. We omit the details, but the ellipsoid also is covered by the patches, although this requires some adjustments of the subdivision points near the poles. Distortions do not cause any gaps in the tiling.

www.manaraa.com

The subdivision points do not lie on the surface itself since they are found by averaging four nodes that lie on the surface. The chart below shows the maximum over the subdivision points of the distance between a subdivision point and the surface of a torus versus the mesh size. Mesh size refers to the average distance between the nodes and their eight nearest neighbors. For simplicity when doing error analysis for the torus, we use $N = M$, i.e., the number of nodes on a radial slice is equal to the number of such slices. For this analysis the torus has large radius 2 and small radius 1. Further discussion on these choices is in 3.3.3. For a subdivision point (x, y, z), the distance to the surface of a torus with large radius R and small radius r is $\left| r - \sqrt{(\sqrt{x^2 + y^2} - R)^2 + z^2} \right|$.

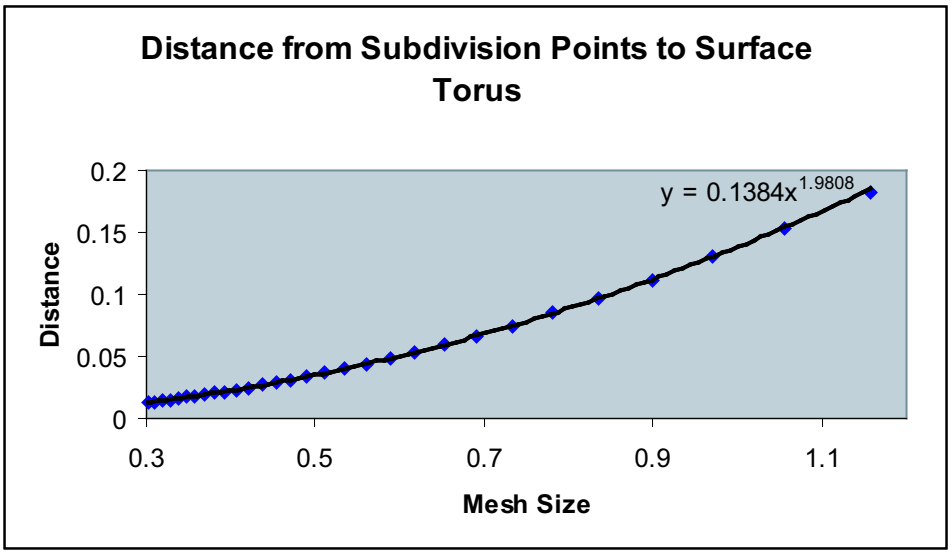

Using Microsoft Excel®, we can fit a function of the form $y = ax^b$ to the data. The error is inversely proportional to the square of the mesh size.

The sphere also has this relationship, as shown below. In the case of a sphere of radius r, the distance from a subdivision point (x, y, z) to the surface is $r - \sqrt{x^2 + y^2 + z^2}$.

www.manaraa.com

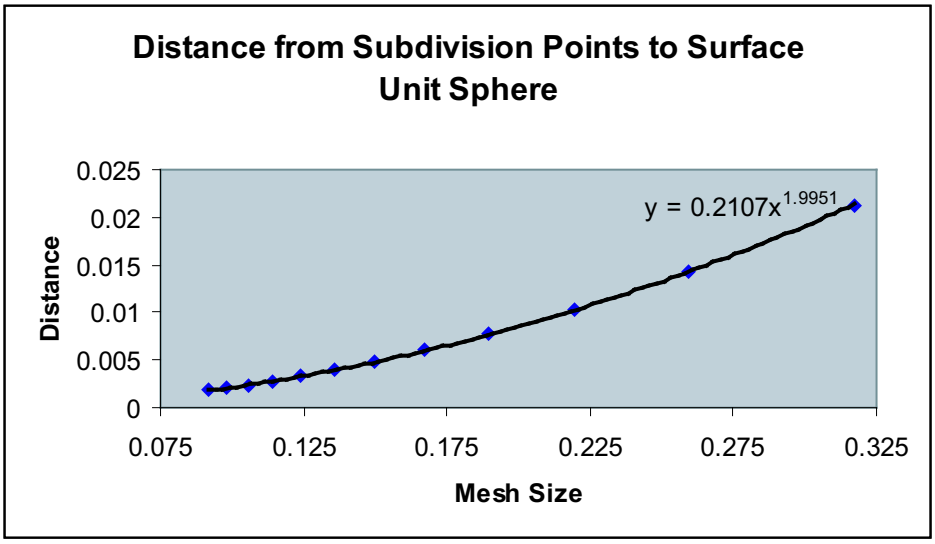

Finding subdivision points which lie nearer to the surface is an area of further work. One possibility is for the subdivision point to lie on the approximating surface through a nearby node (see 3.5).

3.3.2 Patch Area

Given a node and two subdivision points which form the vertices of a patch, we now calculate the area of the patch. We also discuss other options for estimating surface area and why they are not used.

The area of a triangular patch with vertices A, B, and C is simply $\frac{1}{2}\|\overrightarrow{AB} \times \overrightarrow{AC}\|$. Assuming the subdivision points lie on the surface, a more accurate way of calculating the area would be finding the area of the surface itself instead of the triangular patch. However, surface area in general is hard to calculate. Indeed, even for the quadratic surface $z = Ax + By + Cx^2 + Dxy + Ey^2$, to find the area of the surface above the lines connecting $(0,0,0)$, $(a,0,z(a,0))$, and $(0,b,z(0,b))$ we are required to find the integral $\int_0^a \int_0^{\frac{-b}{a}x+b} \sqrt{(A+2Cx+Dy)^2+(B+Dx+2Ey)^2+1}\,dy\,dx$ analytically, which is not an easy task. The first integral of the double integral is not hard to find, but the outer integral would require a numerical algorithm. Ascertaining whether the computational expense is justified by greater accuracy is an area of future work.

www.manaraa.com

A surface simpler than a general quadratic surface is a sphere. Given three nodes P, Q, R on the surface of a sphere with radius R centered at the origin, we let α, β, γ be the angles between the vectors connecting the nodes to the origin. If two of the angles are equal, say $\alpha = \beta$, then the surface area bordered by the arcs connecting P, Q, and R is $\gamma(R^2 - \cos\alpha)$. Otherwise the surface area is $\gamma R^2 \left(1 + \dfrac{\sin\alpha - \sin\beta}{\beta - \alpha}\right)$. Unfortunately this latter formula is extremely sensitive to roundoff error when α is near β, as we have a small number divided by a small number: $\dfrac{\sin\alpha - \sin\beta}{\beta - \alpha}$. A future area of investigation is whether this can be overcome, perhaps by using Taylor series approximations. If we can find a workable formula for the area, the next step would be deciding what radius R is appropriate given any discretized surface.

In view of these difficulties, we use the area of triangles to estimate surface area.

3.3.3 Convergence of Surface Area Estimates

There are two things to consider in analyzing the validity of our surface estimates. First we need that the total area of these estimates converges to the area of the entire surface. Without this latter result, we cannot reasonably ascertain whether the scheme is true to the mathematical model's prediction that surface area is non-increasing (see 4.2). Secondly, we show that the area of a triangular estimate converges to the actual area of the surface "above" the triangle, where the triangle's vertices lie on the surface and convergence is with respect to the maximum length of the sides of a triangle. This helps confirm the validity of integrating over patches as an approximation to integrating over a surface (see 3.7).

To estimate the surface area, we sum the area of all the patches. Numerical convergence results are quite good. For a sphere of radius 1, we have the following tables showing the the relationship between the error and the mesh size. The error is inversely proportional to the square of the mesh size.

www.manaraa.com

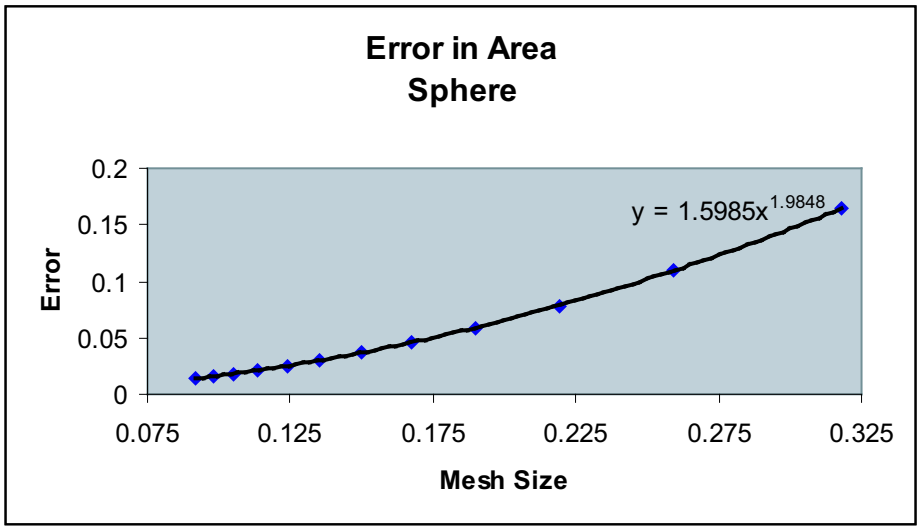

Before continuing the error analysis of surface area estimates, we take a moment to discuss the error analysis tables. Since we directly control the number of nodes rather than the mesh size, we would like to find a relationship between the two. Recall that mesh size is the average distance between the nodes and their eight nearest neighbors. In the argument below we assume patch areas and mesh sizes are approximately the same throughout a surface. Since

$$\begin{aligned} \text{surface area} &\approx (\#\text{ nodes})4(\text{area of patch}) \\ &\approx (\#\text{ nodes})(\text{mesh size})^2 \end{aligned},$$

we have the relationship for some constant k:

$$\#\text{ nodes} \approx \frac{k}{(\text{mesh size})^2}.$$

Experimentally we have this relationship for the unit sphere, as shown below.

www.manaraa.com

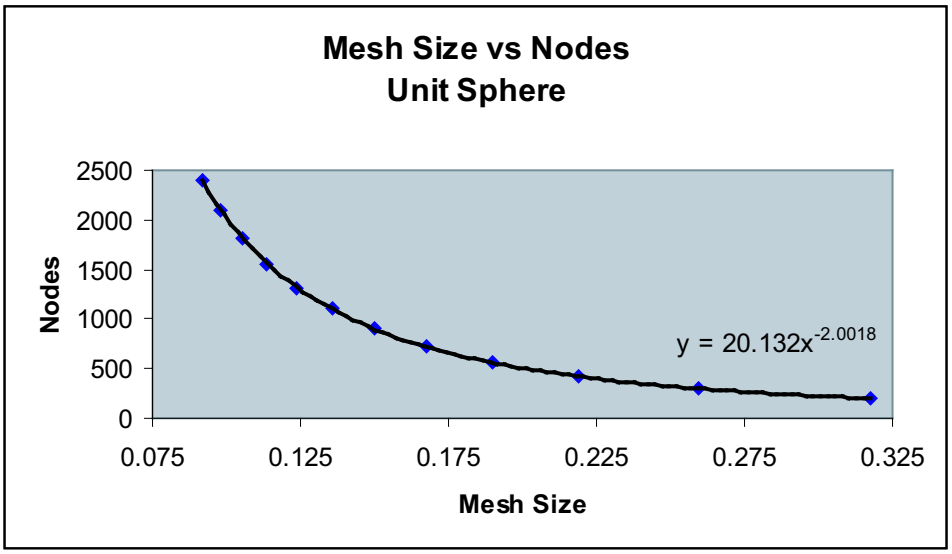

For the torus more care is needed to analyze error. A large number of nodes does not necessarily mean smaller mesh size because the choices of N, the number of radial slices, and M, the number of nodes per radial slice, have a great effect. For example, the torii below all are discretized with $NM = 400$ nodes but have different N and M values and also different mesh sizes.

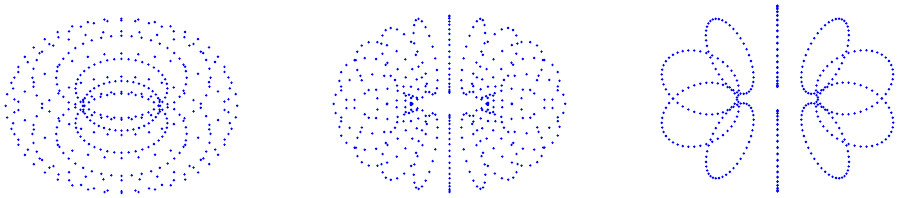

The table below shows the mesh size for different values of N with the number of nodes fixed at 400. The torus has large radius 2 and small radius 1.

www.manaraa.com

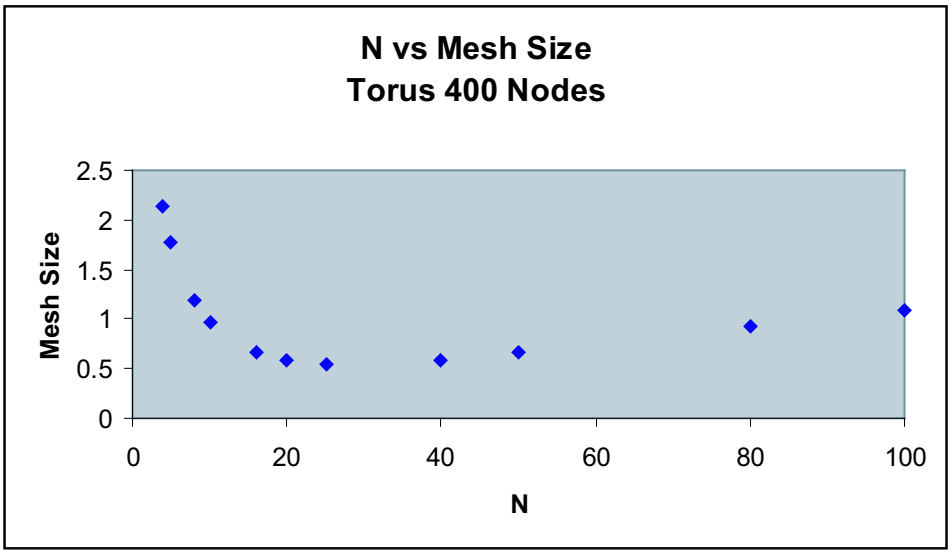

Using $N = M = 20$ gives one of the smaller mesh sizes. In future error analysis with respect to the torus, we will use $N = M$ with large radius 2 and small radius 1. This will give that the nodes on the inner perimeter are the same distance apart as the nodes on each radial slice. Below we show the experimental relationship between number of nodes and mesh size given that $N = M$.

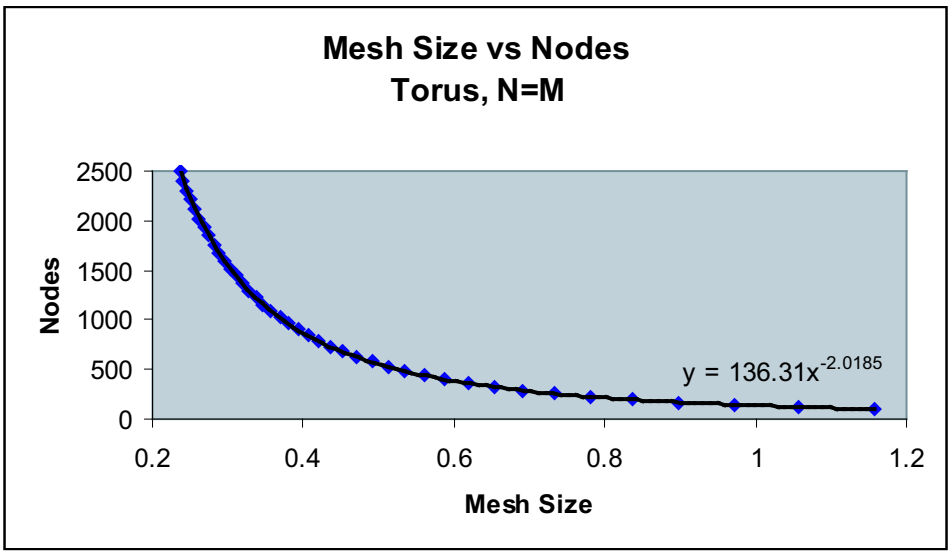

Again we have # nodes $\approx \dfrac{k}{(\text{mesh size})^2}$.

We now return to surface area estimates. For the torus we have the following error:

www.manaraa.com

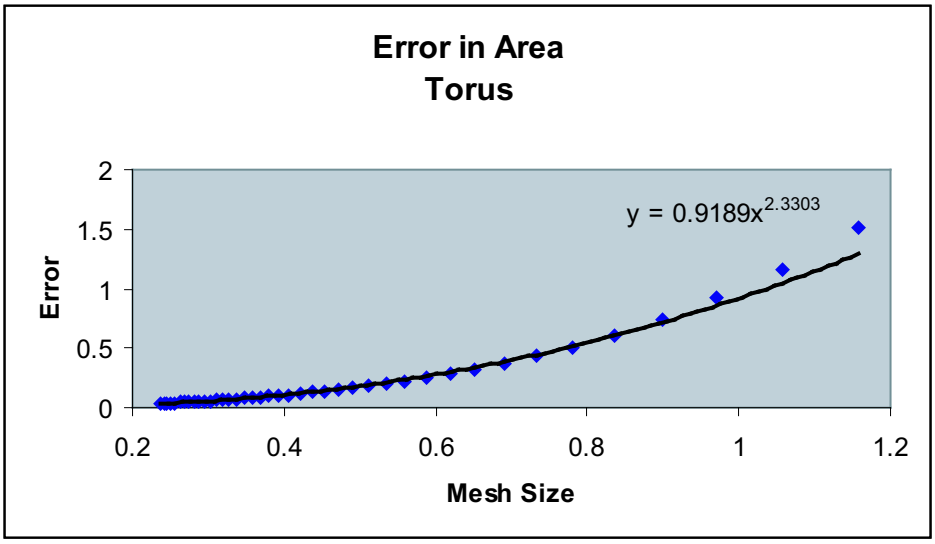

Again we have good convergence.

Next we show analytically that both the total surface area and local surface area patch estimates converge as the mesh size approaches zero. As mentioned previously, surface area in general is hard to find exact formulas for. Therefore we will restrict ourselves to two surfaces for which the area is easier to find: the sphere and the cylinder. We also simplify by using triangles and sometimes rectangles that are larger than the patches constructed above, but this effects the rate of convergence only by a constant.

First we consider the curved side of a cylinder with radius a and height H. Shown below is the cylinder divided into triangles. Each of the triangles has height h and spans an angle β.

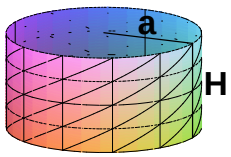

For simplicity we compute the area of the surface enclosed by a rectangular region. Consider the two patches below, both of which have the same vertices. In cylindrical coordinates (r, θ, z) these vertices are $(a, 0, 0)$, $(a, \beta, 0)$, $(a, 0, h)$, and (a, β, h). Recall that a is the radius of the cylinder, β is the angle spanned by the patch, and h is the height of the

www.manaraa.com

patch. In rectangular coordinates the vertices are $(a,0,0)$, $(a\cos\beta, a\sin\beta, 0)$, $(a,0,h)$, and $(a\cos\beta, a\sin\beta, h)$.

The estimated area of the cylindrical patch is simply the base times the height, or $A_{est} = \sqrt{(a\cos\beta - a)^2 - (a\sin\beta)^2}\, h = ah\sqrt{2-2\cos\beta}$. The actual area of the cylindrical patch is simply the arc length times the height, or $A_{act} = a\beta h$. Subtracting the areas and utilizing Taylor series for $\cos\beta$, we have

$$\begin{aligned}
\Delta A &= A_{act} - A_{est} \\
&= ah\sqrt{2-2\cos\beta} - ah\beta \\
&= ah\beta\left(\sqrt{1-\frac{\beta^2}{12}+\mathcal{O}(\beta^4)} - 1\right) \\
&= ah\beta\frac{-\frac{\beta^2}{12}+\mathcal{O}(\beta^4)}{\sqrt{1-\frac{\beta^2}{12}+\mathcal{O}(\beta^4)}+1} \\
&= O\left(h\beta^3\right).
\end{aligned}$$

Hence our estimate on the local level is quite reasonable.

We now consider the sum of the patches as an estimate of the surface area of the entire curved side of the cylinder. The actual area is simply $A_{act} = 2\pi aH$. Now there are $\dfrac{2\pi}{\beta}$ triangles in a slice of height h, and there are $\dfrac{H}{h}$ slices. Therefore the estimated total area is $A_{est} = \dfrac{2\pi}{\beta}\dfrac{H}{h}ah\sqrt{2-2\cos\beta}$. Subtracting these total areas and again utilizing Taylor series, we have

$$\begin{aligned}
\Delta A &= A_{act} - A_{est} \\
&= 2\pi aH - \frac{2\pi aH}{\beta}\sqrt{2-2\cos\beta} \\
&= O\left(\beta^2\right).
\end{aligned}$$

Thus our approximation is second order and again quite reasonable.

For a sphere, we consider an isosceles triangle for simplicity. Consider the two patches below, both of which have the same vertices. In spherical coordinates (ρ,θ,ϕ) these ver-

www.manaraa.com

tices are $(r,0,0)$, $(r,0,\beta)$, and (r,α,β), where r is the radius of the sphere, α is the angle spanned by the base of the patch, and β is angle from the z-axis to the base of the triangle. In rectangular coordinates the vertices are $(0,0,r)$, $(r\sin\beta,0,r\cos\beta)$, and $(r\sin\beta\cos\alpha, r\sin\beta\sin\alpha, r\cos\beta)$. Both α and β are small.

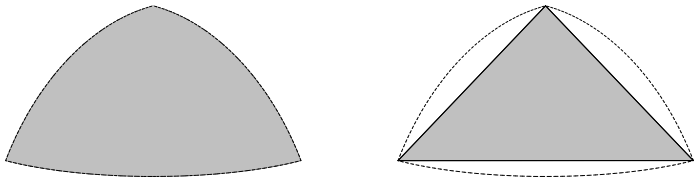

The area of the flat triangular patch is one half the magnitude of the cross product of two of the edge vectors. Thus

$$\begin{aligned}
A_{est} =& \frac{1}{2} \parallel (r\sin\beta, 0, r(\cos\beta - 1) \times (r\sin\beta\,(\cos\alpha - 1), r\sin\beta\sin\alpha, 0) \parallel \\
=& \frac{1}{2}\sqrt{r^4\sin^2\beta\sin^2\alpha(\cos\beta-1)^2 + r^4\sin^2\beta(\cos\alpha-1)^2(\cos\beta-1)^2 + r^4\sin^2\beta\sin^2\alpha} \\
=& \frac{1}{2}\,r^2\sin\beta\sqrt{(1-\cos\alpha)^2(1-\cos\beta)^2 + 2\sin^2\alpha\,(1-\cos\beta)}.
\end{aligned}$$

The actual area of the patch on the sphere is $A_{act} = r^2\alpha(1-\cos\beta)$, which can be found by integration. Subtracting the areas and utilizing Taylor series, we have

$$\begin{aligned}
\Delta A &= A_{act} - A_{est} \\
&= \frac{1}{2}\,r^2\sin\beta\sqrt{(1-\cos\alpha)^2(1-\cos\beta)^2 + 2\sin^2\alpha\,(1-\cos\beta)} - r^2\alpha(1-\cos\beta) \\
&= O(\alpha^n\beta^m).
\end{aligned}$$

where $n+m=5$. Our estimate is again quite reasonable.

Comparing the total area, we make the assumption that $\dfrac{4\pi r^2}{r^2\alpha(1-\cos\beta)}$, which is the surface area of a sphere divided by the actual area of a patch, triangular patches cover the sphere. Then

$$\begin{aligned}
\Delta A &= A_{act} - A_{est} \\
&= 4\pi r^2 - \frac{4\pi r^2}{r^2\alpha(1-\cos\beta)}\,\frac{1}{2}\,r^2\sin\beta\sqrt{(1-\cos\alpha)^2(1-\cos\beta)^2 + 2\sin^2\alpha\,(1-\cos\beta)} \\
&= O(\alpha^2) + O(\beta^2).
\end{aligned}$$

Hence the area of a sphere can be reasonably approximated by triangular patches.

www.manaraa.com

3.4 Volume Estimates

Volume estimates are not necessary for any part of the scheme, but as volume must be preserved, finding a way to accurately measure the volume of particles serves as a way to validate the scheme. How we estimate volume is specific to each type of surface.

3.4.1 Ellipsoid

Approximating generally ellipsoidal surfaces is perhaps the most straightforward. We first calculate the centroid of a (single) particle enclosed by a surface by taking the average over all nodes. Recall that the volume of a prism formed by connecting four nodes is $|(A \times B) \cdot C|$ where A, B, and C are any three vectors formed by the four nodes [41]. For each node we form four such prisms using the subdivision points and the centroid. Finally we sum over all prisms to estimate the volume. Notice that this is an underestimate.

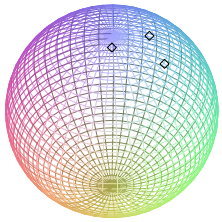

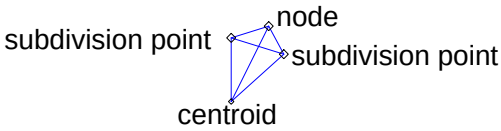

The chart below shows how error in volume relates to mesh size with respect to the unit sphere.

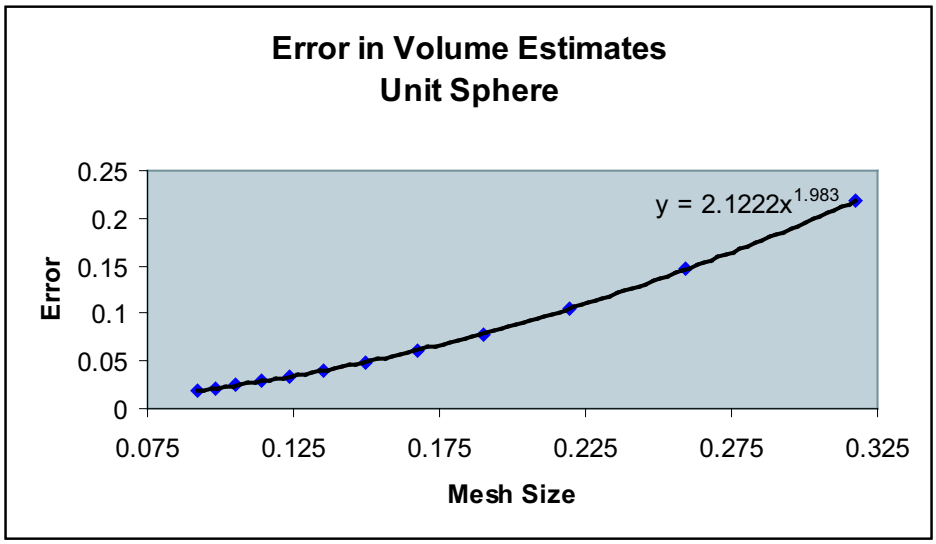

www.manaraa.com

The error is inversely proportional to the square of the mesh size.

3.4.2 Torus

The torus estimate utilizes Pappus' Theorem [41], which states that the volume of a solid of revolution is the area of a cross section multiplied by the distance the centroid of the cross section is revolved. Note that the volume estimate is valid only for axially symmetric objects, so we have no volume estimate for distorted torii. Such a scheme is an area for further investigation. We choose one radial slice of the discretized torus and find the centroid C of the slice by taking the average of its nodes. The area A of the slice is approximated by joining the centroid to the nodes on the perimeter to form triangles and then summing the area of these triangles. We find the area of a triangle with sides $\vec{P}$ and $\vec{Q}$ by $\frac{1}{2}\|\vec{P} \times \vec{Q}\|$. Then the estimated volume is $2\pi\|C\|A$ for a torus centered at the origin.

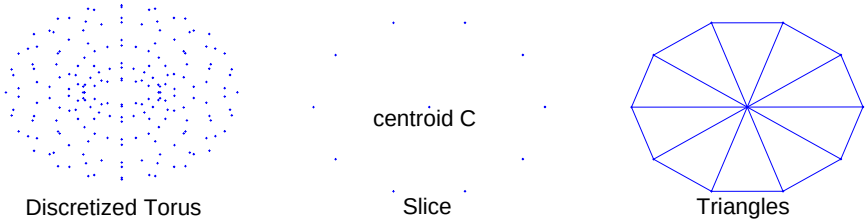

We have the following numerical results for a torus with large radius 2 and small radius 1.

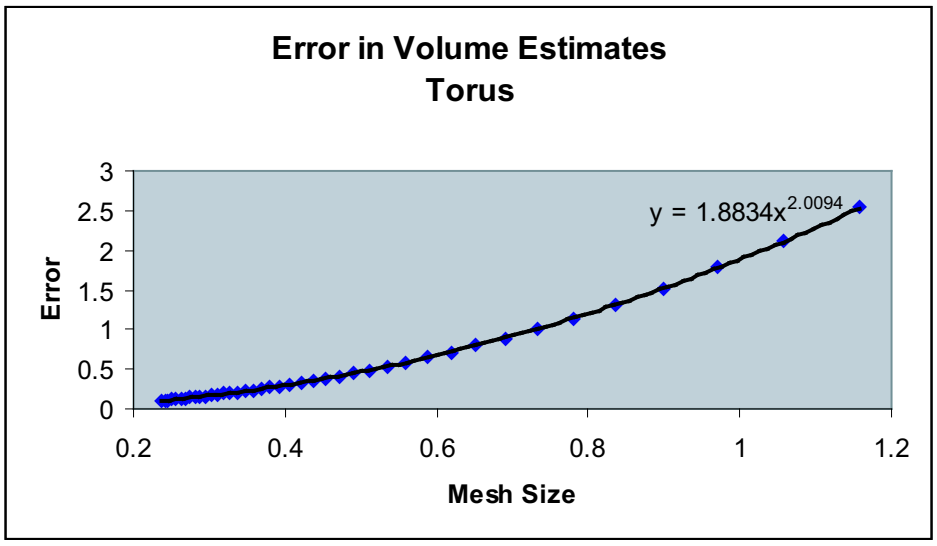

The error shows similar behavior to that of the sphere's error.

www.manaraa.com

3.5 Best Fit Surface and Outward Normal

Given a node and its 8 nearest neighbors, we need a surface so that we can approximate mean curvature and the outward normal at that node. Instead of a surface that goes through all 9 nodes, we use the surface of the form $z = Ax + By + Cx^2 + Dxy + Ey^2$ that best fits the nodes. As shown in [45], through an iterative process we find the coefficients A, B, C, D, and E that minimize the vertical distance between the surface and the nodes and so that the outward unit normal n lies on the z-axis.

The first step is to translate the nodes so that the center node is the origin. Next we choose a coordinate axis so that the nodes will lie on the graph of a function, i.e., we make sure no node is directly above another. There are many ways to do this. We explain first a simple choice, which later on we modify to speed up convergence. Let the basis for the x-axis to be the unit vector passing through the first neighbor. Denoting the i^{th} neighbor as (x_i, y_i, z_i), the vector is

$$\frac{(x_1, y_1, z_1)}{\sqrt{x_1^2 + y_1^2 + z_1^2}}$$

The basis for the z-axis is found by taking the cross product of the vectors passing from the origin to the first and third neighbors and normalizing the result. Thus the vector is

$$\frac{(x_1, y_1, z_1) \times (x_3, y_3, z_3)}{\|(x_1, y_1, z_1) \times (x_3, y_3, z_3)\|}$$

The y-axis is simply the cross product of the other two basis vectors.

To find the best fit surface, we minimize

$$F(A, B, C, D, E) = \sum_{i=1}^{8} \frac{(Ax_i + By_i + Cx_i^2 + Dx_iy_i + Ey_i^2 - z_i)^2}{x_i^2 + y_i^2 + z_i^2}$$

where (x_i, y_i, z_i) is now the i^{th} neighbor in the current coordinate system. The $x_i^2 + y_i^2 + z_i^2$ in the denominator serves to weight nearby nodes more heavily. Thus we need A, B, C, D, and E to satisfy

$$\frac{\partial F}{\partial A} = \sum_{i=1}^{8} \frac{2x_i(Ax_i + By_i + Cx_i^2 + Dx_iy_i + Ey_i^2 - z_i)}{x_i^2 + y_i^2 + z_i^2} = 0$$

$$\frac{\partial F}{\partial B} = \sum_{i=1}^{8} \frac{2y_i(Ax_i + By_i + Cx_i^2 + Dx_iy_i + Ey_i^2 - z_i)}{x_i^2 + y_i^2 + z_i^2} = 0$$

www.manaraa.com

$$\frac{\partial F}{\partial C} = \sum_{i=1}^{8} \frac{2x_i^2(Ax_i + By_i + Cx_i^2 + Dx_iy_i + Ey_i^2 - z_i)}{x_i^2 + y_i^2 + z_i^2} = 0$$

$$\frac{\partial F}{\partial D} = \sum_{i=1}^{8} \frac{2x_iy_i(Ax_i + By_i + Cx_i^2 + Dx_iy_i + Ey_i^2 - z_i)}{x_i^2 + y_i^2 + z_i^2} = 0$$

$$\frac{\partial F}{\partial E} = \sum_{i=1}^{8} \frac{2y_i^2(Ax_i + By_i + Cx_i^2 + Dx_iy_i + Ey_i^2 - z_i)}{x_i^2 + y_i^2 + z_i^2} = 0$$

Equivalently we need to solve the following system of linear equations, where $\|\mathbf{x}_i\|^2$ denotes $x_i^2 + y_i^2 + z_i^2$:

$$\begin{bmatrix} \sum_{i=1}^{8} \frac{x_i^2}{\|\mathbf{x}_i\|^2} & \sum_{i=1}^{8} \frac{x_iy_i}{\|\mathbf{x}_i\|^2} & \sum_{i=1}^{8} \frac{x_i^3}{\|\mathbf{x}_i\|^2} & \sum_{i=1}^{8} \frac{x_i^2y_i}{\|\mathbf{x}_i\|^2} & \sum_{i=1}^{8} \frac{x_iy_i^2}{\|\mathbf{x}_i\|^2} \\ \sum_{i=1}^{8} \frac{x_iy_i}{\|\mathbf{x}_i\|^2} & \sum_{i=1}^{8} \frac{y_i^2}{\|\mathbf{x}_i\|^2} & \sum_{i=1}^{8} \frac{x_i^2y_i}{\|\mathbf{x}_i\|^2} & \sum_{i=1}^{8} \frac{x_iy_i^2}{\|\mathbf{x}_i\|^2} & \sum_{i=1}^{8} \frac{y_i^3}{\|\mathbf{x}_i\|^2} \\ \sum_{i=1}^{8} \frac{x_i^3}{\|\mathbf{x}_i\|^2} & \sum_{i=1}^{8} \frac{x_i^2y_i}{\|\mathbf{x}_i\|^2} & \sum_{i=1}^{8} \frac{x_i^4}{\|\mathbf{x}_i\|^2} & \sum_{i=1}^{8} \frac{x_i^3y_i}{\|\mathbf{x}_i\|^2} & \sum_{i=1}^{8} \frac{x_i^2y_i^2}{\|\mathbf{x}_i\|^2} \\ \sum_{i=1}^{8} \frac{x_i^2y_i}{\|\mathbf{x}_i\|^2} & \sum_{i=1}^{8} \frac{x_iy_i^2}{\|\mathbf{x}_i\|^2} & \sum_{i=1}^{8} \frac{x_i^3y_i}{\|\mathbf{x}_i\|^2} & \sum_{i=1}^{8} \frac{x_i^2y_i^2}{\|\mathbf{x}_i\|^2} & \sum_{i=1}^{8} \frac{x_iy_i^3}{\|\mathbf{x}_i\|^2} \\ \sum_{i=1}^{8} \frac{x_iy_i^2}{\|\mathbf{x}_i\|^2} & \sum_{i=1}^{8} \frac{y_i^3}{\|\mathbf{x}_i\|^2} & \sum_{i=1}^{8} \frac{x_i^2y_i^2}{\|\mathbf{x}_i\|^2} & \sum_{i=1}^{8} \frac{x_iy_i^3}{\|\mathbf{x}_i\|^2} & \sum_{i=1}^{8} \frac{y_i^4}{\|\mathbf{x}_i\|^2} \end{bmatrix} \begin{bmatrix} A \\ B \\ C \\ D \\ E \end{bmatrix} = \begin{bmatrix} \sum_{i=1}^{8} \frac{x_iz_i}{\|\mathbf{x}_i\|^2} \\ \sum_{i=1}^{8} \frac{y_iz_i}{\|\mathbf{x}_i\|^2} \\ \sum_{i=1}^{8} \frac{x_i^2z_i}{\|\mathbf{x}_i\|^2} \\ \sum_{i=1}^{8} \frac{x_iy_iz_i}{\|\mathbf{x}_i\|^2} \\ \sum_{i=1}^{8} \frac{y_i^2z_i}{\|\mathbf{x}_i\|^2} \end{bmatrix}$$

In order to have a unique solution $[A\,B\,C\,D\,E]^T$, the determinant of the coefficient matrix must be nonzero. It is sufficient to show the matrix is positive definite [23]. Again we use the convenient notation $\|\mathbf{x}_i\| = \sqrt{x_i^2 + y_i^2 + z_i^2}$. But the coefficient matrix is the product of a matrix and its transpose, as shown below.

$$\begin{bmatrix} \frac{x_1}{\|\mathbf{x}_1\|} & \frac{x_2}{\|\mathbf{x}_2\|} & \frac{x_3}{\|\mathbf{x}_3\|} & \frac{x_4}{\|\mathbf{x}_4\|} & \frac{x_5}{\|\mathbf{x}_5\|} & \frac{x_6}{\|\mathbf{x}_6\|} & \frac{x_7}{\|\mathbf{x}_7\|} & \frac{x_8}{\|\mathbf{x}_8\|} \\ \frac{y_1}{\|\mathbf{x}_1\|} & \frac{y_2}{\|\mathbf{x}_2\|} & \frac{y_3}{\|\mathbf{x}_3\|} & \frac{y_4}{\|\mathbf{x}_4\|} & \frac{y_5}{\|\mathbf{x}_5\|} & \frac{y_6}{\|\mathbf{x}_6\|} & \frac{y_7}{\|\mathbf{x}_7\|} & \frac{y_8}{\|\mathbf{x}_8\|} \\ \frac{x_1^2}{\|\mathbf{x}_1\|} & \frac{x_2^2}{\|\mathbf{x}_2\|} & \frac{x_3^2}{\|\mathbf{x}_3\|} & \frac{x_4^2}{\|\mathbf{x}_4\|} & \frac{x_5^2}{\|\mathbf{x}_5\|} & \frac{x_6^2}{\|\mathbf{x}_6\|} & \frac{x_7^2}{\|\mathbf{x}_7\|} & \frac{x_8^2}{\|\mathbf{x}_8\|} \\ \frac{x_1y_1}{\|\mathbf{x}_1\|} & \frac{x_2y_2}{\|\mathbf{x}_2\|} & \frac{x_3y_3}{\|\mathbf{x}_3\|} & \frac{x_4y_4}{\|\mathbf{x}_4\|} & \frac{x_5y_5}{\|\mathbf{x}_5\|} & \frac{x_6y_6}{\|\mathbf{x}_6\|} & \frac{x_7y_7}{\|\mathbf{x}_7\|} & \frac{x_8y_8}{\|\mathbf{x}_8\|} \\ \frac{y_1^2}{\|\mathbf{x}_1\|} & \frac{y_2^2}{\|\mathbf{x}_2\|} & \frac{y_3^2}{\|\mathbf{x}_3\|} & \frac{y_4^2}{\|\mathbf{x}_4\|} & \frac{y_5^2}{\|\mathbf{x}_5\|} & \frac{y_6^2}{\|\mathbf{x}_6\|} & \frac{y_7^2}{\|\mathbf{x}_7\|} & \frac{y_8^2}{\|\mathbf{x}_8\|} \end{bmatrix} \begin{bmatrix} \frac{x_1}{\|\mathbf{x}_1\|} & \frac{y_1}{\|\mathbf{x}_1\|} & \frac{x_1^2}{\|\mathbf{x}_1\|} & \frac{x_1y_1}{\|\mathbf{x}_1\|} & \frac{y_1^2}{\|\mathbf{x}_1\|} \\ \frac{x_2}{\|\mathbf{x}_2\|} & \frac{y_2}{\|\mathbf{x}_2\|} & \frac{x_2^2}{\|\mathbf{x}_2\|} & \frac{x_2y_2}{\|\mathbf{x}_2\|} & \frac{y_2^2}{\|\mathbf{x}_2\|} \\ \frac{x_3}{\|\mathbf{x}_3\|} & \frac{y_3}{\|\mathbf{x}_3\|} & \frac{x_3^2}{\|\mathbf{x}_3\|} & \frac{x_3y_3}{\|\mathbf{x}_3\|} & \frac{y_3^2}{\|\mathbf{x}_3\|} \\ \frac{x_4}{\|\mathbf{x}_4\|} & \frac{y_4}{\|\mathbf{x}_4\|} & \frac{x_4^2}{\|\mathbf{x}_4\|} & \frac{x_4y_4}{\|\mathbf{x}_4\|} & \frac{y_4^2}{\|\mathbf{x}_4\|} \\ \frac{x_5}{\|\mathbf{x}_5\|} & \frac{y_5}{\|\mathbf{x}_5\|} & \frac{x_5^2}{\|\mathbf{x}_5\|} & \frac{x_5y_5}{\|\mathbf{x}_5\|} & \frac{y_5^2}{\|\mathbf{x}_5\|} \\ \frac{x_6}{\|\mathbf{x}_6\|} & \frac{y_6}{\|\mathbf{x}_6\|} & \frac{x_6^2}{\|\mathbf{x}_6\|} & \frac{x_6y_6}{\|\mathbf{x}_6\|} & \frac{y_6^2}{\|\mathbf{x}_6\|} \\ \frac{x_7}{\|\mathbf{x}_7\|} & \frac{y_7}{\|\mathbf{x}_7\|} & \frac{x_7^2}{\|\mathbf{x}_7\|} & \frac{x_7y_7}{\|\mathbf{x}_7\|} & \frac{y_7^2}{\|\mathbf{x}_7\|} \\ \frac{x_8}{\|\mathbf{x}_8\|} & \frac{y_8}{\|\mathbf{x}_8\|} & \frac{x_8^2}{\|\mathbf{x}_8\|} & \frac{x_8y_8}{\|\mathbf{x}_8\|} & \frac{y_8^2}{\|\mathbf{x}_8\|} \end{bmatrix}$$

Note that any matrix of the form GG^T is positive semi-definite. since $\mathbf{x}^TGG^T\mathbf{x} = (G^T\mathbf{x})^TG^T\mathbf{x} = \|G^T\mathbf{x}\|^2 \geq 0$. A matrix of this form is called a Gram matrix [23].

www.manaraa.com

To show that the coefficient matrix is positive definite, we investigate when equality holds, i.e., $G^T\mathbf{x} = 0$. Since $\mathbf{x} \neq 0$, this occurs only when the columns of G^T are linearly dependent [23]. Then there exist constants a, b, c, d, and e with at least one constant nonzero such that for $i = 1$ to 8,

$$a\,\frac{x_i}{\|\mathbf{x}_i\|} + b\,\frac{y_i}{\|\mathbf{x}_i\|} + c\,\frac{x_i^2}{\|\mathbf{x}_i\|} + d\,\frac{x_i y_i}{\|\mathbf{x}_i\|} + e\,\frac{y_i^2}{\|\mathbf{x}_i\|} = 0$$

Multiplying through by $\|\mathbf{x}_i\|$, we have that for $i = 1$ to 8,

$$a\,x_i + b\,y_i + c\,x_i^2 + d\,x_i y_i + e\,y_i^2 = 0$$

This means that we have a surface $z = ax + by + cx^2 + dxy + ey^2$ such that all of the 8 neighbor nodes lie on the xy-plane. In this case the mean curvature is simply zero.

We pause to comment on solving this system of linear equations. The coefficient matrix is symmetric, so we use *dsysv*, a library function that uses a diagonal pivoting method to factor the coefficient matrix as UDU^T where U is an upper triangular matrix and D is a symmetric block diagonal matrix. For more detail, see [3].

Now that we have a quadratic surface, we calculate the outward normal, which is needed to advance the surface in time. Since $z = Ax + By + Cx^2 + Dxy + Ey^2$ is a level surface of $f(x, y, z) = z - Ax - By - Cx^2 - Dxy - Ey^2 - z$, we calculate the gradient of f, denoted ∇f, to find the outward normal to the surface. Now $\nabla f = (-A - 2Cx - Dy)\vec{i} + (-B - Dx - 2Ey)\vec{j} + \vec{k}$ evaluated at the origin, or the central node, is $-A\vec{i} - B\vec{j} + \vec{k}$. We normalize this to get the unit vector $\dfrac{-A\vec{i} - B\vec{j} + \vec{k}}{\sqrt{1 + A^2 + B^2}}$. Our hope is that this vector lies on the positive z-axis. Given some small predetermined ϵ, we find the distance between $\dfrac{(-A, -B, 1)}{\sqrt{1 + A^2 + B^2}}$ and $(0, 0, 1)$. If the distance is less than ϵ, we are done. Otherwise we choose a new coordinate system under which $\dfrac{(-A, -B, 1)}{\sqrt{1 + A^2 + B^2}}$ becomes $(0, 0, 1)$.

The new coordinate system is not unique, as there are infinitely many choices of the unit vectors that determine the new x-axis and y-axis. For simplicity we take the new y-axis to be the unit vector along the cross product of the new z-axis and the old x-axis. Thus the new basis for the y-axis is

www.manaraa.com

$$\frac{\frac{(-A,-B,1)}{\sqrt{1+A^2+B^2}} \times (1,0,0)}{\|\frac{(-A,-B,1)}{\sqrt{1+A^2+B^2}} \times (1,0,0)\|} = \frac{(0,1,B)}{\sqrt{1+B^2}}$$

Finally we take the cross product of both of these basis vectors to get the basis vector for the new x-axis, i.e., $\frac{\frac{(-A,-B,1)}{\sqrt{1+A^2+B^2}} \times \frac{(0,1,B)}{\sqrt{1+B^2}}}{\|\frac{(-A,-B,1)}{\sqrt{1+A^2+B^2}} \times \frac{(0,1,B)}{\sqrt{1+B^2}}\|} = \frac{(1+B^2,-AB,A)}{\sqrt{(1+A^2+B^2)(1+B^2)}}$

Using these we can find the change of basis matrix, which is the inverse of the 3×3 matrix having the basis vectors as columns, i.e.,

$$\begin{bmatrix} \frac{1+B^2}{\sqrt{(1+A^2+B^2)(1+B^2)}} & 0 & \frac{-A}{\sqrt{1+A^2+B^2}} \\ \frac{-AB}{\sqrt{(1+A^2+B^2)(1+B^2)}} & \frac{1}{\sqrt{1+B^2}} & \frac{-B}{\sqrt{1+A^2+B^2}} \\ \frac{A}{\sqrt{(1+A^2+B^2)(1+B^2)}} & \frac{B}{\sqrt{1+B^2}} & \frac{1}{\sqrt{1+A^2+B^2}} \end{bmatrix}^{-1}$$

We now multiply each of the 8 neighbor nodes by the change of basis matrix and begin the process of finding A, B, C, D, and E in the new coordinate system. The iterative scheme continues until the outward unit normal to the surface at the origin, $\frac{(-A,-B,1)}{\sqrt{1+A^2+B^2}}$, is within ϵ of $(1,0,0)$ in the current coordinate system. In practice this usually takes about 3 iterations using $\epsilon = 0.0001$. We also set the number of maximum iterations to 50 to prevent infinite looping. Infinite looping will occur in some circumstances, such as when neighbors differ greatly in absolute value. Using $N = 5$ and $M = 80$ when discretizing a torus with large radius 2 and small radius 1 gives rise to this problem. However, using discretizations with nodes fairly evenly spaced is a simple antidote. An area of future study is determining conditions that guarantee convergence.

Below is a node and its eight neighbors and a quadratic surface through those nodes. Also shown is the outward normal, which lies along the z-axis.

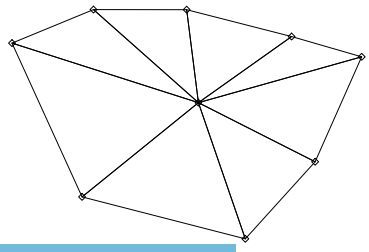

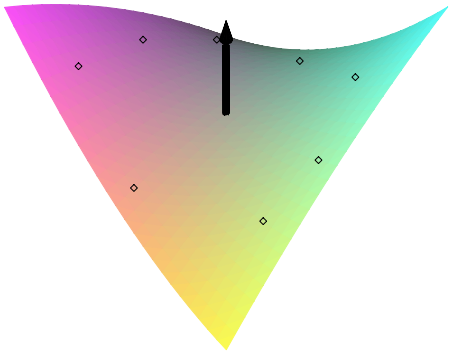

www.manaraa.com

We also look at the error in the outward normal estimates for the unit sphere and a torus with large radius 2 and small radius 1. To find the error, for each node we subtract the estimated and actual normals and find the norm of the result. The average of this norm over all the nodes is the error value used in the charts below.

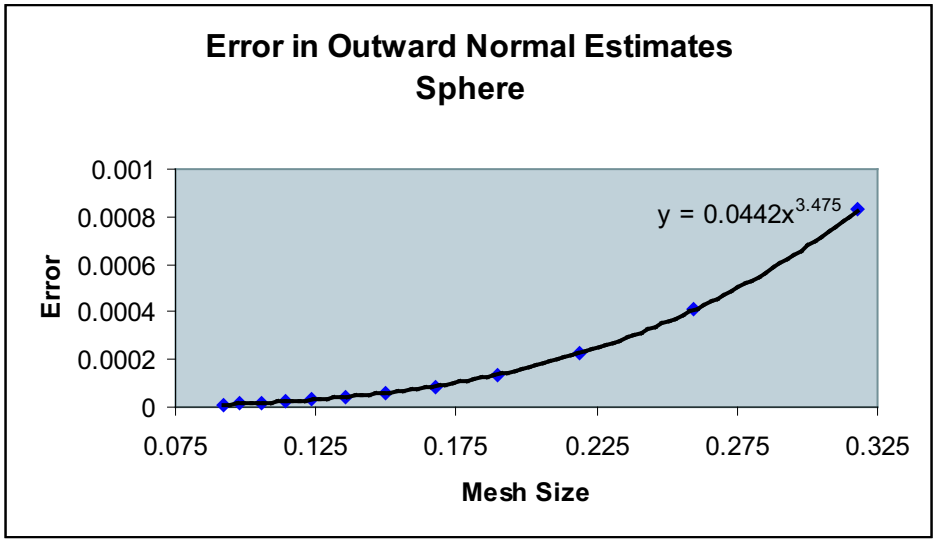

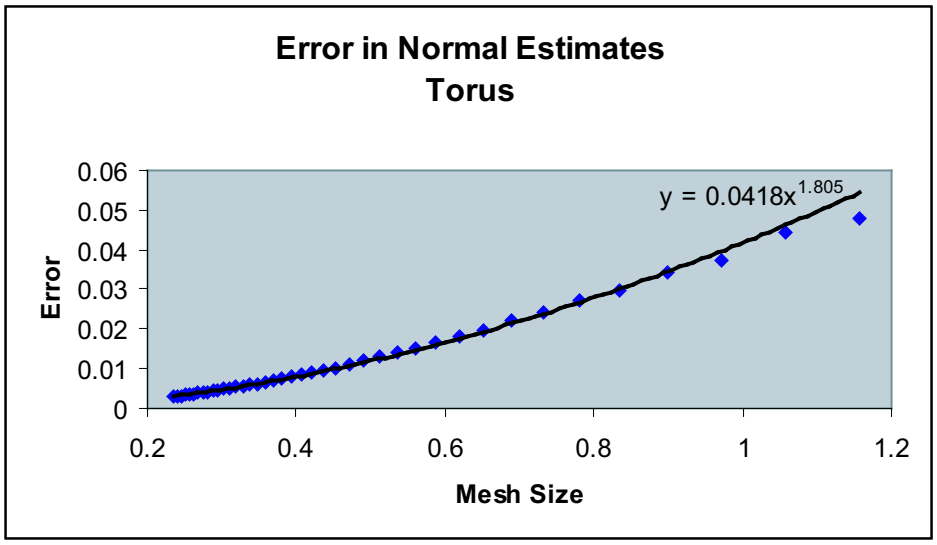

The sphere has extraordinarily good results, but the torus has room for improvement, though the results are acceptable.

www.manaraa.com

3.5.1 Mean Curvature

The mean curvature plays a large part in the Mullins-Sekerka problem as surfaces have a higher normal velocity where the mean curvature is high.

The mean curvature, denoted here as κ, is the average of the principal curvatures, or $\frac{1}{n}\ \mathrm{div}\left(\frac{Du}{\left(1+|Du|^2\right)^{\frac{1}{2}}}\right)$ where $u : \mathbf{R}^n \to \mathbf{R}$ [20]. We choose the convention that the mean curvature of a sphere is negative. By way of example, the mean curvature of a sphere is the negative reciprocal of its radius, and the mean curvature of a plane is 0. A saddle can also have zero mean curvature. For the surface $z = Ax + By + Cx^2 + Dxy + Ey^2$, the mean curvature is

$$\begin{aligned}
\kappa &= \frac{1}{2}\left(\frac{A+2Cx+Dy}{\left(1+\left|(A+2Cx+Dy)\vec{\mathbf{i}}+(B+Dx+2Ey)\vec{j}\right|^2\right)^{\frac{1}{2}}}\right)_x \\
&\quad +\frac{1}{2}\left(\frac{B+Dx+2Ey}{\left(1+\left|(A+2Cx+Dy)\vec{i}+(B+Dx+2Ey)\vec{j}\right|^2\right)^{\frac{1}{2}}}\right)_y \\
&= \frac{1}{2}\left(\frac{2C\left(1+\left|(A+2Cx+Dy)\vec{\mathbf{i}}+(B+Dx+2Ey)\vec{j}\right|^2\right)}{\left(1+\left|(A+2Cx+Dy)\vec{\mathbf{i}}+(B+Dx+2Ey)\vec{j}\right|^2\right)^{\frac{3}{2}}}\right. \\
&\quad \frac{-\frac{1}{2}(A+2Cx+Dy)\left(4C(A+2Cx+Dy)+2D(B+Dx+2Ey)\right)}{\left(1+\left|(A+2Cx+Dy)\vec{\mathbf{i}}+(B+Dx+2Ey)\vec{j}\right|^2\right)^{\frac{3}{2}}} \\
&\quad +\frac{2E\left(1+\left|(A+2Cx+Dy)\vec{\mathbf{i}}+(B+Dx+2Ey)\vec{j}\right|^2\right)}{\left(1+\left|(A+2Cx+Dy)\vec{\mathbf{i}}+(B+Dx+2Ey)\vec{j}\right|^2\right)^{\frac{3}{2}}} \\
&\quad \left.\frac{-\frac{1}{2}(B+Dx+2Ey)\left(2D(A+2Cx+Dy)+4E(B+Dx+2Ey)\right)}{\left(1+\left|(A+2Cx+Dy)\vec{\mathbf{i}}+(B+Dx+2Ey)\vec{j}\right|^2\right)^{\frac{3}{2}}}\right).
\end{aligned}$$

Evaluating this at the point $(0,0)$ gives us

www.manaraa.com

$$
\begin{aligned}
\kappa &= \frac{1}{2}\left(\frac{2C\left(1+A^2+B^2\right)-\frac{1}{2}A\left(4CA+2DB\right)}{\left(1+A^2+B^2\right)^{\frac{3}{2}}}\right. \\
&\quad \left.+\frac{2E\left(1+A^2+B^2\right)-\frac{1}{2}B\left(2DA+4EB\right)}{\left(1+A^2+B^2\right)^{\frac{3}{2}}}\right) \\
&= \frac{\left(C+E\right)\left(1+A^2+B^2\right)-\left(CA^2+EB^2+ADB\right)}{\left(1+A^2+B^2\right)^{\frac{3}{2}}} \\
&= \frac{C+E+EA^2+CB^2-ADB}{\left(1+A^2+B^2\right)^{\frac{3}{2}}}.
\end{aligned}
$$

Note that mean curvature is independent of coordinate system [37] up to a sign.

Below are the error charts for mean curvature. Again we use the unit sphere and a torus with large radius 2 and small radius 1.

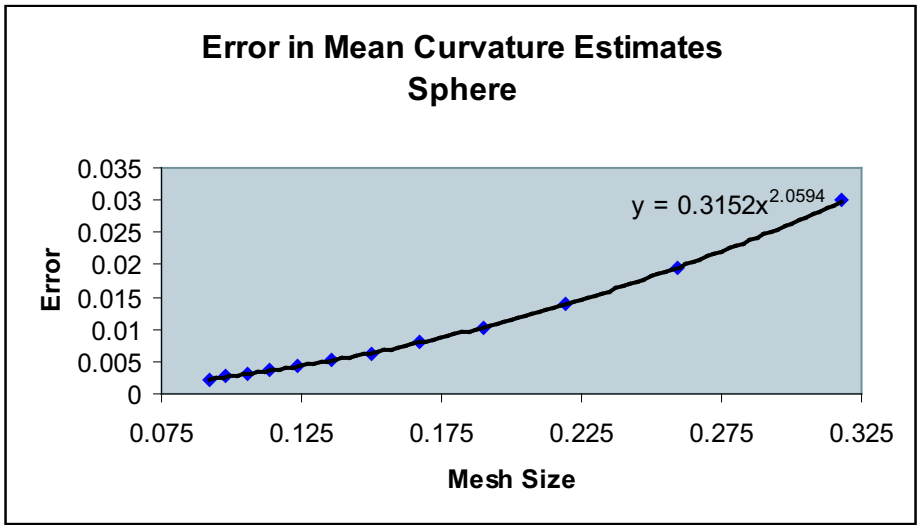

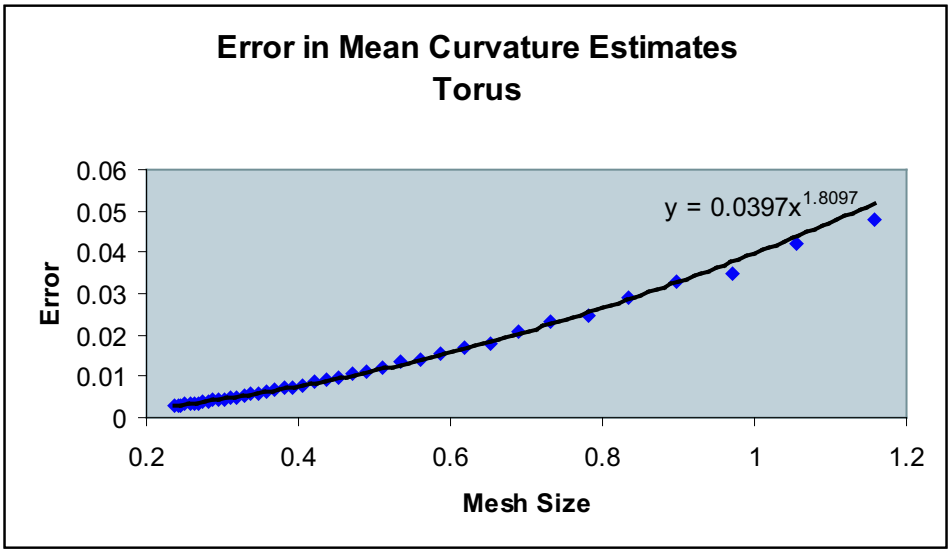

www.manaraa.com

The torus does not perform as well as the sphere. Finding out why is an area of further work

3.5.2 Choice of Initial Coordinate System in Best Fit Surface Scheme

We now analyze the effects of changes in the choice of initial coordinate axes in the iterative process of finding the best fit quadratic surface through a node and its eight nearest neighbors (see 3.5).

We label the node's neighbors as $\{\mathbf{x_i}\}$, $i = 1..8$, once they have been translated so that the node is located at the origin. Recall the initial z-axis is in the direction of $\mathbf{x_1} \times \mathbf{x_3}$, i.e., the cross product of the 1st and 3rd neighbor. The x-axis is simply the first neighbor $\mathbf{x_1}$ normalized. The y-axis is the cross product of the x and z axes.

What happens if the z-axis is chosen differently? The table below shows how the values of A, B, C, D, and E in the quadratic surface $z = Ax + By + Cx^2 + Dxy + Ey^2$ change. We use the selected node $(0.59614731, 0.39251667, 0.70038493)$ on the unit sphere discretized with 420 nodes.

z-axis Direction	A	B	C	D	E
$\mathbf{x_1} \times \mathbf{x_3}$	-1.3e-08	4.0e-08	-0.5078	0.0104	-0.5068
$\mathbf{x_2} \times \mathbf{x_4}$	1.9e-07	-8.0e-09	-0.5121	0.0039	-0.5025
$\mathbf{x_3} \times \mathbf{x_5}$	1.3e-07	5.7e-08	-0.5114	-0.0065	-0.5032
$\mathbf{x_4} \times \mathbf{x_6}$	4.3e-08	2.3e-07	-0.5026	-0.0044	-0.5120
$\mathbf{x_5} \times \mathbf{x_7}$	3.9e-08	3.7e-08	-0.5120	0.0046	-0.5026
$\mathbf{x_6} \times \mathbf{x_8}$	2.4e-07	4.3e-08	-0.5125	-0.0008	-0.5021
$\mathbf{x_7} \times \mathbf{x_1}$	1.1e-07	7.3e-08	-0.5092	-0.0097	-0.5054
$\mathbf{x_8} \times \mathbf{x_2}$	4.1e-08	2.2e-07	-0.5026	-0.0044	-0.5120

The values vary, although A and B approach zero and the others are within a hundredth of each other. This means that even if we start with nodes lying on a quadratic surface we are unlikely to get the same coefficients we began with.

The next table shows the effect of different initial coordinate systems on the mean curvature and normal. The actual mean curvature is -1 and the actual normal is the node itself, $(0.59614731, 0.39251667, 0.70038493)$. Note, however, that the table below is evaluat-

www.manaraa.com

ing how results change with choice of axis, not closeness to the actual values. To improve the estimates for mean curvature and normals, we decrease mesh size, as shown in previous sections. We are looking instead at consistency of error with regard to changing the direction of the z-axis. Here the error is the weighted error between the actual z values of the nodes and the z values that lie on the surface $z = Ax + By + Cx^2 + Dxy + Ey^2$, i.e., $F(A, B, C, D, E) = \sum_{i=1}^{8} \frac{(Ax_i + By_i + Cx_i^2 + Dx_iy_i + Ey_i^2 - z_i)^2}{x_i^2 + y_i^2 + z_i^2}$.

z-axis Direction	Mean Curvature	Error	Normal
$\mathbf{x_1} \times \mathbf{x_3}$	-1.0145942409	5.8e-06	(0.59608416,0.39268448,0.70034461)
$\mathbf{x_2} \times \mathbf{x_4}$	-1.0145942424	5.8e-06	(0.59608433,0.39268437,0.70034453)
$\mathbf{x_3} \times \mathbf{x_5}$	-1.0145942423	5.8e-06	(0.59608429,0.39268438,0.70034456)
$\mathbf{x_4} \times \mathbf{x_6}$	-1.0145942430	5.8e-06	(0.59608435,0.39268433,0.70034453)
$\mathbf{x_5} \times \mathbf{x_7}$	-1.0145942419	5.8e-06	(0.59608415,0.39268443,0.70034465)
$\mathbf{x_6} \times \mathbf{x_8}$	-1.0145942402	5.8e-06	(0.59608399,0.39268455,0.70034472)
$\mathbf{x_7} \times \mathbf{x_1}$	-1.0145942405	5.8e-06	(0.59608408,0.39268451,0.70034466)
$\mathbf{x_8} \times \mathbf{x_2}$	-1.0145942400	5.8e-06	(0.59608402,0.39268455,0.70034469)

Notice that the mean curvature, normal, and the weighted error are consistent with at least six places beyond the decimal point; only the coefficients A, B, C, D, and E of our surface $z = Ax + By + Cx^2 + Dxy + Ey^2$ change. We do not show it here, but the number of iterations needed for the scheme to converge is also consistence. We can reasonably trust that the initial choice of axes is arbitrary as long as no nodes lie on a vertical line, i.e., the nodes lie on a well-defined surface.

However, choosing the initial z-axis to be in the direction of the average of the normalized cross products $\mathbf{x_1} \times \mathbf{x_3}$, $\mathbf{x_3} \times \mathbf{x_5}$, $\mathbf{x_5} \times \mathbf{x_7}$, and $\mathbf{x_7} \times \mathbf{x_1}$ has the effect of reducing the number of iterations required by about one. Hence we choose the normalized average to be the z-axis.

3.5.3 Iteration Limit in Outward Normal Scheme

Now we look at the effects of changing ϵ, the distance the normals must be within each other for the iterative process to stop. Should convergence fail, the iterative process is stopped at 50 iterations to prevent infinite looping. We again use the node $(0.59614731, 0.39251667, 0.70038493)$ on the unit sphere discretized with 420 nodes.

www.manaraa.com

ϵ	Iterations to Converge	Mean Curvature	Surface Error	A	B
1.0e-01	1	-1.0146444129694545	0.0011	-0.017	0.00033
1.0e-02	2	-1.0145940896106787	6.8e-06	0.00046	-0.00012
1.0e-03	2	-1.0145940896106787	6.8e-06	0.00046	-0.00012
1.0e-04	3	-1.0145942069966092	5.8e-06	-1.4e-05	6.1e-06
1.0e-05	4	-1.0145942433475457	5.8e-06	4.2e-07	-2.4e-07
1.0e-06	4	-1.0145942433475457	5.8e-06	4.2e-07	-2.4e-07
1.0e-07	5	-1.0145942413807711	5.8e-06	-1.3e-08	8.9e-09
1.0e-08	6	-1.0145942414606859	5.8e-06	4.3e-10	-3.1e-10
1.0e-09	6	-1.0145942414606859	5.8e-06	4.3e-10	-3.1e-10
1.0e-10	7	-1.0145942414577487	5.8e-06	-1.4e-11	1.1e-11
1.0e-11	8	-1.0145942414578522	5.8e-06	4.7e-13	-3.6e-13
1.0e-12	8	-1.0145942414578522	5.8e-06	4.7e-13	-3.6e-13
1.0e-13	9	-1.0145942414578486	5.8e-06	-1.6e-14	1.2e-14
1.0e-14	10	-1.0145942414578486	5.8e-06	4.8e-16	-4.3e-16
1.0e-15	10	-1.0145942414578486	5.8e-06	4.8e-16	-4.3e-16
1.0e-16	11	-1.0145942414578482	5.8e-06	-6.8e-18	-7.8e-18
1.0e-17	17	-1.0145942414578482	5.8e-06	-2.4e-18	7.6e-18
1.0e-18	50	-1.0145942414578486	5.8e-06	-1.9e-17	-2.4e-18

Although we do not show it here, the normal and coefficients C, D, and E show the same pattern in relation to ϵ as the mean curvature, namely they gradually agree to more and more decimal places. Notice that the surface error stops decreasing. The author conjectures this is because the neighbors lie on a sphere, which cannot be fitted exactly to a quadratic surface in general. Future work includes testing this hypothesis, by using nodes lying on a quadratic surface to see if the error continues decreasing as ϵ decreases.

We conclude that reasonable precision is obtained for $\epsilon = 0.0001$. The last value of ϵ, 10^{-18} is beyond the truncation limits of the computer and presumably is considered 0. Hence the normals never come within ϵ of each other and the iterative process stops when the maximum number of iterations, 50, is reached.

www.manaraa.com

3.6 Integral

3.7 Integral Equations

We now need to solve for the normal velocity V, and the constant c. We have the following system of integral equations to discretize:

$$\begin{aligned} K(x) &= \frac{1}{4\pi}\int_\Gamma \frac{1}{|x-y|}\, V(y)dS_y + c \\ 0 &= \int_\Gamma V(y)dS_y. \end{aligned}$$

We do this by considering the normal velocity V and mean curvature κ to be constant on each of the patches comprising the surface, i.e., we are using a piecewise constant discretization. Let N be the total number of nodes on our discretized surfaces and let $\mathbf{x}_i$ denote the i^{th} node. Note that N is not the same as that used to discretize the torus. Similarly, we denote as κ_i and V_i the mean curvature and normal velocity, respectively, of the surface at $\mathbf{x}_i$. The area of the patch surrounding $\mathbf{x}_i$, really the sum of four triangular patches, is denoted $\Delta_i = \Delta_{i_1} + \Delta_{i_2} + \Delta_{i_3} + \Delta_{i_4}$. Occasionally we abuse notation and use Δ_i to denote the surface rather than its area, but the meaning should be clear from the context.

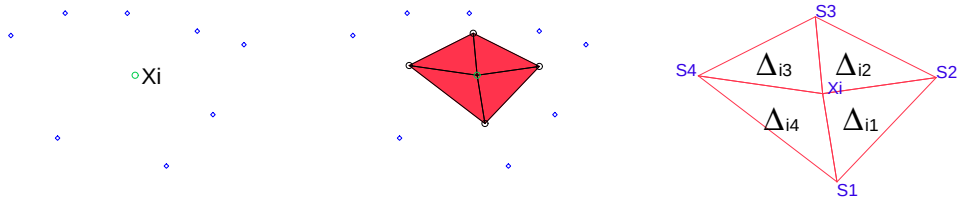

Node and 8 Neighbors Triangular Patches Notation

Then we want to solve the following for $\{V_i\}_{i=1..N}$ and c', where $c' = 4\pi c$.

$$\begin{aligned} 4\pi\kappa_i &= \sum_{j=1}^{i-1} V_j \int_{\Delta_j} \frac{1}{|x_i - y|} dS_y + \int_{\Delta_i} \frac{V_i}{|\mathbf{x}_i - \mathbf{y}|} dS_y + \sum_{j=i+1}^{N} V_j \int_{\Delta_j} \frac{1}{|x_i - y|} dS_y + c' \\ 0 &= \sum_{j=1}^{N} V_j \Delta_j. \end{aligned}$$

We have $N+1$ unknowns and $N+1$ linear equations.

To estimate

www.manaraa.com

$$\int_{\Delta_j} \frac{1}{|x_i - y|} dS_y = \int_{\Delta_{j_1}} \frac{1}{|x_i - y|} dS_y + \int_{\Delta_{j_2}} \frac{1}{|x_i - y|} dS_y + \int_{\Delta_{j_3}} \frac{1}{|x_i - y|} dS_y + \int_{\Delta_{j_4}} \frac{1}{|x_i - y|} dS_y$$

we use a two dimensional version of the trapezoid rule, namely we average the value of $\frac{1}{|x_i - y|}$ on the three vertices of each triangular patch and multiply this by the area of the patch.

The center vertex of Δ_j is y_j. Denote the other vertices forming $\Delta_j = \Delta_{j_1} + \Delta_{j_2} + \Delta_{j_3} + \Delta_{j_4}$ as s_1, s_2, s_3, s_4. Then

$$\begin{aligned}
\int_{\Delta_j} \frac{1}{|x_i - y|} dS_y &= \int_{\Delta_{j_1}} \frac{1}{|x_i - y|} dS_y + \int_{\Delta_{j_2}} \frac{1}{|x_i - y|} dS_y + \int_{\Delta_{j_3}} \frac{1}{|x_i - y|} dS_y + \int_{\Delta_{j_4}} \frac{1}{|x_i - y|} dS_y \\
&\approx \frac{1}{3}\Delta_{j_1}\left(\frac{1}{|x_i - y_j|} + \frac{1}{|x_i - s_1|} + \frac{1}{|x_i - s_2|}\right) \\
&\quad + \frac{1}{3}\Delta_{j_2}\left(\frac{1}{|x_i - y_j|} + \frac{1}{|x_i - s_2|} + \frac{1}{|x_i - s_3|}\right) \\
&\quad + \frac{1}{3}\Delta_{j_3}\left(\frac{1}{|x_i - y_j|} + \frac{1}{|x_i - s_3|} + \frac{1}{|x_i - s_4|}\right) \\
&\quad + \frac{1}{3}\Delta_{j_4}\left(\frac{1}{|x_i - y_j|} + \frac{1}{|x_i - s_4|} + \frac{1}{|x_i - s_1|}\right) \\
&= \frac{1}{3}\left(\frac{\Delta_j}{|x_i - y_j|} + \frac{\Delta_{j_1} + \Delta_{j_4}}{|x_i - s_1|} + \frac{\Delta_{j_1} + \Delta_{j_2}}{|x_i - s_2|} + \frac{\Delta_{j_2} + \Delta_{j_3}}{|x_i - s_3|} + \frac{\Delta_{j_3} + \Delta_{j_4}}{|x_i - s_4|}\right)
\end{aligned}$$

Note that the last step of regrouping cuts computational time approximately in half.

We can calculate $\int_{\Delta_i} \frac{1}{|\mathbf{x}_i - \mathbf{y}|} dS_y$, which has a removable singularity, directly.

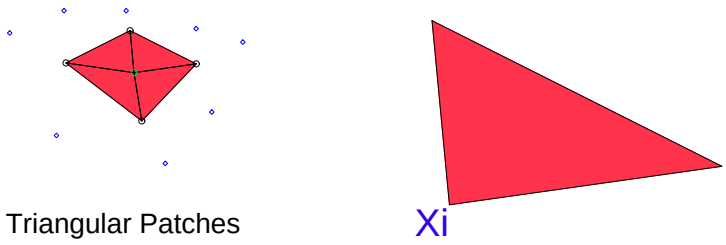

We derive an integral for each of the four triangular patches comprising Δ_i by first translating each triangle (denoted $\triangle$) so that we have the following:

www.manaraa.com

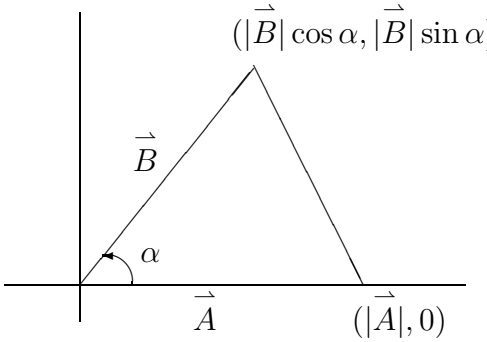

where $\cos\alpha = \dfrac{A \cdot B}{|\vec{A}||\vec{B}|}$ and $\sin\alpha = \sqrt{1-\cos^2\alpha}$. Note that $\sin\alpha$ is necessarily positive, which gives the restriction that $0 < \alpha < \pi$. Then

$$\begin{aligned}\int_{\triangle} \frac{1}{|x-z|}\, dS_z &= \int_0^{\alpha}\int_0^{f(\theta)} \frac{1}{r}\, r dr\, d\theta \\ &= \int_0^{\alpha} f(\theta) d\theta\end{aligned}$$

where $f(\theta)$ describes the line opposite α.

If the line is vertical, its equation is $x = |\vec{A}|$, which in polar coordinates is $r = \dfrac{|\vec{A}|}{\cos\theta}$. Then $\int_0^{\alpha} f(\theta)d\theta = |\vec{A}| \int_0^{\alpha} \sec\theta d\theta = |\vec{A}| \ln|\sec\alpha + \tan\alpha| = |\vec{A}| \ln\left|\frac{1+\sin\alpha}{\cos\alpha}\right|$.

If the line is not vertical, its equation is $y = \dfrac{|\vec{B}|\sin\alpha}{|\vec{B}|\cos\alpha - |\vec{A}|}\, x - \dfrac{|\vec{A}||\vec{B}|\sin\alpha}{|\vec{B}|\cos\alpha - |\vec{A}|}$ which in polar coordinates is $r = \dfrac{m|\vec{A}|}{m\cos\theta - \sin\theta}$ where $m = \dfrac{|\vec{B}|\sin\alpha}{|\vec{B}|\cos\alpha - |\vec{A}|}$ is the slope.

We now evaluate $\displaystyle\int_0^{\alpha} \frac{m|\vec{A}|}{m\cos\theta - \sin\theta}\, d\theta$. Let $\beta = \tan^{-1}(m)$. Note that $-\dfrac{\pi}{2} < \beta < \dfrac{\pi}{2}$, $\cos\beta = \dfrac{1}{\sqrt{m^2+1}}$, and $\sin\beta = \dfrac{m}{\sqrt{m^2+1}}$. Then

$$\begin{aligned} m\cos\theta - \sin\theta &= \sqrt{m^2+1}\left(\frac{m}{\sqrt{m^2+1}}\cos\theta - \frac{1}{\sqrt{m^2+1}}\sin\theta\right) \\ &= \sqrt{m^2+1}(\sin\beta\cos\theta - \cos\beta\sin\theta) \\ &= \sqrt{m^2+1}\,\sin(\beta-\theta).\end{aligned}$$

We now have $\displaystyle\int_0^{\alpha} \frac{m|\vec{A}|}{m\cos\theta - \sin\theta}\, d\theta = \frac{m|\vec{A}|}{\sqrt{m^2+1}} \int_0^{\alpha} \frac{1}{\sin(\beta-\theta)}\, d\theta.$

www.manaraa.com

Before evaluating $\int_0^\alpha \frac{1}{\sin(\beta-\theta)}\,d\theta$, we show $\beta \notin [0,\alpha]$. Suppose to the contrary that $\beta \in [0,\alpha]$. Since $\alpha \in (0,\pi)$, this implies $\sin\beta \geq 0$, which in turn requires that $m > 0$ (note that $m = 0$ is impossible because the triangular patch would have 0 area). Since $m = \dfrac{|\vec{B}|\sin\alpha}{|\vec{B}|\cos\alpha - |\vec{A}|} > 0$, we have $|\vec{B}|\cos\alpha - |\vec{A}| > 0$. Then

$$\begin{aligned}
\sqrt{m^2+1} &= \sqrt{\frac{|\vec{B}|^2\sin^2\alpha}{(|\vec{B}|\cos\alpha - |\vec{A}|)^2} + 1} \\
&= \frac{\sqrt{|\vec{B}|^2\sin^2\alpha + |\vec{B}|^2\cos^2\alpha - 2|\vec{A}|\,|\vec{B}|\cos\alpha + |\vec{A}|^2}}{|\,|\vec{B}|\cos\alpha - |\vec{A}|\,|} \\
&= \frac{\sqrt{|\vec{B}|^2 - 2|\vec{A}|\,|\vec{B}|\cos\alpha + |\vec{A}|^2}}{|\vec{B}|\cos\alpha - |\vec{A}|}
\end{aligned}$$

Now since $\beta \in [0,\alpha]$,

$$\begin{aligned}
\sin\beta \leq \sin\alpha \quad &\Leftrightarrow \quad \frac{m}{\sqrt{m^2+1}} \leq \sin\alpha \\
&\Leftrightarrow \quad \frac{|\vec{B}|\cos\alpha - |\vec{A}|}{\sqrt{|\vec{B}|^2 - 2|\vec{A}|\,|\vec{B}|\cos\alpha + |\vec{A}|^2}} \frac{|\vec{B}|\sin\alpha}{|\vec{B}|\cos\alpha - |\vec{A}|} \leq \sin\alpha \\
&\Leftrightarrow \quad |\vec{B}|^2\sin^2 \leq \sin^2\alpha(|\vec{B}|^2 - 2|\vec{A}|\,|\vec{B}|\cos\alpha + |\vec{A}|^2) \\
&\Leftrightarrow \quad \cos\alpha \leq \frac{|\vec{A}|}{2|\vec{B}|}.
\end{aligned}$$

However, since $m > 0$,

$$|\vec{A}| < |\vec{B}|\cos\alpha \Leftrightarrow \frac{|\vec{A}|}{|\vec{B}|} < \cos\alpha.$$

Then $\dfrac{|\vec{A}|}{|\vec{B}|} < \cos\alpha \leq \dfrac{|\vec{A}|}{2|\vec{B}|}$, which is impossible. Hence $\beta \notin [0,\alpha]$.

We return to the integral $\int_0^\alpha \frac{1}{\sin(\beta-\theta)}\,d\theta$. We want to show $\sin(\beta-\theta) \neq 0$. Since $0 \leq \theta \leq \alpha$, $0 < \alpha < \pi$, and $-\dfrac{\pi}{2} < \beta < \dfrac{\pi}{2}$, we have $-\dfrac{3\pi}{2} < \beta - \theta < \dfrac{\pi}{2}$. Then $\sin(\beta-\theta) =$

www.manaraa.com

$0 \Leftrightarrow \beta = \theta$. But previously we showed $\beta \neq [0, \alpha]$, so $\int_0^\alpha \frac{1}{\sin(\beta - \theta)}\, d\theta$ exists. Then

$$\begin{aligned}
\int_0^\alpha \frac{m|\vec{A}|}{m\cos\theta - \sin\theta}\, d\theta &= \frac{m|\vec{A}|}{\sqrt{m^2+1}} \int_0^\alpha \frac{1}{\sin(\beta-\theta)}\, d\theta \\
&= \frac{-m|\vec{A}|}{\sqrt{m^2+1}} \ln\left|\frac{\csc(\beta-\alpha) - \cot(\beta-\alpha)}{\csc\beta - \cot\beta}\right| \\
&= \frac{m|\vec{A}|}{\sqrt{m^2+1}} \ln\left|\frac{\sin(\beta-\alpha)(1-\cos\beta)}{\sin\beta(1-\cos(\beta-\alpha))}\right|
\end{aligned}$$

Note that $\sin\beta \neq 0$ and $1 - \cos\beta \neq 0$; otherwise $m = 0$, which is impossible. We proved previously that $\beta \neq \alpha$, so $\sin(\beta - \alpha) \neq 0$ and $1 - \cos(\beta - \alpha) \neq 0$.

We simplify further to get

$$\begin{aligned}
\int_0^\alpha \frac{m|\vec{A}|}{m\cos\theta - \sin\theta}\, d\theta &= \frac{m|\vec{A}|}{\sqrt{m^2+1}} \ln\left|\frac{\sin(\beta-\alpha)(\sqrt{m^2+1}-1)}{m(1-\cos(\beta-\alpha))}\right| \\
&= \frac{m|\vec{A}|}{\sqrt{m^2+1}} \ln\left|\frac{(\sin\beta\cos\alpha - \cos\beta\sin\alpha)(\sqrt{m^2+1}-1)}{m(1-[\cos\beta\cos\alpha + \sin\beta\sin\alpha])}\right| \\
&= \frac{m|\vec{A}|}{\sqrt{m^2+1}} \ln\left|\frac{(m\cos\alpha - \sin\alpha)(\sqrt{m^2+1}-1)}{m(\sqrt{m^2+1} - \cos\alpha - m\sin\alpha)}\right| \\
&= \frac{m|\vec{A}|}{\sqrt{m^2+1}} \ln\left|\frac{|\vec{A}|(\sqrt{m^2+1}-1)}{|\vec{B}|(\sqrt{m^2+1} - \cos\alpha - m\sin a)}\right|.
\end{aligned}$$

This last step follows from $r(\alpha) = \frac{m|\vec{A}|}{m\cos\alpha - \sin\alpha} = |\vec{B}|$.

To alleviate the bulky notation in the following explanations, we will denote the discretization of

$$\begin{aligned}
\kappa(x) &= \frac{1}{4\pi}\int_\Gamma \frac{1}{|x-y|}\, V(y) dS_y + c \\
0 &= \int_\Gamma V(y) dS_y
\end{aligned}$$

as

$$\begin{aligned}
4\pi\kappa_i &= \sum_{j=1}^{i-1} \frac{V_j\Delta_j}{|\mathbf{x}_i - \mathbf{x}_j|} + I_i V_i + \sum_{j=i+1}^{N} \frac{V_j\Delta_j}{|\mathbf{x}_i - \mathbf{x}_j|} + c' \\
0 &= \sum_{j=1}^{N} V_j\Delta_j
\end{aligned}$$

www.manaraa.com

where $c' = 4\pi c$, $I_i = \displaystyle\int_{\Delta_i} \frac{1}{|\mathbf{x}_i - \mathbf{y}|} dS_y$, and

$$\frac{V_j \Delta_j}{|\mathbf{x}_i - \mathbf{x}_j|} = \frac{V_j}{3}\left(\frac{\Delta_j}{|x_i - y_j|} + \frac{\Delta_{j_1} + \Delta_{j_4}}{|x_i - s_1|} + \frac{\Delta_{j_1} + \Delta_{j_2}}{|x_i - s_2|} + \frac{\Delta_{j_2} + \Delta_{j_3}}{|x_i - s_3|} + \frac{\Delta_{j_3} + \Delta_{j_4}}{|x_i - s_4|}\right).$$

3.7.1 Particle-Particle Method

We are solving the following for the constants $\{V_i\}_{i=1..N}$ and c'.

$$\begin{aligned} 4\pi\kappa_i &= \sum_{j=1}^{i-1} \frac{V_j \Delta_j}{|\mathbf{x}_i - \mathbf{x}_j|} + I_i V_i + \sum_{j=i+1}^{N} \frac{V_j \Delta_j}{|\mathbf{x}_i - \mathbf{x}_j|} + c' \\ 0 &= \sum_{j=1}^{N} V_j \Delta_j \end{aligned}$$

where $c' = 4\pi c$ and $I_i = \displaystyle\int_{\Delta_i} \frac{1}{|\mathbf{x}_i - \mathbf{y}|} dS_y$, which we calculate directly. The particle-particle method, also called direct summation [27], requires the following system of linear equations to be solved:

$$\begin{bmatrix} I_1 & \frac{\Delta_2}{|\mathbf{x}_1-\mathbf{x}_2|} & \frac{\Delta_3}{|\mathbf{x}_1-\mathbf{x}_3|} & \cdots & \frac{\Delta_{N-1}}{|\mathbf{x}_1-\mathbf{x}_{N-1}|} & \frac{\Delta_N}{|\mathbf{x}_1-\mathbf{x}_N|} & 1 \\ \frac{\Delta_1}{|\mathbf{x}_2-\mathbf{x}_1|} & I_2 & \frac{\Delta_3}{|\mathbf{x}_2-\mathbf{x}_3|} & \cdots & \frac{\Delta_{N-1}}{|\mathbf{x}_2-\mathbf{x}_{N-1}|} & \frac{\Delta_N}{|\mathbf{x}_2-\mathbf{x}_N|} & 1 \\ \frac{\Delta_1}{|\mathbf{x}_3-\mathbf{x}_1|} & \frac{\Delta_2}{|\mathbf{x}_3-\mathbf{x}_2|} & I_3 & \cdots & \frac{\Delta_{N-1}}{|\mathbf{x}_3-\mathbf{x}_{N-1}|} & \frac{\Delta_N}{|\mathbf{x}_3-\mathbf{x}_N|} & 1 \\ \vdots & \vdots & \vdots & \ddots & \vdots & \vdots & \vdots \\ \frac{\Delta_1}{|\mathbf{x}_{N-1}-\mathbf{x}_1|} & \frac{\Delta_2}{|\mathbf{x}_{N-1}-\mathbf{x}_2|} & \frac{\Delta_3}{|\mathbf{x}_{N-1}-\mathbf{x}_3|} & \cdots & I_{N-1} & \frac{\Delta_N}{|\mathbf{x}_{N-1}-\mathbf{x}_N|} & 1 \\ \frac{\Delta_1}{|\mathbf{x}_N-\mathbf{x}_1|} & \frac{\Delta_2}{|\mathbf{x}_N-\mathbf{x}_2|} & \frac{\Delta_3}{|\mathbf{x}_N-\mathbf{x}_3|} & \cdots & \frac{\Delta_{N-1}}{|\mathbf{x}_N-\mathbf{x}_{N-1}|} & I_N & 1 \\ \Delta_1 & \Delta_2 & \Delta_3 & \cdots & \Delta_{N-1} & \Delta_N & 0 \end{bmatrix} \begin{bmatrix} V_1 \\ V_2 \\ V_3 \\ \vdots \\ V_{N-1} \\ V_N \\ c' \end{bmatrix} = \begin{bmatrix} 4\pi\kappa_1 \\ 4\pi\kappa_2 \\ 4\pi\kappa_3 \\ \vdots \\ 4\pi\kappa_{N-1} \\ 4\pi\kappa_N \\ 0 \end{bmatrix}$$

This is a dense, $(N+1) \times (N+1)$ matrix. Filling this matrix is extremely computationally expensive, but can be reduced some by observing that while the coefficient matrix is not symmetric, we can take advantage of repeated denominators. We use the library function *dgesv* to solve the system of linear equations. *dgesv* uses *LU* decomposition with partial pivoting; see [3] for more detail. Solving the system by *LU* decomposition requires $\mathcal{O}(N^3)$

www.manaraa.com

operations [25]. In practice N ranges anywhere from several hundred to several thousand.

3.7.2 Particle-Cluster Method

As filling the coefficient matrix requires a prohibitive amount of computing time, we need to find a more efficient method than the particle-particle method. Hence we turn to the particle-cluster method. See K. Lindsay's PhD thesis [27] and a paper he coauthored with R. Krasny [28] for the application of this method to vortex sheet motion, from which the following argument was adapted.

The particle-cluster method takes a cluster, or group of nearby nodes, and treats them as one. Hence, when we calculate $\dfrac{1}{|\mathbf{x}_i - \mathbf{x}_j|}$, for a cluster of $\mathbf{x}_j$'s sufficiently far away from $\mathbf{x}_i$ we consider their influence as a whole, not individually.

Mathematical Justification

We now establish some notation. Divide the surface into M clusters. Let $\tilde{m} = \{i \,|\, \mathbf{x}_i \in m^{\text{th}}\text{cluster}\}$, that is, $\tilde{m}$ is the set of indices of all nodes in the m^{th} cluster. Let $\tilde{\mathbf{x}}_m$ be a node on the surface representing the m^{th} cluster. $\tilde{\mathbf{x}}_m$ is usually chosen to be the center of mass or geometrical center of the cluster of nodes. In our case we choose a node near or on the geometrical center.

For convenience let $\Psi(\mathbf{x}, \mathbf{y}) = \dfrac{1}{|\mathbf{x} - \mathbf{y}|}$ where $\mathbf{x}, \mathbf{y} \in \mathbb{R}^3$ and $\mathbf{x} \neq \mathbf{y}$. Consider the sum

$$\sum_{j \in \tilde{m}} \frac{1}{|\mathbf{x}_i - \mathbf{x}_j|} V_j \Delta_j = \sum_{j \in \tilde{m}} \Psi(\mathbf{x}_i, \mathbf{x}_j) V_j \Delta_j$$

where $i \notin \tilde{m}$, i.e., we are summing over all nodes $\{\mathbf{x}_j\}$ in a cluster which does not contain $\mathbf{x}_i$.

For $\mathbf{x}_i$ and $\mathbf{x}_j$ sufficiently separated, we can use the Taylor series representation for Ψ where $\mathbf{k} = (k_1, k_2, k_3)$ is a multi-index:

www.manaraa.com

$$\begin{aligned}\sum_{j\in\tilde{m}}\Psi(\mathbf{x}_i,\mathbf{x}_j)V_j\Delta_j &= \sum_{j\in\tilde{m}}\Psi(\mathbf{x}_i,\tilde{\mathbf{x}}_m+(\mathbf{x}_j-\tilde{\mathbf{x}}_m))V_j\Delta_j \\ &= \sum_{j\in\tilde{m}}\left(\sum_{\mathbf{k}}\frac{1}{\mathbf{k}!}D_y^{\mathbf{k}}\Psi(\mathbf{x}_i,\tilde{\mathbf{x}}_m)(\mathbf{x}_j-\tilde{\mathbf{x}}_m)^{\mathbf{k}}\right)V_j\Delta_j \\ &= \sum_{\mathbf{k}}\underbrace{\frac{1}{\mathbf{k}!}D_y^{\mathbf{k}}\Psi(\mathbf{x}_i,\tilde{\mathbf{x}}_m)}_{\text{independent of } j}\underbrace{\sum_{j\in\tilde{m}}(\mathbf{x}_j-\tilde{\mathbf{x}}_m)^{\mathbf{k}}V_j\Delta_j}_{\text{independent of } i}.\end{aligned}$$

Truncating, we have

$$\sum_{j\in\tilde{m}}\Psi(\mathbf{x}_i,\mathbf{x}_j)V_j\Delta_j \approx \sum_{|\mathbf{k}|<p}\frac{1}{\mathbf{k}!}D_y^{\mathbf{k}}\Psi(\mathbf{x}_i,\tilde{\mathbf{x}}_m)\sum_{j\in\tilde{m}}(\mathbf{x}_j-\tilde{\mathbf{x}}_m)^{\mathbf{k}}V_j\Delta_j$$

where p is a positive integer chosen large enough to achieve the desired accuracy. In practice $p=3$ is sufficient.

Recurrence Relation for Taylor Coefficients

We want to find a simple way to calculate the Taylor coefficients $\frac{1}{\mathbf{k}!}D_y^{\mathbf{k}}\Psi(\mathbf{x}_i,\tilde{\mathbf{x}}_m)$ where $\mathbf{k}=(k_1,k_2,k_3)$ is a multi-index. We do this by showing the coefficients satisfy a recurrence relation.

For notational convenience define $C_{\mathbf{k}}(\mathbf{x},\mathbf{y})\equiv\frac{1}{\mathbf{k}!}D_y^{\mathbf{k}}\Psi(\mathbf{x},\mathbf{y})$, i.e.,

$$C_{k_1,k_2,k_3}\equiv\frac{1}{k_1!k_2!k_3!}\frac{\partial^{|\mathbf{k}|}\Psi(\mathbf{x},\mathbf{y})}{\partial^{k_1}y_1\partial^{k_2}y_2\partial^{k_3}y_3}\ .$$

In the case that $k_i<0$ for $i=1,2,$ or 3, we define $C_{\mathbf{k}}=0$.

The following lemma and proof are adapted from a similar one in [27].

Lemma 3.7.1 *$C_{\mathbf{k}}$ satisfies the following recurrence relations:*

(i)
$$\begin{aligned}&|\mathbf{x}-\mathbf{y}|^2C_{k_1,k_2,k_3}-(x_1-y_1)(2-\frac{1}{k_1})C_{k_1-1,k_2,k_3}+(1-\frac{1}{k_1})C_{k_1-2,k_2,k_3}\\&-2(x_2-y_2)C_{k_1,k_2-1,k_3}+C_{k_1,k_2-2,k_3}-2(x_3-y_3)C_{k_1,k_2,k_3-1}+C_{k_1,k_2,k_3-2}=0\quad(k_1\neq0)\end{aligned}$$

(ii)
$$\begin{aligned}&|\mathbf{x}-\mathbf{y}|^2C_{k_1,k_2,k_3}-(x_2-y_2)(2-\frac{1}{k_2})C_{k_1,k_2-1,k_3}+(1-\frac{1}{k_2})C_{k_1,k_2-2,k_3}\\&-2(x_1-y_1)C_{k_1-1,k_2,k_3}+C_{k_1-2,k_2,k_3}-2(x_3-y_3)C_{k_1,k_2,k_3-1}+C_{k_1,k_2,k_3-2}=0\quad(k_2\neq0)\end{aligned}$$

(iii)
$$\begin{aligned}&|\mathbf{x}-\mathbf{y}|^2C_{k_1,k_2,k_3}-(x_3-y_3)(2-\frac{1}{k_3})C_{k_1,k_2,k_3-1}+(1-\frac{1}{k_3})C_{k_1,k_2,k_3-2}\\&-2(x_1-y_1)C_{k_1-1,k_2,k_3}+C_{k_1-2,k_2,k_3}-2(x_2-y_2)C_{k_1,k_2-1,k_3}+C_{k_1,k_2-2,k_3}=0\quad(k_3\neq0)\end{aligned}$$

www.manaraa.com

Proof. First we note that Ψ satisfies the following differential equations for $i = 1, 2, 3$, where $\mathbf{x} = (x_1, x_2, x_3)$ and $\mathbf{y} = (y_1, y_2, y_3)$:

$$|\mathbf{x}-\mathbf{y}|^2 \frac{\partial \Psi}{\partial y_i} - (x_i - y_i)\Psi(\mathbf{x}, \mathbf{y}) = 0 \ .$$

This is shown by direct calculation:

$$|\mathbf{x}-\mathbf{y}|^2 \frac{(x_i - y_i)}{|\mathbf{x}-\mathbf{y}|^3} - (x_i - y_i)\frac{1}{|\mathbf{x}-\mathbf{y}|} = 0 \ .$$

We will prove (i). The proofs of (ii) and (iii) are similar. Now given that

$$|\mathbf{x}-\mathbf{y}|^2 \frac{\partial \Psi}{\partial y_1} - (x_1 - y_1)\Psi(\mathbf{x}, \mathbf{y}) = 0 \ .$$

differentiate $k_1 - 1$ times with respect to y_1. Utilizing Leibnitz Rule, we get

$$\begin{aligned} \frac{(k_1-1)(k_1-2)}{2} 2\Psi^{k_1-2} - (k_1-1)2(x_1-y_1)\Psi^{k_1-1} & \\ +|\mathbf{x}-\mathbf{y}|^2\Psi^{k_1} + (k_1-1)\Psi^{k_1-2} - (x_1-y_1)\Psi^{k_1-1} &= 0 \\ \Leftrightarrow \quad |\mathbf{x}-\mathbf{y}|^2\Psi^{k_1} - (2k_1-1)(x_1-y_1)\Psi^{k_1-1} + (k_1-1)^2\Psi^{k_1-2} &= 0 \ . \end{aligned}$$

Next differentiate with respect to y_2 k_2 times to get

$$\begin{aligned} |\mathbf{x}-\mathbf{y}|^2\Psi^{k_1,k_2} - (2k_1-1)(x_1-y_1)\Psi^{k_1-1,k_2} + (k_1-1)^2\Psi^{k_1-2,k_2} & \\ -2k_2(x_2-y_2)\Psi^{k_1,k_2-1} + k_2(k_2-1)\Psi^{k_1,k_2-2} &= 0 \ . \end{aligned}$$

Now differentiate with respect to y_3 k_3 times to get

$$\begin{aligned} |\mathbf{x}-\mathbf{y}|^2\Psi^{k_1,k_2,k_3} - (2k_1-1)(x_1-y_1)\Psi^{k_1-1,k_2,k_3} + (k_1-1)^2\Psi^{k_1-2,k_2,k_3} & \\ -2k_2(x_2-y_2)\Psi^{k_1,k_2-1,k_3} + k_2(k_2-1)\Psi^{k_1,k_2-2,k_3} & \\ -2k_3(x_3-y_3)\Psi^{k_1,k_2,k_3-1} + k_3(k_3-1)\Psi^{k_1,k_2,k_3-2} &= 0 \ . \end{aligned}$$

Finally, divide by $k_1!k_2!k_3!$ to get our desired recurrence relation. □

Error Analysis

We now analyze the error incurred by truncating the Taylor series in the approximation

$$\sum_{j\in\tilde{m}} \Psi(\mathbf{x}_i, \mathbf{x}_j)V_j\Delta_j \approx \sum_{|\mathbf{k}|<p} \frac{1}{\mathbf{k}!} D_y^{\mathbf{k}}\Psi(\mathbf{x}_i, \tilde{\mathbf{x}}_m) \sum_{j\in\tilde{m}} (\mathbf{x}_j - \tilde{\mathbf{x}}_m)^{\mathbf{k}} V_j\Delta_j \ .$$

We do this by showing the absolute value of the terms in the Taylor series approximation of Ψ decreases geometrically.

Recall that $C_{\mathbf{k}}(\mathbf{x}, \mathbf{y}) \equiv \frac{1}{\mathbf{k}!} D_y^{\mathbf{k}}\Psi(\mathbf{x}, \mathbf{y})$, i.e.,

$$C_{k_1,k_2,k_3} \equiv \frac{1}{k_1!k_2!k_3!} \frac{\partial^{|\mathbf{k}|}\Psi(\mathbf{x}, \mathbf{y})}{\partial^{k_1}y_1\partial^{k_2}y_2\partial^{k_3}y_3}$$

and in the case that $k_i < 0$ for $i = 1, 2$, or 3, we define $C_{\mathbf{k}} = 0$. Define $T_n \equiv \sum_{|\mathbf{k}|=n} \frac{1}{\mathbf{k}!} D_y^{\mathbf{k}}\Psi(\mathbf{x}_i, \tilde{\mathbf{x}}_m)(\mathbf{x}_j - \tilde{\mathbf{x}}_m)^{\mathbf{k}}$, i.e.,

www.manaraa.com

$$T_n \equiv \sum_{|\mathbf{k}|=n} C_{\mathbf{k}}(\mathbf{x}_i, \tilde{\mathbf{x}}_m)(\mathbf{x}_j - \tilde{\mathbf{x}}_m)^{\mathbf{k}}.$$

Here $i \in \{1, 2, ..., N\}$, N being the number of nodes on our discretized surface, and $i \notin \tilde{m}$ where $\tilde{m}$ is the set of indices of the nodes contained in the m^{th} cluster. $\tilde{\mathbf{x}}_m$ is the central node of the m^{th} cluster. We also have that $j \in \tilde{m}$. Hence T_n is the sum of all terms in the Taylor series with $k_1+k_2+k_3 = n$. We will eventually show that $|T_n|$ decreases geometrically with n.

The following is modified from a similar lemma in [27].

Lemma 3.7.2 *The following recurrence relation is satisfied by T_n for all $i \notin \tilde{m}, j \in \tilde{m}, n \in \mathbf{Z}^+$, and $n \geq 3$:*

$$|\mathbf{x}_i - \tilde{\mathbf{x}}_m|^2 T_n - (\mathbf{x}_i - \tilde{\mathbf{x}}_m) \cdot (\mathbf{x}_j - \tilde{\mathbf{x}}_m)(2 - \frac{1}{n}) T_{n-1} + |\mathbf{x}_j - \tilde{\mathbf{x}}_m|^2 T_{n-2} = 0.$$

Proof. We take a linear combination of the recurrence relations satisfied by $C_{\mathbf{k}}$ with $k_1 + k_2 + k_3 = n, k_1, k_2, k_3 > 0, \mathbf{x} = \mathbf{x}_i = (x_{i1}, x_{i2}, x_{i3})$, $\mathbf{y} = \tilde{\mathbf{x}}_m = (\tilde{x}_{m1}, \tilde{x}_{m2}, \tilde{x}_{m3})$.

www.manaraa.com

$$
\begin{aligned}
&\frac{k_1}{n}(i)+\frac{k_2}{n}(ii)+\frac{k_1}{n}(iii) \Leftrightarrow \\
&\quad \frac{k_1}{n} \quad \Big(|\mathbf{x}_i-\tilde{\mathbf{x}}_m|^2 C_{k_1,k_2,k_3}-(x_{i1}-\tilde{x}_{m1})(2-\frac{1}{k_1})C_{k_1-1,k_2,k_3}+(1-\frac{1}{k_1})C_{k_1-2,k_2,k_3} \\
&\qquad -2(x_{i2}-\tilde{x}_{m2})C_{k_1,k_2-1,k_3}+C_{k_1,k_2-2,k_3}-2(x_{i3}-\tilde{x}_{m3})C_{k_1,k_2,k_3-1}+C_{k_1,k_2,k_3-2}\Big) \\
&+\frac{k_2}{n} \quad \Big(|\mathbf{x}_i-\tilde{\mathbf{x}}_m|^2 C_{k_1,k_2,k_3}-(x_{i2}-\tilde{x}_{m2})(2-\frac{1}{k_2})C_{k_1,k_2-1,k_3}+(1-\frac{1}{k_2})C_{k_1,k_2-2,k_3} \\
&\qquad -2(x_{i1}-\tilde{x}_{m1})C_{k_1-1,k_2,k_3}+C_{k_1-2,k_2,k_3}-2(x_{i3}-\tilde{x}_{m3})C_{k_1,k_2,k_3-1}+C_{k_1,k_2,k_3-2}\Big) \\
&+\frac{k_3}{n} \quad \Big(|\mathbf{x}_i-\tilde{\mathbf{x}}_m|^2 C_{k_1,k_2,k_3}-(x_{i3}-\tilde{x}_{m3})(2-\tfrac{1}{k_3})C_{k_1,k_2,k_3-1}+(1-\tfrac{1}{k_3})C_{k_1,k_2,k_3-2} \\
&\qquad -2(x_{i1}-\tilde{x}_{m1})C_{k_1-1,k_2,k_3}+C_{k_1-2,k_2,k_3}-2(x_{i2}-\tilde{x}_{m2})C_{k_1,k_2-1,k_3}+C_{k_1,k_2-2,k_3}\Big) \quad = 0
\end{aligned}
$$

$$
\begin{aligned}
&\Leftrightarrow \\
&\left(\frac{k_1}{n}+\frac{k_2}{n}+\frac{k_3}{n}\right)|\mathbf{x}_i-\tilde{\mathbf{x}}_m|^2\, C_{k_1,k_2,k_3} \\
&-\left(\frac{k_1}{n}(x_{i1}-\tilde{x}_{m1})(2-\frac{1}{k_1})+\frac{k_2}{n}2(x_{i1}-\tilde{x}_{m1})+\frac{k_3}{n}2(x_{i1}-\tilde{x}_{m1})\right) C_{k_1-1,k_2,k_3} \\
&+\left(\frac{k_1}{n}(1-\frac{1}{k_1})+\frac{k_2}{n}+\frac{k_3}{n}\right) C_{k_1-2,k_2,k_3} \\
&-\left(\frac{k_1}{n}2(x_{i2}-\tilde{x}_{m2})+\frac{k_2}{n}(x_{i2}-\tilde{x}_{m2})(2-\frac{1}{k_2})+\frac{k_3}{n}2(x_{i2}-\tilde{x}_{m2})\right) C_{k_1,k_2-1,k_3} \\
&+\left(\frac{k_1}{n}+\frac{k_2}{n}(1-\frac{1}{k_2})+\frac{k_3}{n}\right) C_{k_1,k_2-2,k_3} \\
&-\left(\frac{k_1}{n}2(x_{i3}-\tilde{x}_{m3})+\frac{k_2}{n}2(x_{i3}-\tilde{x}_{m3})+\frac{k_3}{n}(x_{i3}-\tilde{x}_{m3})(2-\frac{1}{k_3})\right) C_{k_1,k_2,k_3-1} \\
&+\left(\frac{k_1}{n}+\frac{k_2}{n}+\frac{k_3}{n}(1-\frac{1}{k_3})\right) C_{k_1,k_2,k_3-2}=0
\end{aligned}
$$

$$
\begin{aligned}
&\Leftrightarrow \\
&|\mathbf{x}_i-\tilde{\mathbf{x}}_m|^2\, C_{k_1,k_2,k_3} \\
&-\left(2-\frac{1}{n}\right)((x_{i1}-\tilde{x}_{m1})C_{k_1-1,k_2,k_3}+(x_{i2}-\tilde{x}_{m2})C_{k_1,k_2-1,k_3}+(x_{i3}-\tilde{x}_{m3})C_{k_1,k_2,k_3-1}) \\
&+\left(1-\frac{1}{n}\right)(C_{k_1-2,k_2,k_3}+C_{k_1,k_2-2,k_3}+C_{k_1,k_2,k_3-2})=0.
\end{aligned}
$$

www.manaraa.com

Recall the notation $(\mathbf{x}-\mathbf{y})^{\mathbf{k}} = (\mathbf{x}-\mathbf{y})^{(k_1,k_2,k_3)} = (x_1-y_1)^{k_1}(x_2-y_2)^{k_2}(x_3-y_3)^{k_3}$. We now multiply the above equation through by $(\mathbf{x}_j-\tilde{\mathbf{x}}_m)^{\mathbf{k}}$ where $k_1+k_2+k_3=n$. Sum over all such $\mathbf{k}$ to get

$$
\begin{aligned}
&|\mathbf{x}_i-\tilde{\mathbf{x}}_m|^2 \sum_{|\mathbf{k}|=n} C_{k_1,k_2,k_3}(\mathbf{x}_j-\tilde{\mathbf{x}}_m)^{\mathbf{k}} \\
&-\left(2-\frac{1}{n}\right) \quad \Bigg[(x_{i1}-\tilde{x}_{m1})(x_{j1}-\tilde{x}_{m1}) \sum_{k_1-1+k_2+k_3=n-1} C_{k_1-1,k_2,k_3}\,(\mathbf{x}_j-\tilde{\mathbf{x}}_m)^{(k_1-1,k_2,k_3)} \\
&\qquad +(x_{i2}-\tilde{x}_{m2})(x_{j2}-\tilde{x}_{m2}) \sum_{k_1+k_2-1+k_3=n-1} C_{k_1,k_2-1,k_3}\,(\mathbf{x}_j-\tilde{\mathbf{x}}_m)^{(k_1,k_2-1,k_3)} \\
&\qquad +(x_{i3}-\tilde{x}_{m3})(x_{j3}-\tilde{x}_{m3}) \sum_{k_1+k_2+k_3-1=n-1} C_{k_1,k_2,k_3-1}\,(\mathbf{x}_j-\tilde{\mathbf{x}}_m)^{(k_1,k_2,k_3-1)}\Bigg] \\
&+\left(1-\frac{1}{n}\right) \quad \Bigg[(x_{j1}-\tilde{x}_{m1})^2 \sum_{k_1-2+k_2+k_3=n-2} C_{k_1-2,k_2,k_3}\,(\mathbf{x}_j-\tilde{\mathbf{x}}_m)^{(k_1-2,k_2,k_3)} \\
&\qquad +(x_{j2}-\tilde{x}_{m2})^2 \sum_{k_1+k_2-2+k_3=n-2} C_{k_1,k_2-2,k_3}\,(\mathbf{x}_j-\tilde{\mathbf{x}}_m)^{(k_1,k_2-2,k_3)} \\
&\qquad +(x_{j3}-\tilde{x}_{m3})^2 \sum_{k_1+k_2+k_3-2=n-2} C_{k_1,k_2,k_3-2}\,(\mathbf{x}_j-\tilde{\mathbf{x}}_m)^{(k_1,k_2,k_3-2)}\Bigg] = 0
\end{aligned}
$$

$\Leftrightarrow$

$$
|\mathbf{x}_i-\tilde{\mathbf{x}}_m|^2\,T_n - (\mathbf{x}_i-\tilde{\mathbf{x}}_m)\cdot(\mathbf{x}_j-\tilde{\mathbf{x}}_m)\left(2-\frac{1}{n}\right)T_{n-1} + |\mathbf{x}_j-\tilde{\mathbf{x}}_m|^2\,T_{n-2} = 0
$$

Since

$$
\begin{aligned}
T_{n-1} &= \sum_{k_1-1+k_2+k_3=n-1} C_{k_1-1,k_2,k_3}\,(\mathbf{x}_j-\tilde{\mathbf{x}}_m)^{(k_1-1,k_2,k_3)} \\
&= \sum_{k_1+k_2-1+k_3=n-1} C_{k_1,k_2-1,k_3}\,(\mathbf{x}_j-\tilde{\mathbf{x}}_m)^{(k_1,k_2-1,k_3)} \\
&= \sum_{k_1+k_2+k_3-1=n-1} C_{k_1,k_2,k_3-1}\,(\mathbf{x}_j-\tilde{\mathbf{x}}_m)^{(k_1-1,k_2,k_3-1)}\ .
\end{aligned}
$$

T_{n-2} can be written similarly. Thus we have our desired recurrence relation. $\square$

www.manaraa.com

We now relate T_n to the Legendre polynomials P_n, defined as follows [24]:

$P_0(x) = 1, P_1(x) = x, P_n(x) = \frac{1}{n!2^n}\frac{d^n}{dx^n}(x^2-1)^n$

Be aware that there are different, albeit related ways of defining the polynomials [25]. We eventually use the inequality $|P_n(x)| \leq 1$ for $|x| \leq 1$ [24] when we bound T_n.

The following lemma and proof are adapted from [27].

Lemma 3.7.3 *For $n \geq 2$,*

$$T_n = \frac{|\mathbf{x}_j - \tilde{\mathbf{x}}_m|^n}{|\mathbf{x}_i - \tilde{\mathbf{x}}_m|^{n+1}} P_n\left(\frac{(\mathbf{x}_i - \tilde{\mathbf{x}}_m)\cdot(\mathbf{x}_j - \tilde{\mathbf{x}}_m)}{|\mathbf{x}_i - \tilde{\mathbf{x}}_m||\mathbf{x}_j - \tilde{\mathbf{x}}_m|}\right) .$$

Proof. Define S_n to be the right hand side of the above equation. To prove that $S_n = T_n$, it is sufficient to show that $S_0 = T_0$, $S_1 = T_1$, and that S_n satisfies the same recurrence relation as T_n satisfies, given in the previous lemma. We have

$$\begin{aligned} T_0 &= \sum_{|\mathbf{k}|=0} \frac{1}{\mathbf{k}!} D_y^{\mathbf{k}} \frac{1}{|\mathbf{x}_i - \tilde{\mathbf{x}}_m|} (\mathbf{x}_j - \tilde{\mathbf{x}}_m)^{\mathbf{k}} \\ &= \frac{1}{|\mathbf{x}_i - \tilde{\mathbf{x}}_m|} \\ &= S_0. \end{aligned}$$

Also,

$$\begin{aligned} T_1 &= \sum_{|\mathbf{k}|=1} \frac{1}{\mathbf{k}!} D_y^{\mathbf{k}} \frac{1}{|\mathbf{x}_i - \tilde{\mathbf{x}}_m|} (\mathbf{x}_j - \tilde{\mathbf{x}}_m)^{\mathbf{k}} \\ &= \frac{(\mathbf{x}_{i1} - \tilde{\mathbf{x}}_{m1})(\mathbf{x}_{j1} - \tilde{\mathbf{x}}_{m1})}{|\mathbf{x}_i - \tilde{\mathbf{x}}_m|^3} + \frac{(\mathbf{x}_{i2} - \tilde{\mathbf{x}}_{m2})(\mathbf{x}_{j2} - \tilde{\mathbf{x}}_{m2})}{|\mathbf{x}_i - \tilde{\mathbf{x}}_m|^3} + \frac{(\mathbf{x}_{i3} - \tilde{\mathbf{x}}_{m3})(\mathbf{x}_{j3} - \tilde{\mathbf{x}}_{m3})}{|\mathbf{x}_i - \tilde{\mathbf{x}}_m|^3} \\ &= \frac{(\mathbf{x}_i - \tilde{\mathbf{x}}_m)\cdot(\mathbf{x}_j - \tilde{\mathbf{x}}_m)}{|\mathbf{x}_i - \tilde{\mathbf{x}}_m|^3} \\ &= S_1. \end{aligned}$$

Now the Legendre polynomials satisfy the following recurrence relation for $n \geq 2$ [24].

$P_n(x) - x(2 - \frac{1}{n})\, P_{n-1}(x) + (1 - \frac{1}{n})\, P_{n-2}(x) = 0.$

Let $x = \frac{(\mathbf{x}_i - \tilde{\mathbf{x}}_m)\cdot(\mathbf{x}_j - \tilde{\mathbf{x}}_m)}{|\mathbf{x}_i - \tilde{\mathbf{x}}_m||\mathbf{x}_j - \tilde{\mathbf{x}}_m|}$ and multiply through by $\frac{|\mathbf{x}_j - \tilde{\mathbf{x}}_m|^n}{|\mathbf{x}_i - \tilde{\mathbf{x}}_m|^{n+1}}$ to get

www.manaraa.com

$$\frac{|\mathbf{x}_j-\tilde{\mathbf{x}}_m|^n}{|\mathbf{x}_i-\tilde{\mathbf{x}}_m|^{n+1}} P_n\left(\frac{(\mathbf{x}_i-\tilde{\mathbf{x}}_m)\cdot(\mathbf{x}_j-\tilde{\mathbf{x}}_m)}{|\mathbf{x}_i-\tilde{\mathbf{x}}_m||\mathbf{x}_j-\tilde{\mathbf{x}}_m|}\right)$$

$$-\frac{|\mathbf{x}_j-\tilde{\mathbf{x}}_m|^n}{|\mathbf{x}_i-\tilde{\mathbf{x}}_m|^{n+1}}(2-\frac{1}{n})\frac{(\mathbf{x}_i-\tilde{\mathbf{x}}_m)\cdot(\mathbf{x}_j-\tilde{\mathbf{x}}_m)}{|\mathbf{x}_i-\tilde{\mathbf{x}}_m||\mathbf{x}_j-\tilde{\mathbf{x}}_m|} P_{n-1}\left(\frac{(\mathbf{x}_i-\tilde{\mathbf{x}}_m)\cdot(\mathbf{x}_j-\tilde{\mathbf{x}}_m)}{|\mathbf{x}_i-\tilde{\mathbf{x}}_m||\mathbf{x}_j-\tilde{\mathbf{x}}_m|}\right)$$

$$+\frac{|\mathbf{x}_j-\tilde{\mathbf{x}}_m|^n}{|\mathbf{x}_i-\tilde{\mathbf{x}}_m|^{n+1}}(1-\frac{1}{n})\, P_{n-2}\left(\frac{(\mathbf{x}_i-\tilde{\mathbf{x}}_m)\cdot(\mathbf{x}_j-\tilde{\mathbf{x}}_m)}{|\mathbf{x}_i-\tilde{\mathbf{x}}_m||\mathbf{x}_j-\tilde{\mathbf{x}}_m|}\right) = 0$$

$$\Leftrightarrow$$

$$S_n - \left(2-\frac{1}{n}\right)\frac{(\mathbf{x}_i-\tilde{\mathbf{x}}_m)\cdot(\mathbf{x}_j-\tilde{\mathbf{x}}_m)}{|\mathbf{x}_i-\tilde{\mathbf{x}}_m|^2} S_{n-1} + \left(1-\frac{1}{n}\right)\frac{|\mathbf{x}_j-\tilde{\mathbf{x}}_m|^2}{|\mathbf{x}_i-\tilde{\mathbf{x}}_m|^2} S_{n-2} = 0$$

$$\Leftrightarrow$$

$$|\mathbf{x}_i-\tilde{\mathbf{x}}_m|^2 S_n - \left(2-\frac{1}{n}\right)(\mathbf{x}_i-\tilde{\mathbf{x}}_m)\cdot(\mathbf{x}_j-\tilde{\mathbf{x}}_m) S_{n-1} + \left(1-\frac{1}{n}\right)|\mathbf{x}_j-\tilde{\mathbf{x}}_m|^2 S_{n-2} = 0$$

which is the same recurrence relation satisfied by T_n. □

We next bound T_n. Since $\frac{(\mathbf{x}_i-\tilde{\mathbf{x}}_m)\cdot(\mathbf{x}_j-\tilde{\mathbf{x}}_m)}{|\mathbf{x}_i-\tilde{\mathbf{x}}_m||\mathbf{x}_j-\tilde{\mathbf{x}}_m|}$ is the cosine of the angle between the vectors $\mathbf{x}_i-\tilde{\mathbf{x}}_m$ and $\mathbf{x}_j-\tilde{\mathbf{x}}_m$, we have $\left|\frac{(\mathbf{x}_i-\tilde{\mathbf{x}}_m)\cdot(\mathbf{x}_j-\tilde{\mathbf{x}}_m)}{|\mathbf{x}_i-\tilde{\mathbf{x}}_m||\mathbf{x}_j-\tilde{\mathbf{x}}_m|}\right| \le 1$. Since $|P_n(x)| \le 1$ for $|x| \le 1$ [24], we have $\left|P_n\left(\frac{(\mathbf{x}_i-\tilde{\mathbf{x}}_m)\cdot(\mathbf{x}_j-\tilde{\mathbf{x}}_m)}{|\mathbf{x}_i-\tilde{\mathbf{x}}_m||\mathbf{x}_j-\tilde{\mathbf{x}}_m|}\right)\right| \le 1$. Therefore $|T_n| \le \frac{|\mathbf{x}_j-\tilde{\mathbf{x}}_m|^n}{|\mathbf{x}_i-\tilde{\mathbf{x}}_m|^{n+1}}$.

We now put restrictions on our clusters. Let $R = \max_{j\in\tilde{m}} |\mathbf{x}_j-\tilde{\mathbf{x}}_m|$, i.e., the maximum distance from the m^{th} cluster's center node $\tilde{\mathbf{x}}_m$ to a node $\mathbf{x}_j$ in the cluster. We require the center of the cluster containing $\mathbf{x}_i$ to be at least $3R$ units away from $\tilde{\mathbf{x}}_m$. Then $|\mathbf{x}_j-\tilde{\mathbf{x}}_m| \le R$ and $|\mathbf{x}_i-\tilde{\mathbf{x}}_m| \le 2R$. Under these restrictions we have

$$|T_n| \le \frac{R^n}{(2R)^{n+1}} = \frac{1}{R\,2^{n+1}} .$$

Hence, the magnitude of T_n decreases geometrically.

A similar result to the following lemma was previously proved in [27].

Lemma 3.7.4 *The error incurred by truncating Taylor series is bounded by* $\frac{1}{R\,2^p}$.

Proof. Because the magnitude of T_n decreases geometrically, the following inequalities hold:

$$\sum_{n\ge p} T_n \le T_{p-1} \le \frac{1}{R\,2^p} .$$

www.manaraa.com

But $T_{p-1} = \sum_{\mathbf{k}} \frac{1}{\mathbf{k}!} D_y^{\mathbf{k}} \left(\frac{1}{\mathbf{x}_i - \tilde{\mathbf{x}}_m} \right) (\mathbf{x}_j - \tilde{\mathbf{x}}_m)^{\mathbf{k}} - \sum_{|\mathbf{k}|<p} \frac{1}{\mathbf{k}!} D_y^{\mathbf{k}} \left(\frac{1}{\mathbf{x}_i - \tilde{\mathbf{x}}_m} \right) (\mathbf{x}_j - \tilde{\mathbf{x}}_m)^{\mathbf{k}}$. Hence, the error is bounded by $\frac{1}{R\,2^p}$. □

3.7.3 Efficiency

Recall that we are solving the following for the constants $\{V_i\}_{i=1..N}$ and c'.

$$\begin{aligned} 4\pi\kappa_i &= \sum_{j=1}^{i-1} \frac{V_j \Delta_j}{|\mathbf{x}_i - \mathbf{x}_j|} + I_i V_i + \sum_{j=i+1}^{N} \frac{V_j \Delta_j}{|\mathbf{x}_i - \mathbf{x}_j|} + c' \ , \\ 0 &= \sum_{j=1}^{N} V_j \Delta_j \ . \end{aligned}$$

We rewrite

$$4\pi\kappa_i = \sum_{j=1}^{i-1} \frac{V_j \Delta_j}{|\mathbf{x}_i - \mathbf{x}_j|} + I_i\, V_i + \sum_{j=i+1}^{N} \frac{V_j \Delta_j}{|\mathbf{x}_i - \mathbf{x}_j|} + c'$$

as

$$4\pi\kappa_i = \underbrace{\sum_{j \neq i} \frac{V_j \Delta_j}{|\mathbf{x}_i - \mathbf{x}_j|}}_{\substack{\mathbf{x}_j \text{ in clusters} \\ \text{near or} \\ \text{containing } \mathbf{x}_i}} + \underbrace{\sum_{j} \frac{V_j \Delta_j}{|\mathbf{x}_i - \mathbf{x}_j|}}_{\substack{\mathbf{x}_j \text{ in} \\ \text{clusters not} \\ \text{neighboring } \mathbf{x}_i}} + I_i V_i + c'.$$

We have split the sum in order to keep the particle-particle method for nodes near $\mathbf{x}_i$, but we want to apply the particle-cluster method for clusters sufficiently separated from the cluster containing $\mathbf{x}_i$. In the latter case we use the following approximation, where M is the number of clusters and $\tilde{\mathbf{x}}_m$ is the center node of the m^{th} cluster, and $\tilde{m}$ is the set of all indices j such that $\mathbf{x}_j$ is in the m^{th} cluster:

$$\underbrace{\sum_{j} \frac{V_j \Delta_j}{|\mathbf{x}_i - \mathbf{x}_j|}}_{\substack{\mathbf{x}_j \text{ in} \\ \text{clusters not} \\ \text{neighboring } \mathbf{x}_i}} \approx \underbrace{\sum_{m \in M}}_{\substack{m^{\text{th}} \text{ cluster} \\ \text{far from } \mathbf{x}_i}} \sum_{|\mathbf{k}|<p} \frac{1}{\mathbf{k}!} D_y^{\mathbf{k}} \left(\frac{1}{|\mathbf{x}_i - \tilde{\mathbf{x}}_m|} \right) \sum_{j \in \tilde{m}} (\mathbf{x}_j - \tilde{\mathbf{x}}_m)^{\mathbf{k}} V_j \Delta_j.$$

For each i, calculating $\sum_{|\mathbf{k}|<p} \frac{1}{\mathbf{k}!} D_y^{\mathbf{k}} \left(\frac{1}{|\mathbf{x}_i - \tilde{\mathbf{x}}_m|} \right)$ requires $\mathcal{O}(p^3 M)$ operations.

www.manaraa.com

Cluster Formation

We describe how to divide our surfaces into clusters. There are many ways this can be done, with preference given to ways that give the most flexibility in terms of changing cluster size and numbers of clusters.

For ellipsoids we simply let each face of the icosahedron from which the discretization was derived be a cluster.

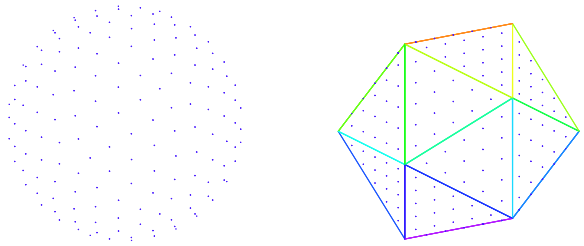

Recall that the torus is based on an N by M rectangular array. We designate the number of clusters h in the horizontal direction and the number of clusters v in the vertical direction and partition the rectangular array appropriately. The clusters do not have to be the same size, as h and v may not divide N and M evenly. Below are the clusters for a torus discretized by a 30 by 10 rectangular array with $h = 4$ and $v = 2$.

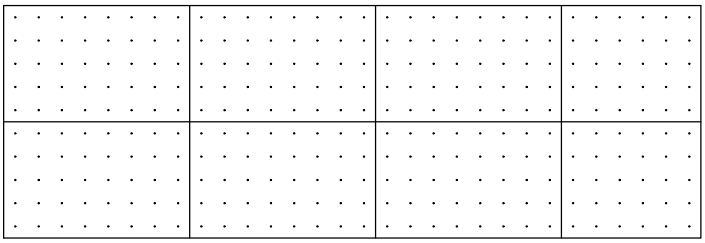

Time Savings

The particle-cluster method is indeed faster for small p, where p is the highest order of derivative in the truncated Taylor series. For a unit sphere discretized by 420 nodes, the particle-cluster method is faster than the particle-particle method for $p = 0$ and $p = 1$. For $p = 2$ the two methods are equal. For $p \geq 3$ the particle-particle method is faster.

The time savings is greater for increased nodes. For a sphere with 4200 nodes and $p = 1$, the time savings is approximately 10 seconds per iteration. For 9300 nodes the

www.manaraa.com

particle-cluster scheme is roughly 45 seconds faster per iteration. For the latter surface, one iteration takes approximately 10 minutes on an SGI Onyx2 Origin 2000 supercomputer. As the surfaces evolve through hundreds and often thousands of iterations, further time savings techniques are necessary for the particle-cluster method to be practical. The approach shows promise and is an area of further work.

3.7.4 Advancing the Surface

Once we have solved for the normal velocity, there are many ways to estimate $\Gamma(t+\Delta t)$. The easiest methods are explicit in nature, but require an extremely small time step. Instead we develop a semi-implicit scheme based on the Implicit Trapezoid method [9]:

$$\begin{aligned} \Gamma(0) &= \Gamma_0 \\ \Gamma(t+\Delta t) &= \Gamma(t) + \frac{\Delta t}{2}\left[n(t+\Delta t)V(t+\Delta t) + n(t)V(t)\right] . \end{aligned}$$

Thus we are averaging the advancement of Γ at times t and $t+\Delta t$. Instead of finding $n(t+\Delta t)$ we use a $\mathcal{O}(\Delta t^2)$ approximation, namely $n(t+\Delta t) \approx n(t) + \Delta t\, n_t(t)$. Since the normal to the surface $z = Ax + By + Cx^2 + Dxy + Ey^2$ is $\dfrac{(-A,-B,1)}{\sqrt{1+A^2+B^2}}$ we calculate

$$\frac{\partial n_i}{\partial t} = \frac{\partial n_i}{\partial A}\frac{\partial A}{\partial t} + \frac{\partial n_i}{\partial B}\frac{\partial B}{\partial t}$$

for $i = 1..3$, where $n = (n_1, n_2, n_3)$. Finding $\dfrac{\partial n_i}{\partial A}$ and $\dfrac{\partial n_i}{\partial B}$ is straightforward differentiation.

$$\begin{aligned} \frac{\partial n_1}{\partial A} &= -\frac{1+B^2}{(1+A^2+B^2)^{\frac{3}{2}}} , \\ \frac{\partial n_1}{\partial B} &= \frac{AB}{(1+A^2+B^2)^{\frac{3}{2}}} , \\ \frac{\partial n_2}{\partial A} &= \frac{AB}{(1+A^2+B^2)^{\frac{3}{2}}} , \\ \frac{\partial n_2}{\partial B} &= -\frac{1+A^2}{(1+A^2+B^2)^{\frac{3}{2}}} , \\ \frac{\partial n_3}{\partial A} &= -\frac{A}{(1+A^2+B^2)^{\frac{3}{2}}} , \\ \frac{\partial n_3}{\partial B} &= -\frac{B}{(1+A^2+B^2)^{\frac{3}{2}}} . \end{aligned}$$

Calculating $\dfrac{\partial A}{\partial t}$ and $\dfrac{\partial B}{\partial t}$ is more involved. Since we will need $\dfrac{\partial C}{\partial t}$, $\dfrac{\partial D}{\partial t}$, and $\dfrac{\partial E}{\partial t}$ in

www.manaraa.com

future approximations, we show how to find these quantities also. Now A, B, C, D, and E are found by solving the system of linear equations shown below. Recall $\|\mathbf{x}_i\|^2$ denotes $x_i^2 + y_i^2 + z_i^2$:

$$\begin{bmatrix} \sum_{i=1}^{8} \frac{x_i^2}{\|\mathbf{x}_i\|^2} & \sum_{i=1}^{8} \frac{x_i y_i}{\|\mathbf{x}_i\|^2} & \sum_{i=1}^{8} \frac{x_i^3}{\|\mathbf{x}_i\|^2} & \sum_{i=1}^{8} \frac{x_i^2 y_i}{\|\mathbf{x}_i\|^2} & \sum_{i=1}^{8} \frac{x_i y_i^2}{\|\mathbf{x}_i\|^2} \\ \sum_{i=1}^{8} \frac{x_i y_i}{\|\mathbf{x}_i\|^2} & \sum_{i=1}^{8} \frac{y_i^2}{\|\mathbf{x}_i\|^2} & \sum_{i=1}^{8} \frac{x_i^2 y_i}{\|\mathbf{x}_i\|^2} & \sum_{i=1}^{8} \frac{x_i y_i^2}{\|\mathbf{x}_i\|^2} & \sum_{i=1}^{8} \frac{y_i^3}{\|\mathbf{x}_i\|^2} \\ \sum_{i=1}^{8} \frac{x_i^3}{\|\mathbf{x}_i\|^2} & \sum_{i=1}^{8} \frac{x_i^2 y_i}{\|\mathbf{x}_i\|^2} & \sum_{i=1}^{8} \frac{x_i^4}{\|\mathbf{x}_i\|^2} & \sum_{i=1}^{8} \frac{x_i^3 y_i}{\|\mathbf{x}_i\|^2} & \sum_{i=1}^{8} \frac{x_i^2 y_i^2}{\|\mathbf{x}_i\|^2} \\ \sum_{i=1}^{8} \frac{x_i^2 y_i}{\|\mathbf{x}_i\|^2} & \sum_{i=1}^{8} \frac{x_i y_i^2}{\|\mathbf{x}_i\|^2} & \sum_{i=1}^{8} \frac{x_i^3 y_i}{\|\mathbf{x}_i\|^2} & \sum_{i=1}^{8} \frac{x_i^2 y_i^2}{\|\mathbf{x}_i\|^2} & \sum_{i=1}^{8} \frac{x_i y_i^3}{\|\mathbf{x}_i\|^2} \\ \sum_{i=1}^{8} \frac{x_i y_i^2}{\|\mathbf{x}_i\|^2} & \sum_{i=1}^{8} \frac{y_i^3}{\|\mathbf{x}_i\|^2} & \sum_{i=1}^{8} \frac{x_i^2 y_i^2}{\|\mathbf{x}_i\|^2} & \sum_{i=1}^{8} \frac{x_i y_i^3}{\|\mathbf{x}_i\|^2} & \sum_{i=1}^{8} \frac{y_i^4}{\|\mathbf{x}_i\|^2} \end{bmatrix} \begin{bmatrix} A \\ B \\ C \\ D \\ E \end{bmatrix} = \begin{bmatrix} \sum_{i=1}^{8} \frac{x_i z_i}{\|\mathbf{x}_i\|^2} \\ \sum_{i=1}^{8} \frac{y_i z_i}{\|\mathbf{x}_i\|^2} \\ \sum_{i=1}^{8} \frac{x_i^2 z_i}{\|\mathbf{x}_i\|^2} \\ \sum_{i=1}^{8} \frac{x_i y_i z_i}{\|\mathbf{x}_i\|^2} \\ \sum_{i=1}^{8} \frac{y_i^2 z_i}{\|\mathbf{x}_i\|^2} \end{bmatrix}.$$

We will demonstrate how to find $\frac{\partial A}{\partial t}$. The method for finding $\frac{\partial B}{\partial t}$, $\frac{\partial C}{\partial t}$, $\frac{\partial D}{\partial t}$, and $\frac{\partial E}{\partial t}$ is similar.

A depends on the components of the neighbors $\{x_i, y_i, z_i | i = 1 \dots 8\}$, so $\frac{\partial A}{\partial t} = \sum_{i=1}^{8} \left(\frac{\partial A}{\partial x_i} \frac{\partial x_i}{\partial t} + \frac{\partial A}{\partial y_i} \frac{\partial y_i}{\partial t} +$

By Cramer's rule [26],

$$A = \frac{\begin{vmatrix} \sum \frac{x_i^2}{\|\mathbf{x}_i\|^2} & \sum \frac{x_i y_i}{\|\mathbf{x}_i\|^2} & \sum \frac{x_i^3}{\|\mathbf{x}_i\|^2} & \sum \frac{x_i^2 y_i}{\|\mathbf{x}_i\|^2} & \sum \frac{x_i y_i^2}{\|\mathbf{x}_i\|^2} \\ \sum \frac{x_i y_i}{\|\mathbf{x}_i\|^2} & \sum \frac{y_i^2}{\|\mathbf{x}_i\|^2} & \sum \frac{x_i^2 y_i}{\|\mathbf{x}_i\|^2} & \sum \frac{x_i y_i^2}{\|\mathbf{x}_i\|^2} & \sum \frac{y_i^3}{\|\mathbf{x}_i\|^2} \\ \sum \frac{x_i^3}{\|\mathbf{x}_i\|^2} & \sum \frac{x_i^2 y_i}{\|\mathbf{x}_i\|^2} & \sum \frac{x_i^4}{\|\mathbf{x}_i\|^2} & \sum \frac{x_i^3 y_i}{\|\mathbf{x}_i\|^2} & \sum \frac{x_i^2 y_i^2}{\|\mathbf{x}_i\|^2} \\ \sum \frac{x_i^2 y_i}{\|\mathbf{x}_i\|^2} & \sum \frac{x_i y_i^2}{\|\mathbf{x}_i\|^2} & \sum \frac{x_i^3 y_i}{\|\mathbf{x}_i\|^2} & \sum \frac{x_i^2 y_i^2}{\|\mathbf{x}_i\|^2} & \sum \frac{x_i y_i^3}{\|\mathbf{x}_i\|^2} \\ \sum \frac{x_i y_i^2}{\|\mathbf{x}_i\|^2} & \sum \frac{y_i^3}{\|\mathbf{x}_i\|^2} & \sum \frac{x_i^2 y_i^2}{\|\mathbf{x}_i\|^2} & \sum \frac{x_i y_i^3}{\|\mathbf{x}_i\|^2} & \sum \frac{y_i^4}{\|\mathbf{x}_i\|^2} \end{vmatrix}}{\begin{vmatrix} \sum \frac{x_i z_i}{\|\mathbf{x}_i\|^2} & \sum \frac{x_i y_i}{\|\mathbf{x}_i\|^2} & \sum \frac{x_i^3}{\|\mathbf{x}_i\|^2} & \sum \frac{x_i^2 y_i}{\|\mathbf{x}_i\|^2} & \sum \frac{x_i y_i^2}{\|\mathbf{x}_i\|^2} \\ \sum \frac{y_i z_i}{\|\mathbf{x}_i\|^2} & \sum \frac{y_i^2}{\|\mathbf{x}_i\|^2} & \sum \frac{x_i^2 y_i}{\|\mathbf{x}_i\|^2} & \sum \frac{x_i y_i^2}{\|\mathbf{x}_i\|^2} & \sum \frac{y_i^3}{\|\mathbf{x}_i\|^2} \\ \sum \frac{x_i^2 z_i}{\|\mathbf{x}_i\|^2} & \sum \frac{x_i^2 y_i}{\|\mathbf{x}_i\|^2} & \sum \frac{x_i^4}{\|\mathbf{x}_i\|^2} & \sum \frac{x_i^3 y_i}{\|\mathbf{x}_i\|^2} & \sum \frac{x_i^2 y_i^2}{\|\mathbf{x}_i\|^2} \\ \sum \frac{x_i y_i z_i}{\|\mathbf{x}_i\|^2} & \sum \frac{x_i y_i^2}{\|\mathbf{x}_i\|^2} & \sum \frac{x_i^3 y_i}{\|\mathbf{x}_i\|^2} & \sum \frac{x_i^2 y_i^2}{\|\mathbf{x}_i\|^2} & \sum \frac{x_i y_i^3}{\|\mathbf{x}_i\|^2} \\ \sum \frac{y_i^2 z_i}{\|\mathbf{x}_i\|^2} & \sum \frac{y_i^3}{\|\mathbf{x}_i\|^2} & \sum \frac{x_i^2 y_i^2}{\|\mathbf{x}_i\|^2} & \sum \frac{x_i y_i^3}{\|\mathbf{x}_i\|^2} & \sum \frac{y_i^4}{\|\mathbf{x}_i\|^2} \end{vmatrix}}.$$

We use this formula for A to find $\frac{\partial A}{\partial x_i}$, $\frac{\partial A}{\partial y_i}$, and $\frac{\partial A}{\partial z_i}$ for $i = 1 \dots 8$. This is not as tedious as it seems, for we can reduce the 5×5 determinants to the sum of constant multiples of 4×4, 3×3, and finally 2×2 determinants, the majority of which are repeated. Details are

www.manaraa.com

omitted.

The last derivatives to find are $\frac{\partial x_i}{\partial t}$, $\frac{\partial y_i}{\partial t}$, and $\frac{\partial z_i}{\partial t}$ for $i = 1 \ldots 8$. This is simply the normal velocity of (x_i, y_i, z_i) multiplied by the x, y, or z coordinate of the normal at (x_i, y_i, z_i).

Thus we have found the necessary quantities to calculate $n(t + \Delta t) \approx n(t) + \Delta t\, n_t(t)$.

We now find a $\mathcal{O}(\Delta t)$ approximation of $V(t+\Delta t)$. Now V is found by solving the matrix equation

$$\begin{bmatrix} I_1 & \frac{\Delta_2}{|\mathbf{x}_1-\mathbf{x}_2|} & \frac{\Delta_3}{|\mathbf{x}_1-\mathbf{x}_3|} & \cdots & \frac{\Delta_{N-1}}{|\mathbf{x}_1-\mathbf{x}_{N-1}|} & \frac{\Delta_N}{|\mathbf{x}_1-\mathbf{x}_N|} & 1 \\ \frac{\Delta_1}{|\mathbf{x}_2-\mathbf{x}_1|} & I_2 & \frac{\Delta_3}{|\mathbf{x}_2-\mathbf{x}_3|} & \cdots & \frac{\Delta_{N-1}}{|\mathbf{x}_2-\mathbf{x}_{N-1}|} & \frac{\Delta_N}{|\mathbf{x}_2-\mathbf{x}_N|} & 1 \\ \frac{\Delta_1}{|\mathbf{x}_3-\mathbf{x}_1|} & \frac{\Delta_2}{|\mathbf{x}_3-\mathbf{x}_2|} & I_3 & \cdots & \frac{\Delta_{N-1}}{|\mathbf{x}_3-\mathbf{x}_{N-1}|} & \frac{\Delta_N}{|\mathbf{x}_3-\mathbf{x}_N|} & 1 \\ \vdots & \vdots & \vdots & \ddots & \vdots & \vdots & \vdots \\ \frac{\Delta_1}{|\mathbf{x}_{N-1}-\mathbf{x}_1|} & \frac{\Delta_2}{|\mathbf{x}_{N-1}-\mathbf{x}_2|} & \frac{\Delta_3}{|\mathbf{x}_{N-1}-\mathbf{x}_3|} & \cdots & I_{N-1} & \frac{\Delta_N}{|\mathbf{x}_{N-1}-\mathbf{x}_N|} & 1 \\ \frac{\Delta_1}{|\mathbf{x}_N-\mathbf{x}_1|} & \frac{\Delta_2}{|\mathbf{x}_N-\mathbf{x}_2|} & \frac{\Delta_3}{|\mathbf{x}_N-\mathbf{x}_3|} & \cdots & \frac{\Delta_{N-1}}{|\mathbf{x}_N-\mathbf{x}_{N-1}|} & I_N & 1 \\ \Delta_1 & \Delta_2 & \Delta_3 & \cdots & \Delta_{N-1} & \Delta_N & 0 \end{bmatrix} \begin{bmatrix} V_1 \\ V_2 \\ V_3 \\ \vdots \\ V_{N-1} \\ V_N \\ c' \end{bmatrix} = \begin{bmatrix} 4\pi\kappa_1 \\ 4\pi\kappa_2 \\ 4\pi\kappa_3 \\ \vdots \\ 4\pi\kappa_{N-1} \\ 4\pi\kappa_N \\ 0 \end{bmatrix}.$$

We find a $\mathcal{O}(\Delta t^2)$ approximations of $\kappa(t + \Delta t)$, namely $\kappa(t + \Delta t) \approx \kappa(t) + \Delta t\, \kappa_t(t)$. We then solve the above system of equations for $V(t + \Delta t)$. Note that this will only be a $\mathcal{O}(\Delta t)$ approximation since all entries in the coefficient matrix are at time t.

We now calculate $\frac{\partial \kappa(x)}{\partial t}$. We use the chain rule. Recall $\kappa = \frac{C + E + EA^2 + CB^2 - ADB}{(1 + A^2 + B^2)^{\frac{3}{2}}}$ where $z = Ax + By + Cx^2 + Dxy + Ey^2$ is the equation of the surface. Then $\frac{\partial \kappa}{\partial t} = \frac{\partial \kappa}{\partial A}\frac{\partial A}{\partial t} + \frac{\partial \kappa}{\partial B}\frac{\partial B}{\partial t} + \frac{\partial \kappa}{\partial C}\frac{\partial C}{\partial t} + \frac{\partial \kappa}{\partial D}\frac{\partial D}{\partial t} + \frac{\partial \kappa}{\partial E}\frac{\partial E}{\partial t}$.

It is straightforward to calculate the following:

www.manaraa.com

$$
\begin{aligned}
\frac{\partial \kappa}{\partial A} &= \frac{(2EA - DB)(1 + A^2 + B^2) - 3A(C + E + EA^2 + CB^2 - ADB)}{(1 + A^2 + B^2)^{\frac{5}{2}}} \\
\frac{\partial \kappa}{\partial B} &= \frac{(2CB - AD)(1 + A^2 + B^2) - 3B(C + E + EA^2 + CB^2 - ADB)}{(1 + A^2 + B^2)^{\frac{5}{2}}} \\
\frac{\partial \kappa}{\partial C} &= \frac{1 + B^2}{(1 + A^2 + B^2)^{\frac{3}{2}}} \\
\frac{\partial \kappa}{\partial D} &= \frac{-AB}{(1 + A^2 + B^2)^{\frac{3}{2}}} \\
\frac{\partial \kappa}{\partial E} &= \frac{1 + A^2}{(1 + A^2 + B^2)^{\frac{3}{2}}}.
\end{aligned}
$$

We found $\frac{\partial A}{\partial t}$, $\frac{\partial B}{\partial t}$, $\frac{\partial C}{\partial t}$, $\frac{\partial D}{\partial t}$, and $\frac{\partial E}{\partial t}$ previously. Thus we have an approximation of $\kappa(t + \Delta t)$.

www.manaraa.com

www.manaraa.com

Chapter 4

Validation of Scheme

To validate the scheme we look for properties that the solution should have, namely conservation of volume, non-increasing area, and the tendency of Γ to become spherical, and see if the numerical solution exhibits these behaviors. If anomalies occur, we analyze the limitations of the scheme and what restrictions, if any, need to be placed on node spacing, time step size (Δt), etc.

A problem that occurs during the numerical evolution of surfaces is the bunching, or clustering, of nodes in areas of high mean curvature. With the torus, which is especially prone to this bunching on its inner perimeter, a redistribution scheme alleviates the bunching. Other means of improving the scheme specifically involving the torus include taking advantage of symmetry and getting past the point of topology change. We explain the algorithms and compare actual and predicted behavior before and after these adaptations.

We also can find the analytic solution to the system of boundary integral equations for special situations; namely, the single sphere, spheres of equal radii, and concentric spheres. We compare the analytic solutions to the numerical ones and discuss the correlation.

4.1 Volume Conservation

A binary alloy will preserve the amount of each species as it undergoes the coarsening process as described in the Introduction. The mathematical model also obeys preservation of species. Recall that Ω is a bounded and simply connected domain in $\mathbb{R}^3$ and Γ_0 is a finite collection

www.manaraa.com

of smooth, simple closed surfaces in the domain. We follow the convention that $V > 0$ if the surface of a sphere is expanding. Letting $Vol(t)$ denote the volume enclosed by $\Gamma(t)$, we have by Green's First Identity

$$\frac{d}{dt}Vol(t) = \int_{\Gamma(t)} V dS = \int_{\Gamma(t)} \left[\frac{\partial u}{\partial n}\right] dS = -\int_{\partial\Omega} \frac{\partial u}{\partial n}\, dS + \int_{\Omega\setminus\Gamma(t)} \Delta u\, d\mathbf{x} = 0$$

Hence the volume is constant. This result is proved for the two dimensional case in [2, 13, 46] with the argument given for arbitrary dimensions in [17]. In [18], $Vol(\cdot)$ is shown to belong to $C^\infty((0,T),\mathbb{R})$. If $\Omega = \mathbb{R}^3$ and $\nabla u = \mathcal{O}\left(\frac{1}{|x|^3}\right)$ as $|x| \to \infty$, we have for a ball B_R of radius R sufficiently large

$$\frac{d}{dt}Vol(t) = -\int_{\partial B_R} \frac{\partial u}{\partial n}\, dS = 4\pi R^2 \mathcal{O}\left(\frac{1}{R^3}\right) = \mathcal{O}\left(\frac{1}{R}\right) \to 0 \text{ as } R \to \infty$$

4.2 Non-increasing Area

An important question to ask about the evolution of the interface Γ is what happens to surface area over time. To find out what the model predicts, we take the derivative of the area $A(t)$ with respect to time and utilize Green's First Identity. We follow the convention that $\kappa < 0$ for a sphere. We have

$$\begin{aligned}
\frac{1}{2}\frac{d}{dt}A(t) = -\int_{\Gamma(t)} \kappa V dS &= -\int_{\Gamma(t)} u \left[\frac{\partial u}{\partial n}\right] dS \\
&= \int_{\partial\Omega} u\frac{\partial u}{\partial n}\, dS - \int_{\Omega\setminus\Gamma(t)} \left(u\triangle u + |\nabla u|^2\right) d\mathbf{x} \\
&= -\int_{\Omega\setminus\Gamma(t)} |\nabla u|^2 d\mathbf{x} \\
&\leq 0.
\end{aligned}$$

Thus area is non-increasing. This is proved for the two dimensional case in [2, 13, 46]. In [17] the result is proved for arbitrary dimensions. In [18], $A(\cdot)$ is shown to belong to $C^\infty((0,T),\mathbb{R})$. If $\Omega = \mathbb{R}^3$ and $\nabla u = \mathcal{O}\left(\frac{1}{|x|^3}\right)$ as $|x| \to \infty$, we have for a ball B_R of radius R sufficiently large

$$\frac{1}{2}\frac{d}{dt}A(t) = \int_{\partial B_R} u\frac{\partial u}{\partial n}\, dS - \int_{\Omega\setminus\Gamma(t)} |\nabla u|^2 d\mathbf{x} = \mathcal{O}\left(\frac{1}{R}\right) - \int_{\Omega\setminus\Gamma(t)} |\nabla u|^2 d\mathbf{x} \leq 0 \text{ as } R \to \infty.$$

The above calculations also show that particles will tend towards spheres, since $\frac{d}{dt}A(t) = 0 \iff \nabla u = 0 \iff u = k$ for some constant k. Then $\kappa = k$ and $\Gamma(t)$ is the surface of a

www.manaraa.com

sphere of radius $-\frac{1}{k}$.

4.3 Numerical Volume and Area Results

4.3.1 Ellipsoid

We use an ellipsoid $\frac{x^2}{a^2}+\frac{y^2}{b^2}+\frac{z^2}{c^2}=1$ with $a=1, b=1.5$, and $c=2$ discretized by 420 nodes with $\Delta t = 0.0005$. As shown below, it indeed tends towards a sphere.

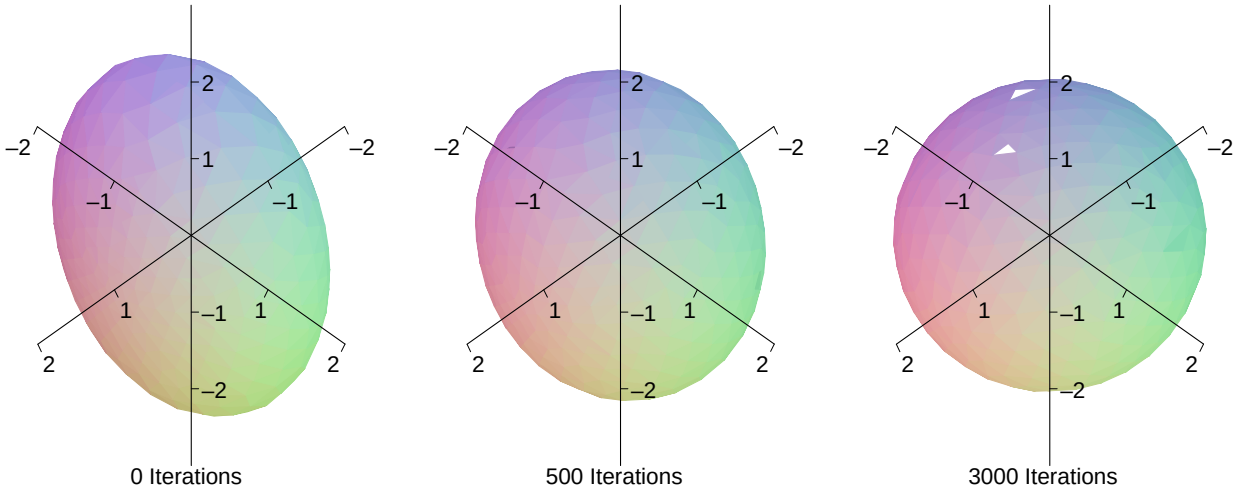

The volume enclosed by the surface $\frac{x^2}{a^2}+\frac{y^2}{b^2}+\frac{z^2}{c^2}=1$ is $\frac{4}{3}\pi abc$. An ellipsoid with $a=1, b=1.5$, and $c=2$ has volume $4\pi \approx 12.57$. We track the volume enclosed by the discretized surface as it evolves over time.

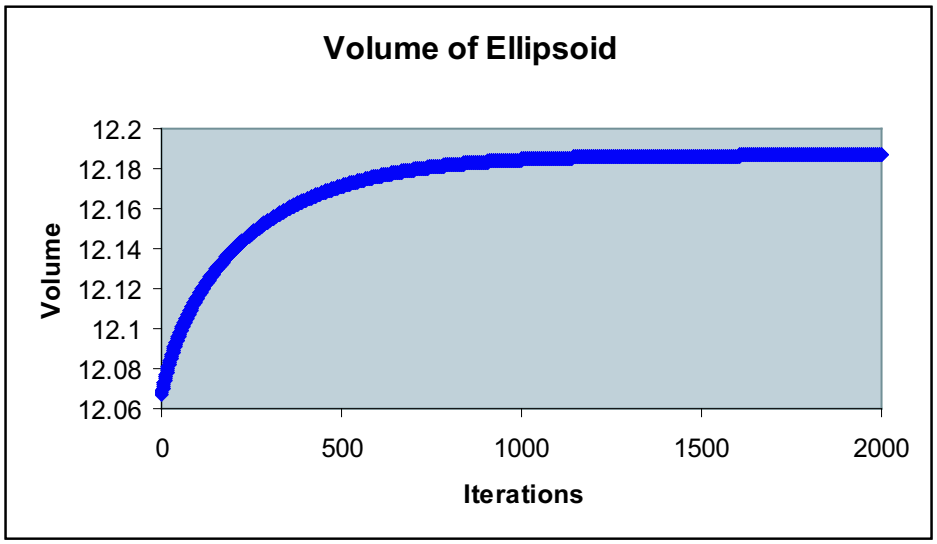

www.manaraa.com

The volume initially increases until stabilizing after about 700 iterations. The increase is about 0.12, or 1% of the ellipsoid's volume. We must bear in mind that the volumes themselves are estimates: the estimate of the initial volume of the ellipsoid is 12.07 compared to the actual value of 12.57, a discrepancy of 0.5. Thus a deviation in ideally constant volume of 0.12 not unreasonable, and the numerical model behaves as predicted.

The area of the surface $\frac{x^2}{a^2} + \frac{y^2}{b^2} + \frac{z^2}{c^2} = 1$ does not have a simple formula, but can be calculated numerically for given a, b, c. An ellipsoid with $a = 1, b = 1.5$, and $c = 2$, has surface area 27.89 as calculated using Maple®. The chart below shows the ellipsoid's area versus iterations.

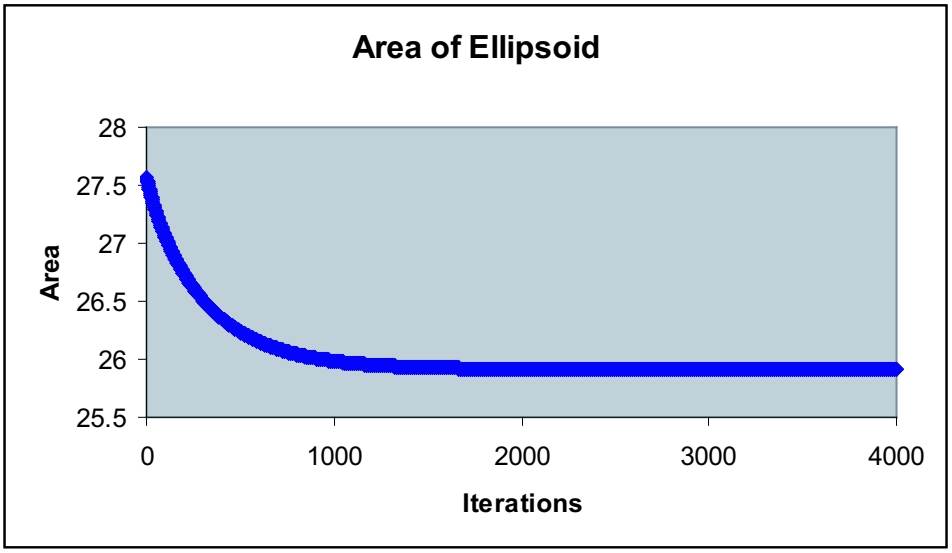

The surface area decreases, as hoped. We can predict the surface area of the sphere of eventual equilibrium. Since the volume of the initial ellipsoid is $\frac{4}{3}\pi(1)\left(\frac{3}{2}\right)(2) = 4\pi \approx 12.57$, the radius of the sphere can be found using $\frac{4}{3}\pi r^3 = 4\pi$. Then the predicted surface area of the sphere is $4\pi r^2 = 4\pi(\sqrt[3]{3})^2 \approx 26.14$. The numerical surface area begins at 27.57, rather than the actual value of 27.89, and after 3000 iterations has stabilized at 25.91, which is 0.23 less than the projected value. This error is quite reasonable.

www.manaraa.com

4.3.2 Multiple Spheres of Unequal Radii

As multiple spheres with differing radii evolve over time, larger spheres absorb the volume of the smaller spheres. The spheres below have radii of 1, 1.1, and 1.2 and centers $(2, 0, 0)$, $(-2, 0, 0)$, and $(0, 4, 0)$, respectively. The two smaller spheres are discretized with 300 nodes while the largest sphere has 420 nodes. Here $\Delta t = 0.0004$.

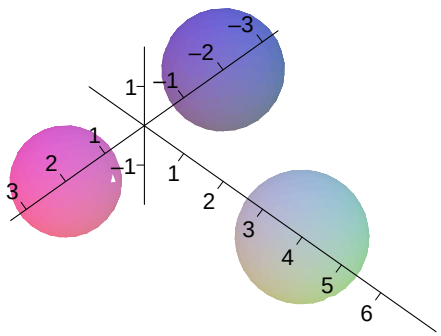

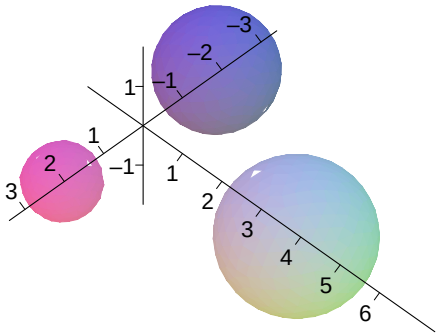

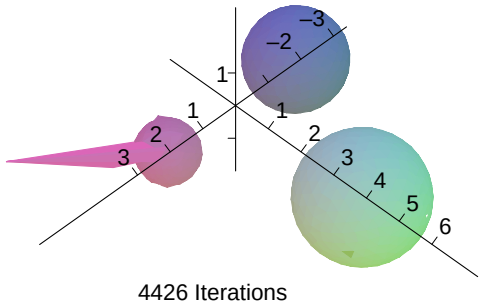

The smallest sphere "blows" at 4426 iterations as a result of extremely high normal velocities. However, the model actually loses its validity long before, as shown by the graph of the volume.

www.manaraa.com

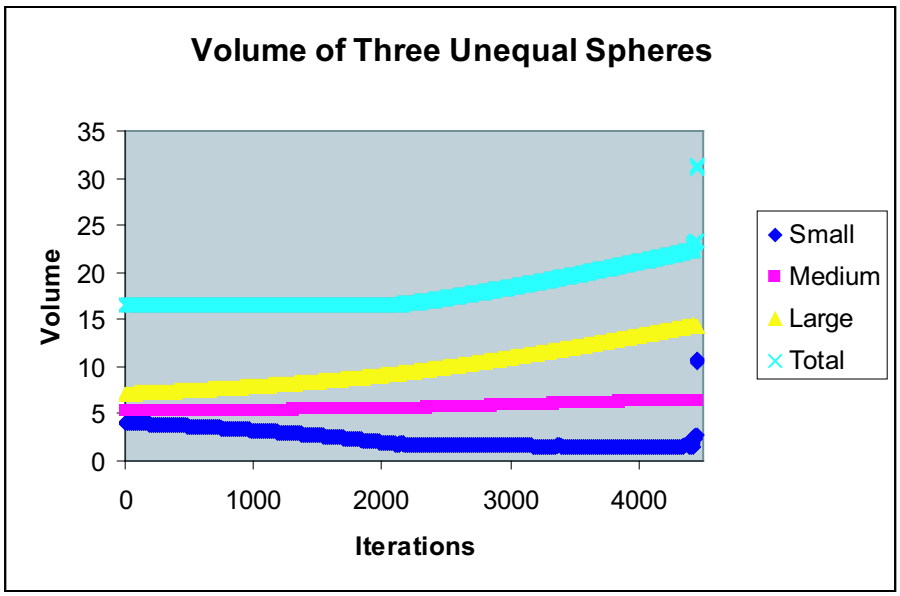

The total volume stays within a hundredth of the initial value until about 2100 iterations, or $t = 0.84$, when it begins gradually increasing. The surface area also decreases as desired until about 2100 iterations.

Two ways to prolong the valid numerical evolution of these spheres are reducing the time step and re-discretizing the spheres so that the largest sphere has more nodes and the smallest sphere has fewer, as problems occur when nodes become too crowded.

The latter is done by approximating the evolved sphere by averaging the distance from each node to the centroid. We take this average and use it as the radius of a new sphere. The new spheres are discretized with more or less nodes as appropriate for their radii. After regenerating the spheres there is a difference in volume, as the spheres lose their shapes over time. Evolving the new spheres allow us to retain the validity of the model longer.

Decreasing the time step allows us to extend the scheme even longer than rediscretizing. However, there is a large run time cost.

Combining the two techniques by reducing the time step size and regenerating the smallest surface with fewer nodes gives about the same total time with less run time than just reducing the time step. However, we still have the loss of accuracy when we approximate the surfaces, although this could be overcome by a more sophisticated approximation scheme.

www.manaraa.com

We conclude that a careful watch on the volume is necessary, and that the validity of the scheme may be prolonged by reducing the time step and/or rediscretizing shrinking surfaces.

4.3.3 Torus

Shown below is a torus with large radius 2 and small radius 1 discretized with 400 nodes. We use $\Delta t = 0.005$. The surface indeed tends to a sphere, as the both the outer and inner perimeters decrease.

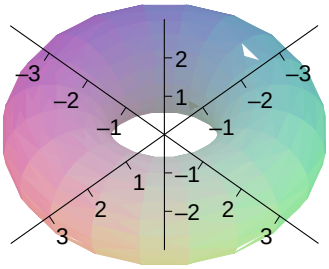

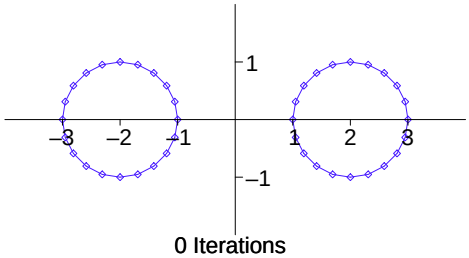

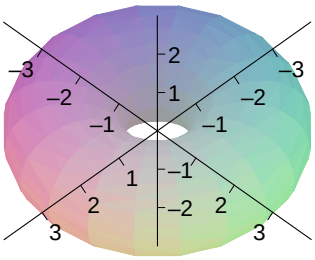

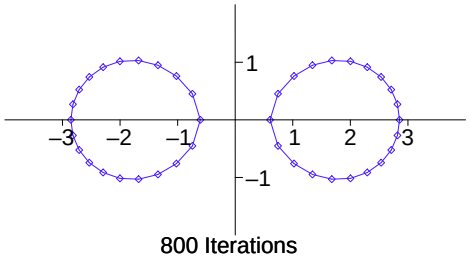

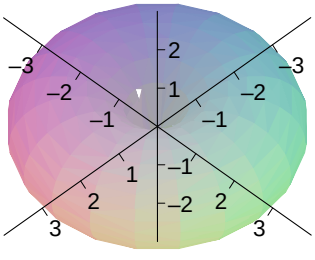

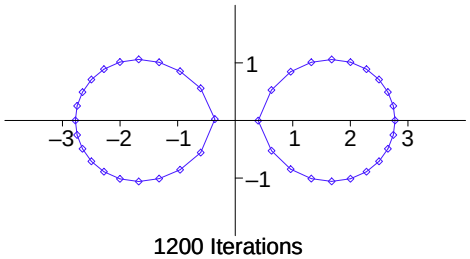

The exact volume of the torus is $2\pi^2 Rr^2 \approx 39.48$. Unfortunately the volume of the discretized torus bears no resemblance of being constant. Instead it steadily increases.

www.manaraa.com

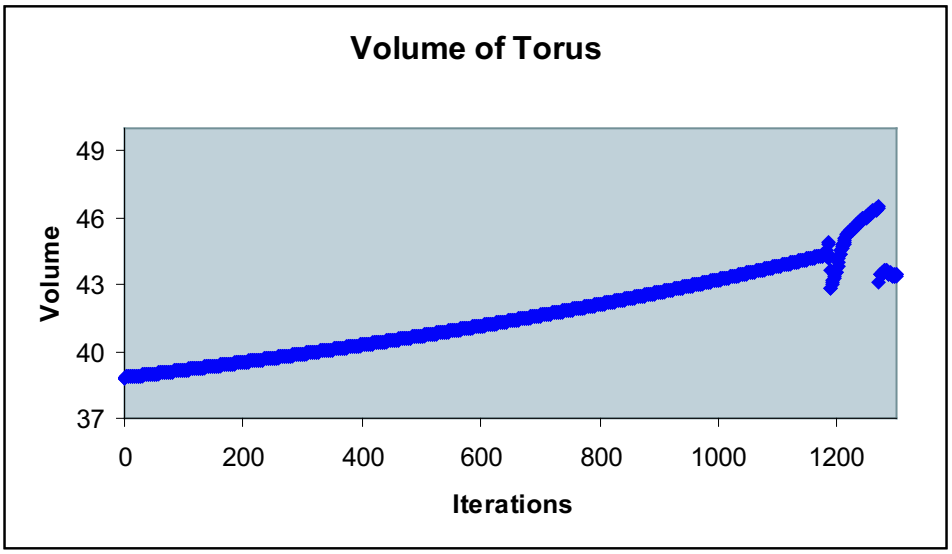

An adaptation of the scheme is necessary. An examination of cross sections reveals that nodes are bunching on the outer perimeter and the opposite is occurring on the inner perimeter. This behavior is likely a result of the higher normal velocities that result from higher mean curvatures on the inner perimeter. Hence we utilize a redistribution scheme to alleviate bunching with the goal to keep the volume constant.

4.3.4 Torus with Redistribution

We use a redistribution technique adapted from the two-dimensional version found in X. Deng's Master's thesis [16]. We redistribute by taking three nodes, say A, B, and C, and moving node B along the unique circle passing through the three nodes so B is equidistant from A and C. The new position of B is

$$\frac{(\|B-C\|-\|B-A\|)\left(\frac{\overrightarrow{B-A}}{\|B-A\|}+\frac{\overrightarrow{C-B}}{\|C-B\|}\right)}{2\left(1+\frac{\overrightarrow{B-A}}{\|B-A\|}\cdot\frac{\overrightarrow{C-B}}{\|C-B\|}\right)},$$

which is derived in two-dimensions in [16] and the vector argument is almost exactly the same for three-dimensions.

www.manaraa.com

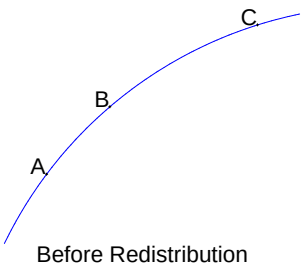

Before Redistribution

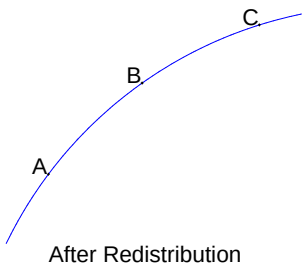

After Redistribution

To implement this redistribution for the torus, we take the top half of one side of a radial slice. The outermost node is assumed to lie on the xy-plane.

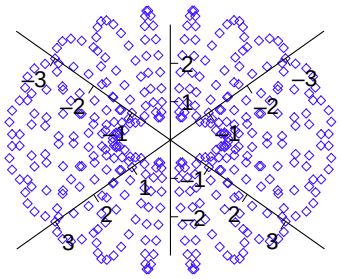
Discretized Torus

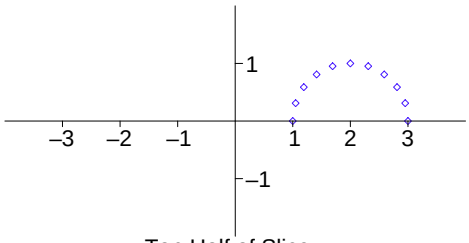
Top Half of Slice

We perform the above centering procedure beginning with the outermost three nodes and progressing inward. The we utilize the symmetry of the torus with respect to the xy-plane reflect the top half to the bottom half. We redistribute each slice in this manner after every iteration. The result for the torus with large radius 2 and small radius 1 discretized with 400 nodes, $\Delta t = 0.005$, is shown below.

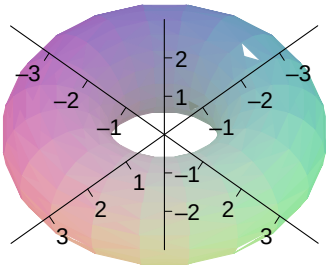
0 Iterations

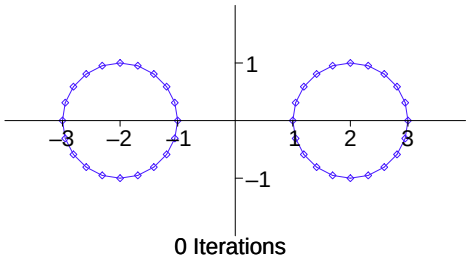
0 Iterations

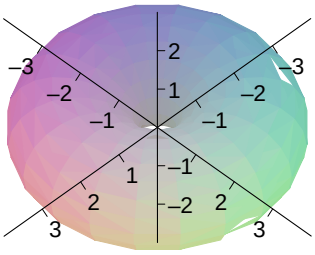
1100 Iterations

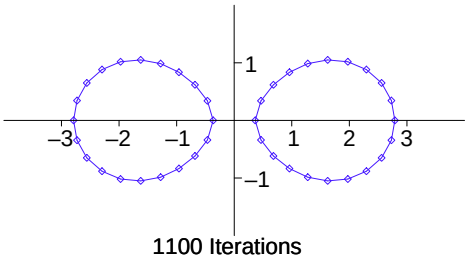
1100 Iterations

www.manaraa.com

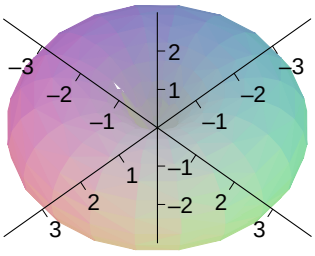

1121 Iterations

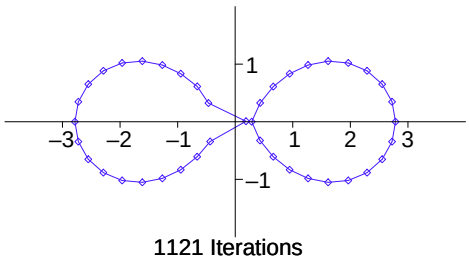

1121 Iterations

The volume is fairly close to being constant until about 1100 iterations. We would like to see the nodes on the inner perimeter converge closer to the origin before we lose validity, so we next try utilizing the radial symmetry of the torus.

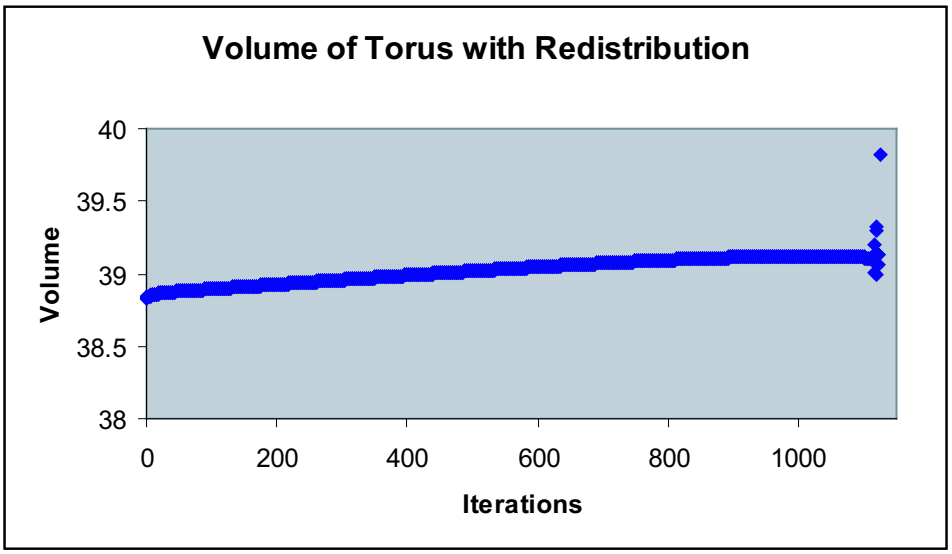

4.3.5 Torus with Symmetry and Redistribution

Given the slice lying on the xz-axis with x positive, we generate the rest of the torus by taking each node on this slice, say (x, y, z), and for $j = 1..N$ where N is the number of radial slices, generate the nodes $\left(x\cos\left(\frac{2\pi j}{N}\right), y\sin\left(\frac{2\pi j}{N}\right), z\right)$. Again we evolve a torus with large radius 2 and small radius 1 discretized with 400 nodes, $\Delta t = 0.005$. Here $N = 20$.

www.manaraa.com

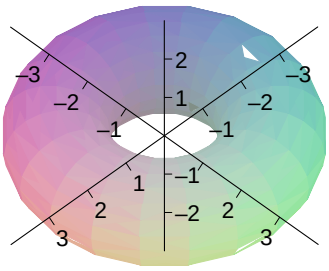

0 Iterations

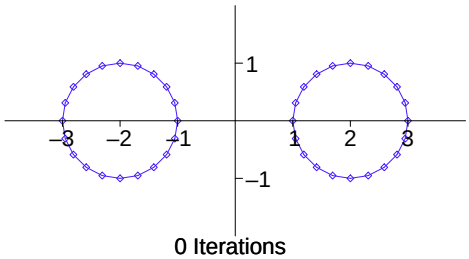

0 Iterations

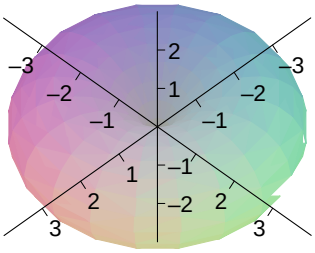

1200 Iterations

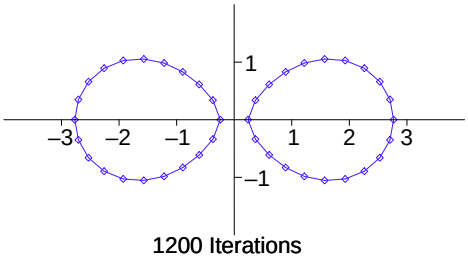

1200 Iterations

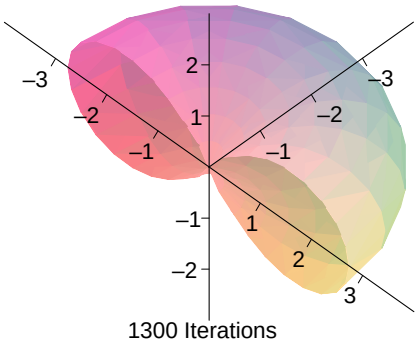

1300 Iterations

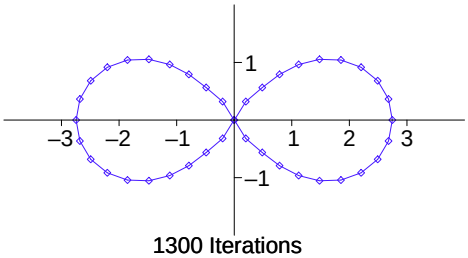

1300 Iterations

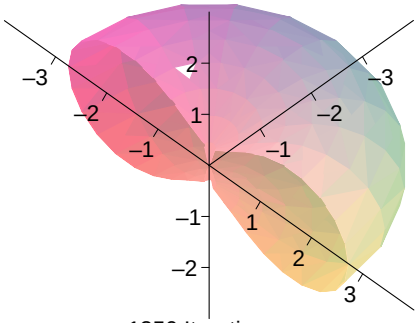

1350 Iterations

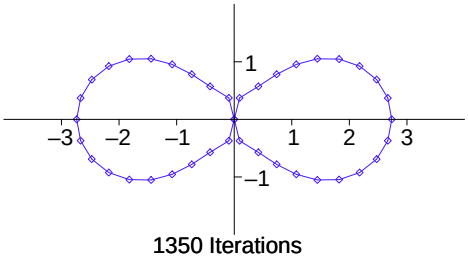

1350 Iterations

The inner perimeter shrinks to zero and the torus pushes up against itself. The volume starts to deviate at this critical evolutionary phase.

www.manaraa.com

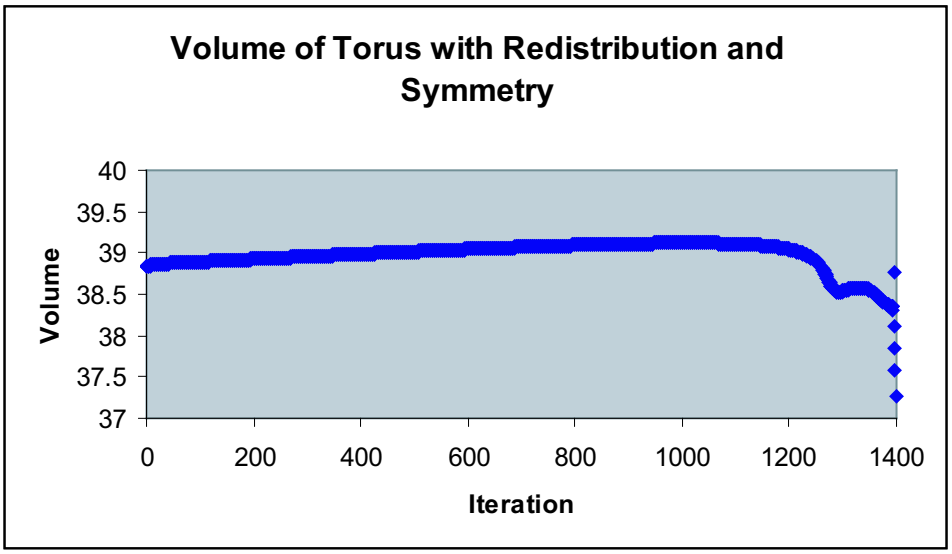

Further adaptation is needed to take the torus to the point where it is no longer a deformed torus but a deformed sphere.

4.3.6 Torus Taken Past Topology Change

To take the torus past its topology change, we project a sphere onto the torus when the innermost nodes reach the origin. Because the discretizations of the torus and sphere are quite difference, we need to have a surface to project the sphere onto. First we take the nodes lying on the xz-plane with z positive and use linear interpolation to form a curve. A cubic spline interpolation would seem to follow the round surface of a torus better, but there are unwanted oscillations with when a node is almost directly above another, like the outermost nodes.

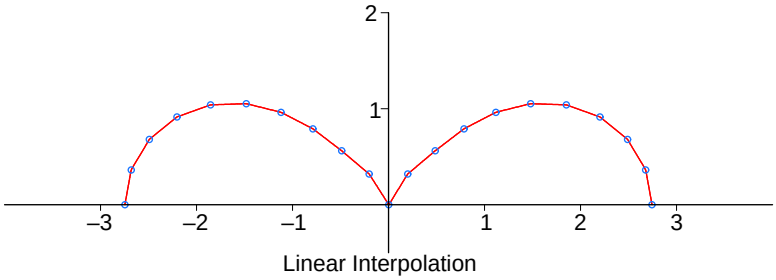

The outermost node on the positive x-axis determines the radius of the sphere that will be projected onto the torus. Once this sphere is generated, we take each node, say (x, y, z) and find its length. We find the equation of the interpolated line above $(\sqrt{x^2 + y^2 + z^2}, 0)$

www.manaraa.com

on the xz-plane, say $y = mx + b$. The projected node will be $(x, y, \pm(mx + b))$ with the sign determined by z. Below we take the previous torus and project a sphere with 560 nodes onto it. The projected sphere will not pinch at the origin because the discretization of the sphere has no nodes on the z-axis.

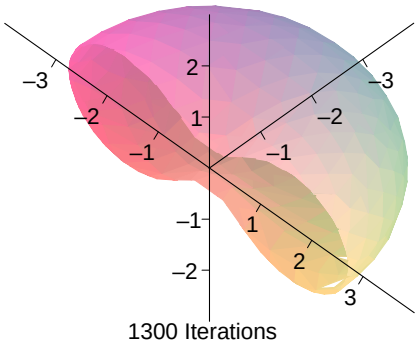

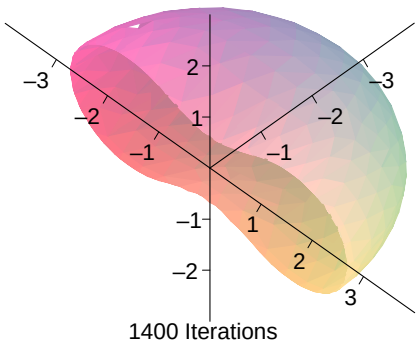

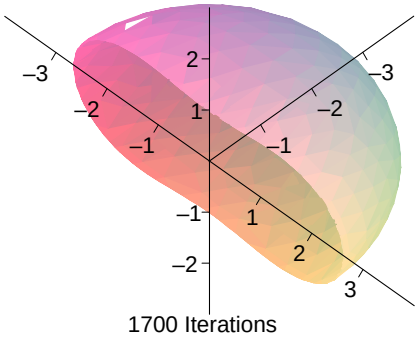

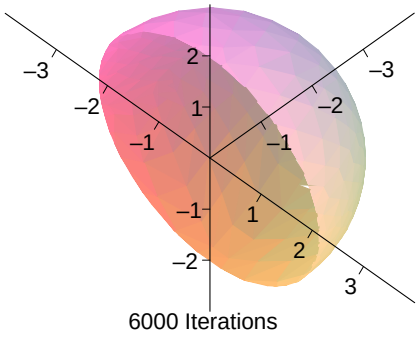

The volume has a jump when the surface is rediscretized; however, the projected sphere should have a lightly larger volume because of the missing pinch at the origin. This is explained partly by the volume lost through linear interpolation. Also, the volume is only estimated, and the volume chart can give us qualitative information but not precise quantitative information.

www.manaraa.com

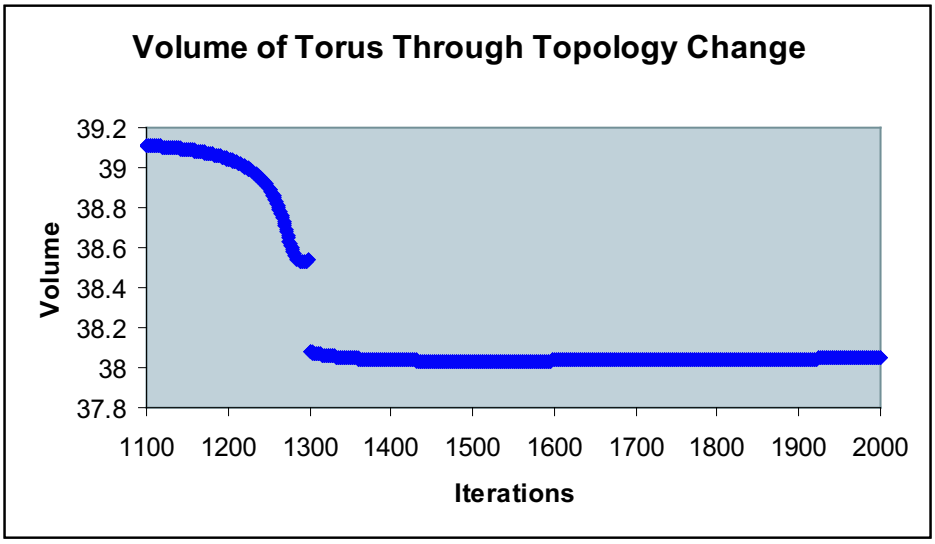

The area behaves as desired, namely it decreases until the surface stabilizes to a sphere, where it is constant.

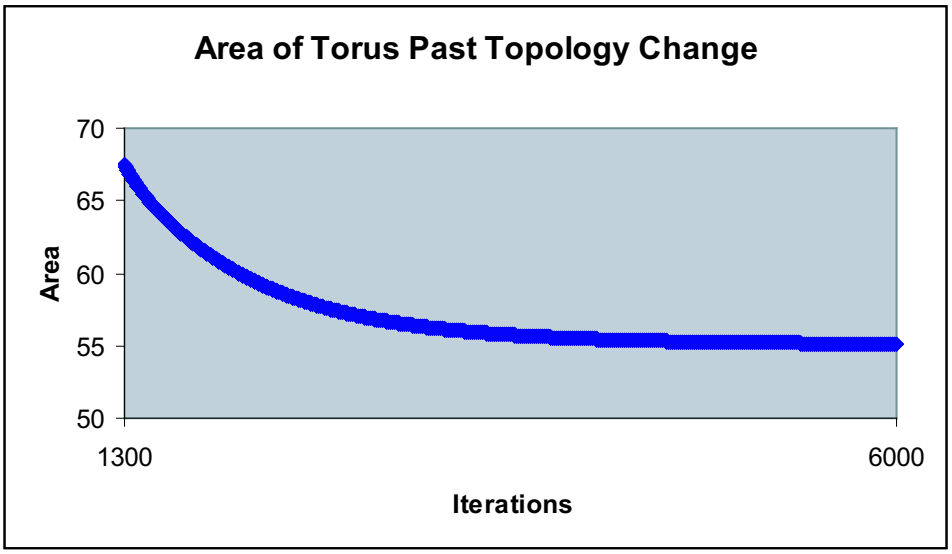

Thus the torus exhibits good behavior provided we make adaptations to keep nodes distributed evenly and to take it past its topology change.

4.3.7 Distorted Sphere

All the surfaces under consideration up to this point have had some sort of symmetry. We would like to see if volume is constant and surface area decreases for non-symmetrical surfaces. Below we have a distorted sphere with 420 nodes evolved through 1000 iterations

www.manaraa.com

using $\Delta t = 0.0008$.

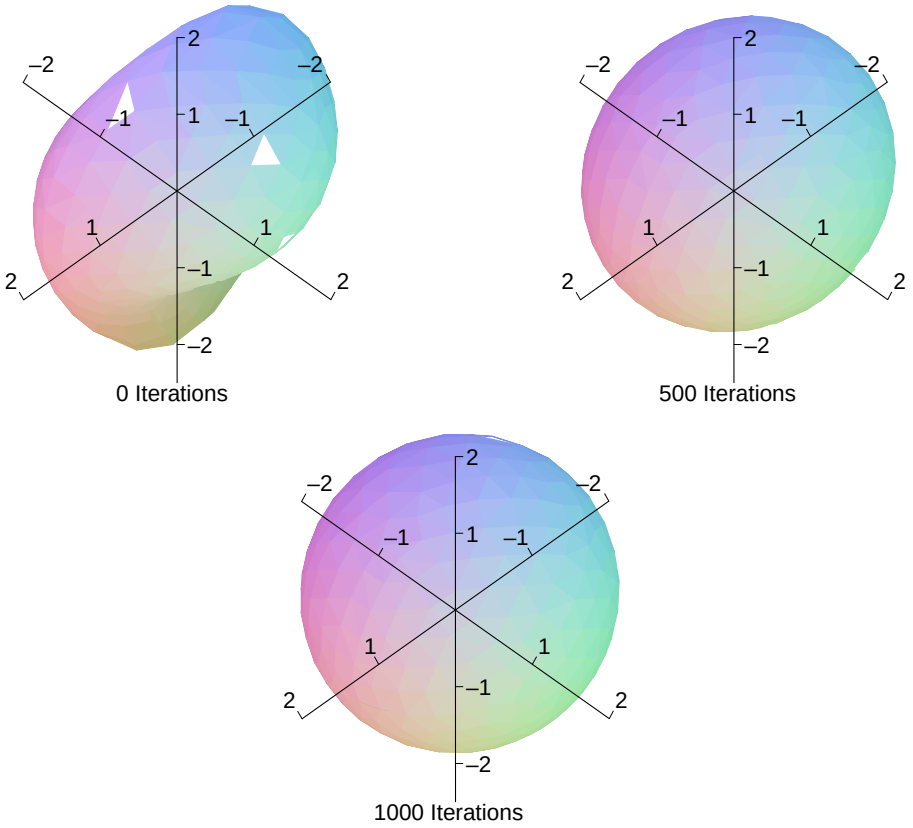

The volume is initially 13.03 and deviates only 0.12 from that amount after 1000 iterations. The area decreases but eventually stabilizes as the surface becomes spherical. Also of interest are the maximum and minimum values of the normal velocity.

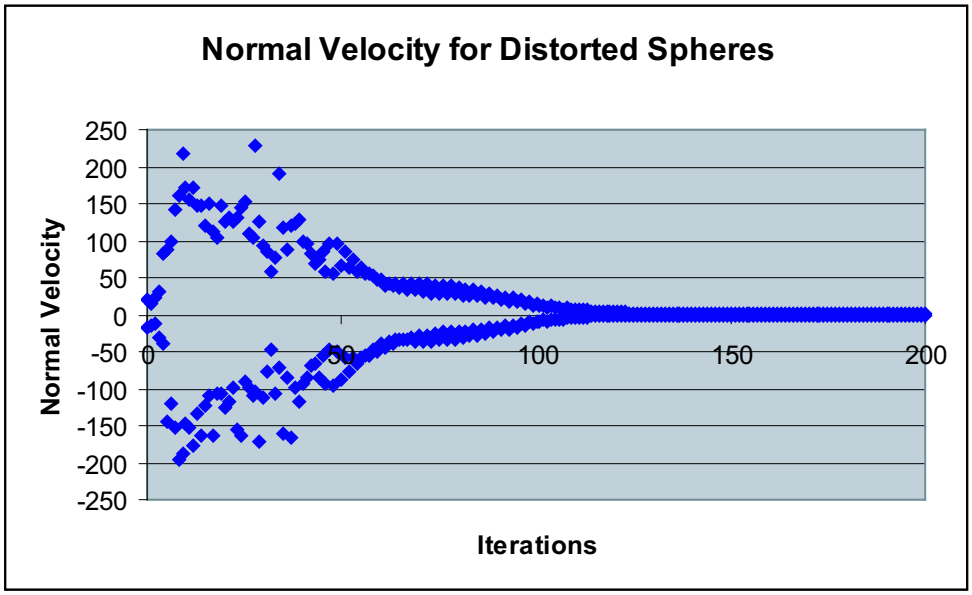

www.manaraa.com

The values quickly tend to zero as the surface tends to a sphere. The maximum and minimum values of mean curvature for each iteration also tend towards the negative reciprocal of the radius of the eventual sphere.

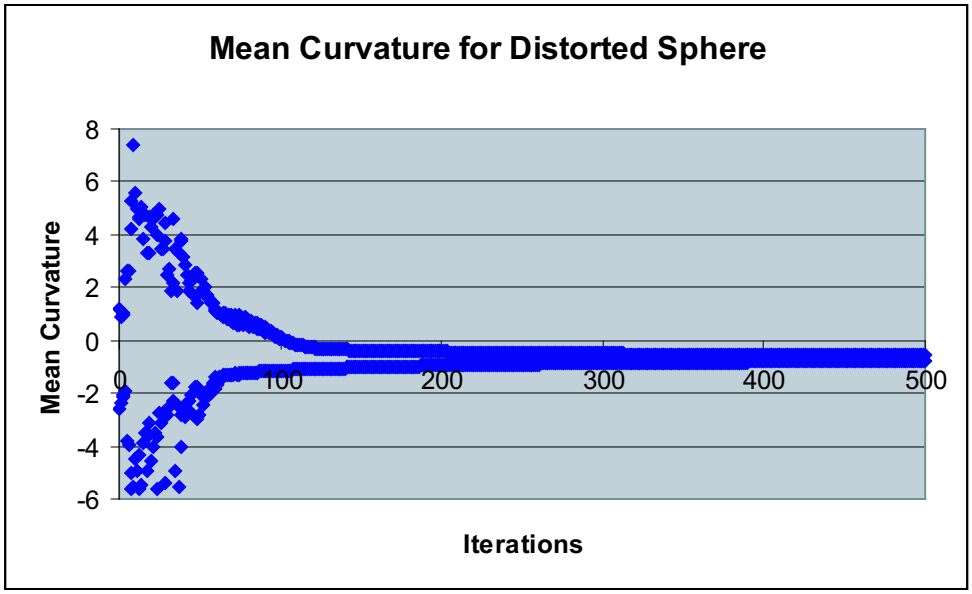

Thus the distorted sphere is an example of a non-symmetrical surface that behaves as desired.

4.4 Analytic Solution

We find the exact solution to Mullins-Sekerka flow for a single sphere, spheres of equal radii, and concentric spheres.

4.4.1 Sphere

For a sphere of radius R, $u = -\frac{1}{R}$ satisfies

$$\begin{aligned} \Delta u &= 0 && \text{in } R^3 \backslash \Gamma(t) \\ u &= \kappa && \text{on } \Gamma(t) \\ \nabla u &= \mathcal{O}\left(\frac{1}{|x|^3}\right) && \text{as } |x| \to \infty. \end{aligned}$$

where κ is the mean curvature with the convention that $\kappa < 0$ for a sphere. By uniqueness of smooth solutions to the Mullins-Sekerka problem [1] this is the only possible solution to

www.manaraa.com

$$
\begin{aligned}
&\text{i)} \quad \Delta u(\cdot, t) = 0 && \text{in } \mathbb{R}^3 \backslash \Gamma(t) \\
&\text{ii)} \quad \nabla u = \mathcal{O}\left(\frac{1}{|x|^3}\right) && \text{as } |x| \to \infty \\
&\text{iii)} \quad u = \kappa && \text{on } \Gamma(t) \\
&\text{iv)} \quad \left[\frac{\partial u}{\partial n}\right]_{\Gamma(t)} = V && \text{on } \Gamma(t) \\
&\text{v)} \quad \Gamma(0) = \Gamma_0
\end{aligned}
$$

The normal velocity V is uniquely determined by Theorem 2.4.1. Since the sum of the outward normal derivatives $\left[\frac{\partial u}{\partial n}\right]_{\Gamma(t)} = 0$, the normal velocity V is 0.

The model predicts that the surface area of a sphere should remain constant as well as its volume, and as hoped for, a unit sphere discretized using 420 nodes remains at equilibrium. In fact, after 500 iterations with $\Delta t = 0.0004$, the volume and surface area remain constant through four decimal places.

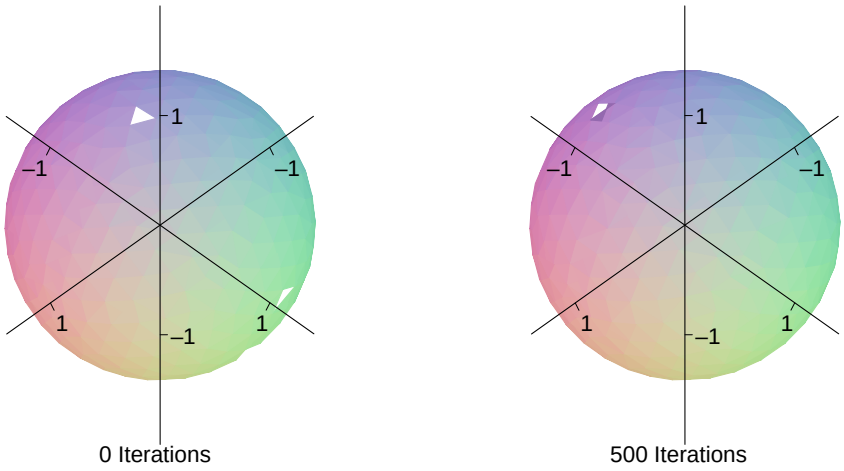

Below we show the maximum and minimum numerically calculated normal velocities over all of the nodes for the first 100 iterations.

www.manaraa.com

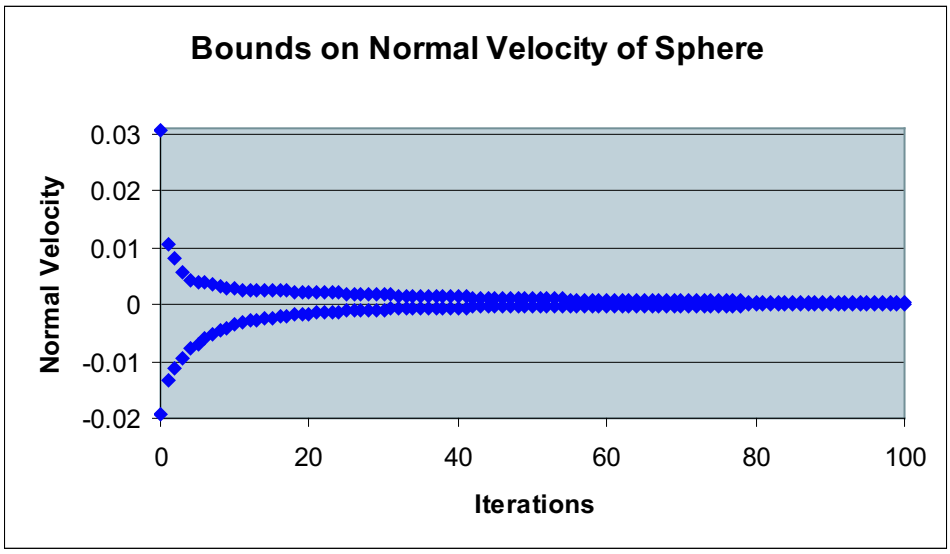

Only about 50 iterations are required for the normal velocity to be within three decimal places of zero.

The numerical method is quite sensitive to time step size. The charts below demonstrate the effects of increasing Δt on the area and volume of the unit sphere.

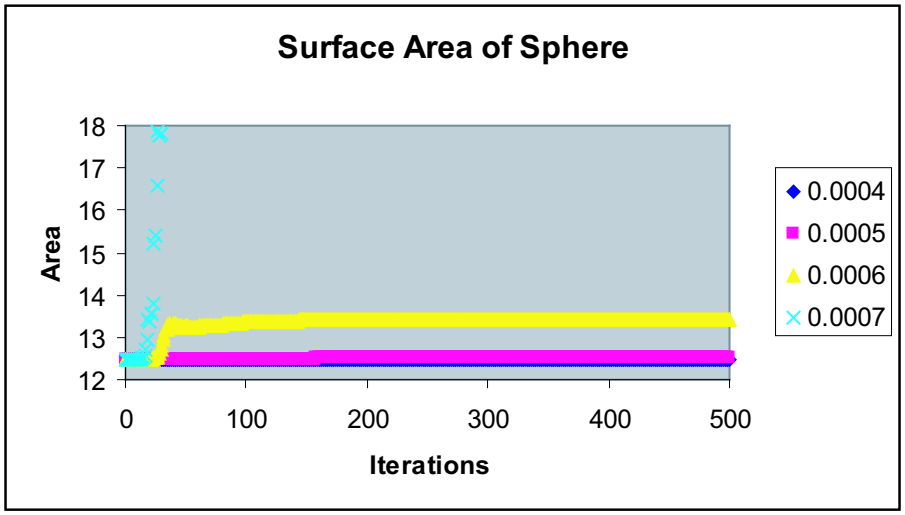

www.manaraa.com

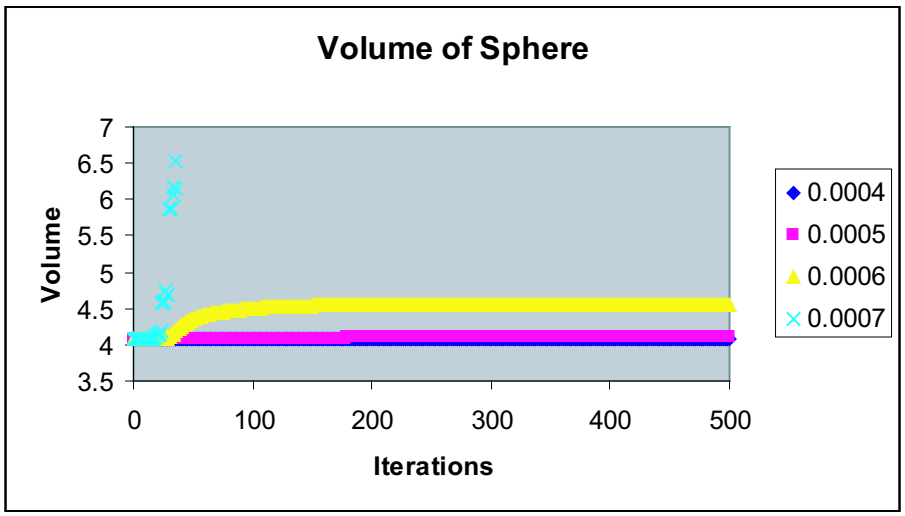

Hence the sphere is both analytically and numerically an equilibrium solution provided the time step Δt is chosen small enough.

4.4.2 Multiple Spheres of Equal Radii

For Γ the union of spheres of radius R, $u = -\dfrac{1}{R}$ is the unique solution to the Mullins Sekerka problem. Just as in the case of the single sphere, we have the normal velocity $V = \left[\dfrac{\partial u}{\partial n}\right]_{\Gamma(t)} = 0$ and Γ is at equilibrium. Below we show the numerical model's results for four spheres of radius 1 centered at $(2,0,0)$, $(2,4,2)$, $(0,2,-2)$, and $(-2,0,0)$. Each is discretized by 420 nodes and $\Delta t = 0.0004$.

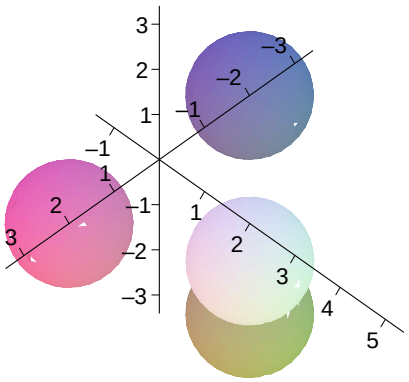

0 Iterations

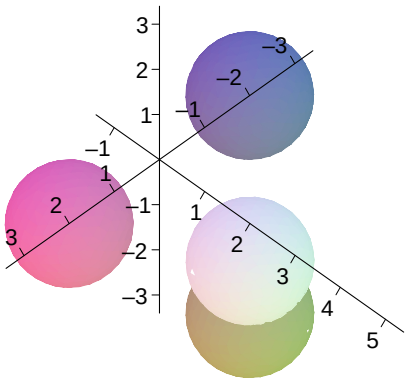

500 Iterations

After 500 iterations the total volume and surface area have both deviated less than 10^{-5} from the initial values. After about 50 iterations, the normal velocity is less than 0.001 in absolute value. Thus the numerical model agrees with the analytical solution.

www.manaraa.com

4.4.3 Concentric Spheres

Suppose $\Gamma(t)$ is the boundary of two concentric spheres with radii $0 < R_1(t) < R_2(t)$. We consider $\Gamma(t)$ as enclosing $\{\vec{x} \,|\, R_1 < |\vec{x}| < R_2\}$. For ease of notation we abbreviate $R_1(t)$ and $R_2(t)$ as R_1 and R_2, respectively.

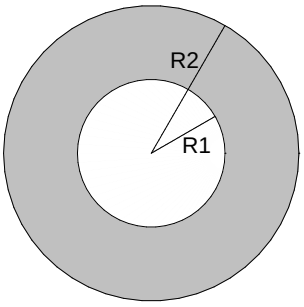

We are looking for solutions of

$$\begin{aligned} \Delta u &= 0 && \text{in } \mathbb{R}^3 \backslash \Gamma(t) \\ u &= \kappa && \text{on } \Gamma(t) \\ \nabla u &= \mathcal{O}\left(\frac{1}{|\vec{x}|^3}\right) && \text{as } |\vec{x}| \to \infty. \end{aligned}$$

Then for $|\vec{x}| \leq R_1$, $u(\vec{x}) = \dfrac{1}{R_1}$ and for $|\vec{x}| \geq R_2$, $u(\vec{x}) = -\dfrac{1}{R_2}$ satisfy the requirements. For $R_1 < |\vec{x}| < R_2$, we note that a function of the form $u(\vec{x}) = a + \dfrac{b}{|\vec{x}|}$ is harmonic. Letting $a = \dfrac{-2}{R_2 - R_1}$ and $b = \dfrac{R_1 + R_2}{R_2 - R_1}$ insures that u is continuous on $\Gamma(t)$. Hence u is a solution to

$$\begin{aligned} &\text{i)} && \Delta u(\cdot, t) = 0 && \text{in } \mathbb{R}^3 \backslash \Gamma(t) \\ &\text{ii)} && \nabla u = \mathcal{O}\left(\frac{1}{|\vec{x}|^3}\right) && \text{as } |\vec{x}| \to \infty \\ &\text{iii)} && u = \kappa && \text{on } \Gamma(t) \\ &\text{iv)} && \left[\frac{\partial u}{\partial n}\right]_{\Gamma(t)} = V && \text{on } \Gamma(t) \\ &\text{v)} && \Gamma(0) = \Gamma_0. \end{aligned}$$

Uniqueness of solutions to the Mullins-Sekerka problem requires u to be sufficiently smooth [1], which it is not. However, under certain assumptions about the exterior Dirichlet problem, κ uniquely determines the normal velocity V by Theorem 2.4.1.

www.manaraa.com

We next determine the normal velocity V at time t. For $|\vec{x}| = R_1$, the outward normal is $n = \dfrac{(-x,-y,-z)}{R_1}$ and for $|\vec{x}| = R_2$, the outward normal is $n = \dfrac{(x,y,z)}{R_2}$. Now $V = \left[\dfrac{\partial u}{\partial n}\right]_{\Gamma(t)}$ is the jump in the normal derivative of u across $\Gamma(t)$. Then for $|\vec{x}| = R_1$,

$$\begin{aligned} V_{R_1} = \left[\frac{\partial u}{\partial n}\right]_{\Gamma(t)} &= \partial_{n^-} u - \partial_{n^+} u \\ &= \partial_{n^-}\left(\frac{-2}{R_2 - R_1} + \frac{R_1 + R_2}{R_2 - R_1}\,\frac{1}{|\vec{x}|}\right) - \partial_{n^+}\left(\frac{1}{R_1}\right) \\ &= \frac{(-x,-y,-z)}{R_1} \cdot \frac{R_1 + R_2}{R_2 - R_1}\,\frac{(-x,-y,-z)}{R_1^3} - 0 \\ &= \frac{(R_1 + R_2)}{(R_2 - R_1)R_1^2}. \end{aligned}$$

For $|\vec{x}| = R_2$, a similar calculation yields $V_{R_2} = -\dfrac{(R_1 + R_2)}{(R_2 - R_1)R_2^2}$. Now the volume enclosed by $\Gamma(t)$ is

$$\mathrm{Vol}(t) = \frac{4}{3}\,\pi R_2^3 - \frac{4}{3}\,\pi R_1^3.$$

Then utilizing the normal velocities $V_{R_1} = -\dfrac{dR_1}{dt}$ and $V_{R_2} = \dfrac{dR_2}{dt}$, we have

$$\begin{aligned} \frac{\partial \mathrm{Vol}}{\partial t} &= 4\pi\, R_2^2\,\frac{dR_2}{dt} - 4\pi\, R_1^2\,\frac{dR_1}{dt} \\ &= -4\pi\, R_2^2\,\frac{(R_1 + R_2)}{(R_2 - R_1)R_2^2} + 4\pi\, R_1^2\,\frac{(R_1 + R_2)}{(R_2 - R_1)R_1^2} \\ &= 0. \end{aligned}$$

Hence, the enclosed volume is constant.

Let this volume be $\dfrac{4}{3}\,\pi M$. Then $M = R_2^3 - R_1^3$ and $R_2 = (M + R_1^3)^{\frac{1}{3}}$. Now $V_{R_1} = -\dfrac{dR_1}{dt} = \dfrac{(R_1 + R_2)}{(R_2 - R_1)R_1^2}$, so we have

$$\frac{R_1^2\left(R_1 - (M + R_1^3)^{\frac{1}{3}}\right)}{(M + R_1^3)^{\frac{1}{3}} + R_1}\,dR_1 = dt.$$

We can now solve for $R_1(t)$ implicitly using

$$t = \int_{R_1(0)}^{R_1(t)} \frac{r^2\left(r - (M + r^3)^{\frac{1}{3}}\right)}{(M + r^3)^{\frac{1}{3}} + r}\,dr$$

www.manaraa.com

Using Romberg's method for integration [9] in combination with a bisection method we determine $R_1(t)$, the inner radius, given t. This is done by evaluating successive guesses, denoted here as $\tilde{R}_1(t)$, to $R_1(t)$ until $\int_{R_1(0)}^{\tilde{R}_1(t)} \frac{r^2\left(r-(M+r^3)^{\frac{1}{3}}\right)}{(M+r^3)^{\frac{1}{3}}+r}\,dr$ is within a specified tolerance to t. Since $0 \le R_1(t) \le R_1(0)$, we use the initial guess $\tilde{R}_1(t) = \frac{R_1(0)}{2}$. In general, given an upper bound U and lower bound L of $R_1(t)$, we use the approximation $\tilde{R}_1(t) = \frac{U+L}{2}$. If $\int_{R_1(0)}^{\tilde{R}_1(t)} \frac{r^2\left(r-(M+r^3)^{\frac{1}{3}}\right)}{(M+r^3)^{\frac{1}{3}}+r}\,dr < t$, the estimate $\tilde{R}_1(t)$ is too large, and we let $U = \tilde{R}_1(t)$ for finding the next approximation to $R_1(t)$. If $\int_{R_1(0)}^{\tilde{R}_1(t)} \frac{r^2\left(r-(M+r^3)^{\frac{1}{3}}\right)}{(M+r^3)^{\frac{1}{3}}+r}\,dr > t$, then $\tilde{R}_1(t)$ is an underestimate, and we let $L = \tilde{R}_1(t)$. In this manner we find a sequence $\{\tilde{R}_1(t)\}$ that converges to $R_1(t)$ as the integral converges to t. The integrals cannot be evaluated algebraically, so we use Romberg's method with code adapted from [9] to evaluate the integrals numerically. Once we find $R_1(t)$, we find the outer radius $R_2(t)$ via the formula $R_2 = (M + R_1^3)^{\frac{1}{3}}$

Below is the evolution of concentric spheres as determined analytically via the method explained above. Here $R_1(0) = 1$ and $R_2(0) = 2$.

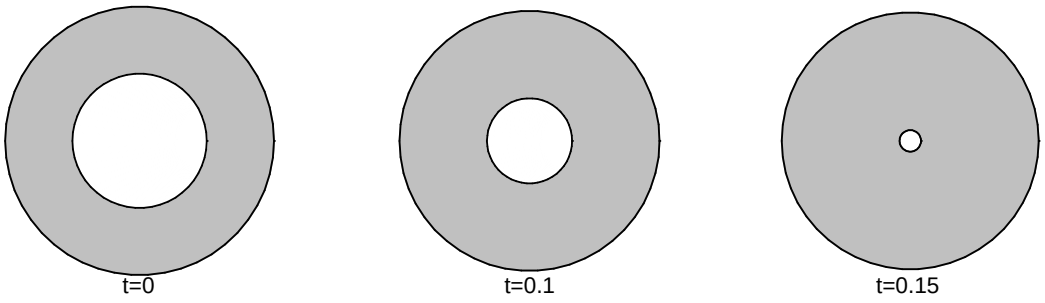

The results from our numerical scheme as compared to the analytical solution are shown below. The correlation disappears as the inner radius shrinks to zero since the numerical scheme cannot handle very small spheres, but initially the numerical scheme is a good approximation. We used 200 nodes to discretize the smaller sphere and 720 nodes for the larger. The time step is $\Delta t = 0.0002$.

www.manaraa.com

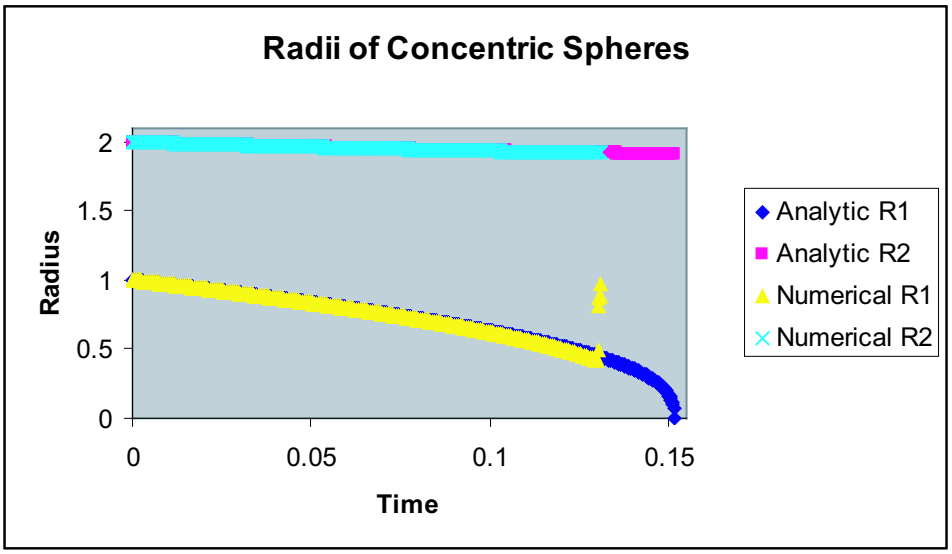

Below is the numerical evolution of the concentric spheres from $t = 0$ to $t = 0.12$.

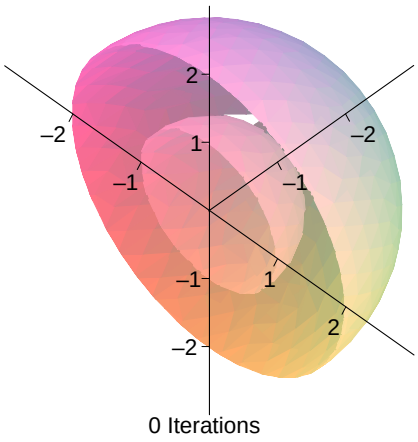

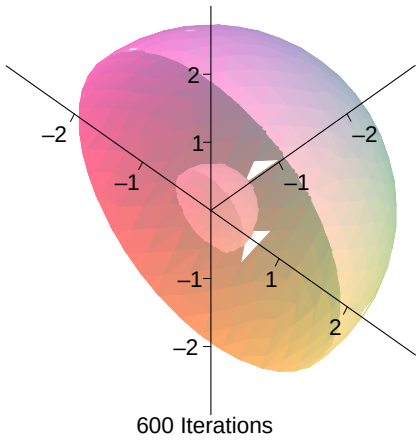

While overall the results for the concentric spheres are very good, the numerical values of the normal velocities are necessitating the small time step. The actual normal velocities of the initial surfaces are $V_{R_1} = \dfrac{(R_1 + R_2)}{(R_2 - R_1)R_1^2} = 3$ and $V_{R_2} = -\dfrac{(R_1 + R_2)}{(R_2 - R_1)R_2^2} = -\dfrac{3}{4}$, where $R_1 = 1$ and $R_2 = 2$. With regard to V_{R_1}, the average of the numerical normal velocities for the smaller sphere discretized by 200 nodes at $t = 0$ is 3.05 with a standard deviation of 0.15, not as close as hoped for to the actual value of 3. The velocities vary widely between 2.85 and 3.36, as shown in the table below where the nodes are labelled 1 through 200 for convenience.

www.manaraa.com

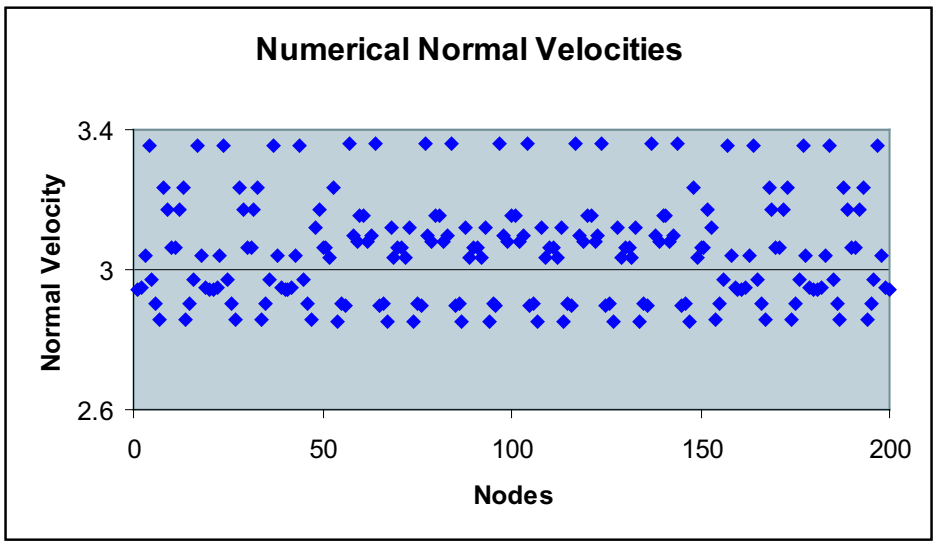

The symmetries are presumably a result of the discretization based on the 20 faces of the icosahedron. Unfortunately, increasing the number of nodes does not significantly improve the numerically calculated normal velocities. For example, using the same radii but with 720 nodes yields an average of 3.00 with standard deviation 0.12, but the range is 2.77 to 3.38, worse than before. By way of comparison, the average mean curvature estimates for the smaller sphere (actual value 1) goes from 1.03 to 1.0079 with standard deviation decreasing from 0.0011 to 0.00045 when we increase the number of nodes from 200 to 720.

Recall that the normal velocities V_i are found by solving the following matrix, which is derived from using a piecewise constant discretization to estimate surface integrals.

www.manaraa.com

$$\begin{bmatrix} I_1 & \frac{\Delta_2}{|\mathbf{x}_1-\mathbf{x}_2|} & \frac{\Delta_3}{|\mathbf{x}_1-\mathbf{x}_3|} & \cdots & \frac{\Delta_{N-1}}{|\mathbf{x}_1-\mathbf{x}_{N-1}|} & \frac{\Delta_N}{|\mathbf{x}_1-\mathbf{x}_N|} & 1 \\ \frac{\Delta_1}{|\mathbf{x}_2-\mathbf{x}_1|} & I_2 & \frac{\Delta_3}{|\mathbf{x}_2-\mathbf{x}_3|} & \cdots & \frac{\Delta_{N-1}}{|\mathbf{x}_2-\mathbf{x}_{N-1}|} & \frac{\Delta_N}{|\mathbf{x}_2-\mathbf{x}_N|} & 1 \\ \frac{\Delta_1}{|\mathbf{x}_3-\mathbf{x}_1|} & \frac{\Delta_2}{|\mathbf{x}_3-\mathbf{x}_2|} & I_3 & \cdots & \frac{\Delta_{N-1}}{|\mathbf{x}_3-\mathbf{x}_{N-1}|} & \frac{\Delta_N}{|\mathbf{x}_3-\mathbf{x}_N|} & 1 \\ \vdots & \vdots & \vdots & \ddots & \vdots & \vdots & \vdots \\ \frac{\Delta_1}{|\mathbf{x}_{N-1}-\mathbf{x}_1|} & \frac{\Delta_2}{|\mathbf{x}_{N-1}-\mathbf{x}_2|} & \frac{\Delta_3}{|\mathbf{x}_{N-1}-\mathbf{x}_3|} & \cdots & I_{N-1} & \frac{\Delta_N}{|\mathbf{x}_{N-1}-\mathbf{x}_N|} & 1 \\ \frac{\Delta_1}{|\mathbf{x}_N-\mathbf{x}_1|} & \frac{\Delta_2}{|\mathbf{x}_N-\mathbf{x}_2|} & \frac{\Delta_3}{|\mathbf{x}_N-\mathbf{x}_3|} & \cdots & \frac{\Delta_{N-1}}{|\mathbf{x}_N-\mathbf{x}_{N-1}|} & I_N & 1 \\ \Delta_1 & \Delta_2 & \Delta_3 & \cdots & \Delta_{N-1} & \Delta_N & 0 \end{bmatrix} \begin{bmatrix} V_1 \\ V_2 \\ V_3 \\ \vdots \\ V_{N-1} \\ V_N \\ c' \end{bmatrix} = \begin{bmatrix} 4\pi\kappa_1 \\ 4\pi\kappa_2 \\ 4\pi\kappa_3 \\ \vdots \\ 4\pi\kappa_{N-1} \\ 4\pi\kappa_N \\ 0 \end{bmatrix}$$

Note that as the number of nodes increases, the patch areas $\triangle_i$ becomes very small, along with some of the $|\mathbf{x}_i-\mathbf{x}_j|$'s. Roundoff error can be very large when dividing a small number by a small number. Using the actual values of the mean curvature κ improves the numerically calculated normal velocities slightly, but we still don't see significant improvement when the number of nodes is increased. This is an indicator that the roundoff error nullifies the increased accuracy gained by increasing the number of nodes. Remedying this is an area for further work.

4.5 Summary

Overall, our scheme agrees very well with theoretically predicted behavior and analytically derived solutions. Care must be taken, however, with large time step sizes, bunched nodes, and topological changes.

Thus our scheme loses validity for a time step size that borders the stability region, as the change in surface area makes small oscillations.

As this surface actually has a significant increase in area, we conclude that a careful watch on time step size is necessary, but within the stable range for Δt we have very good results.

www.manaraa.com

www.manaraa.com

Chapter 5

Numerical Results

Here we show how particles evolve over time. We use the Particle-Particle Method with the first order implicit scheme.

5.1 Various Surfaces

5.1.1 Distorted Torus

We distort a torus of large radius 3 and small radius 1 discretized with 800 nodes. The time step size is 0.0004. We redistribute each radial slice after each iteration. We note that the redistribution for a distorted torus is slightly different from a non-perturbed torus because we cannot utilized the symmetry with respect to the xy-plane.

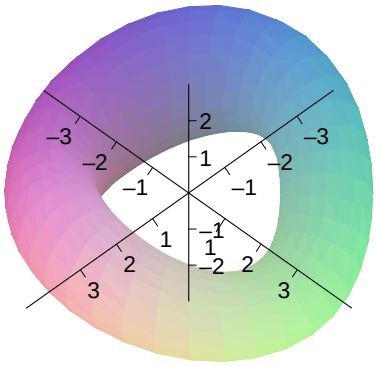

0 Iterations

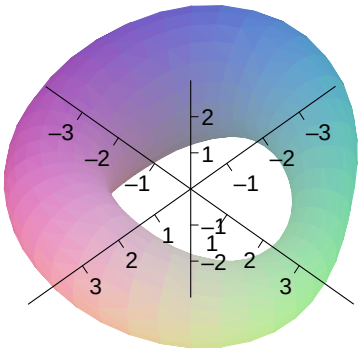

1000 Iterations

www.manaraa.com

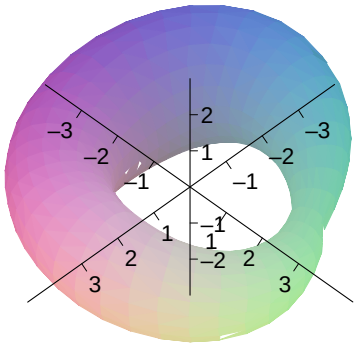

1650 Iterations

The scheme is not valid after 1650 iterations because surface area no longer decreases. The bulging parts of the torus get fatter and the skinny part gets even skinnier as the inner perimeter shrinks. This suggests that pinching off may occur. An area of work in the future is creating a discretization that will allow the evolution to progress even farther by reducing the number of nodes at the narrow neck and increasing the density of nodes at the bulge.

5.1.2 Two Spheres of Unequal Radii

The following spheres have radii 1.5 and 1. Here $\Delta t = 0.0004$. Below we show the surfaces at 0 and 3000 iterations.

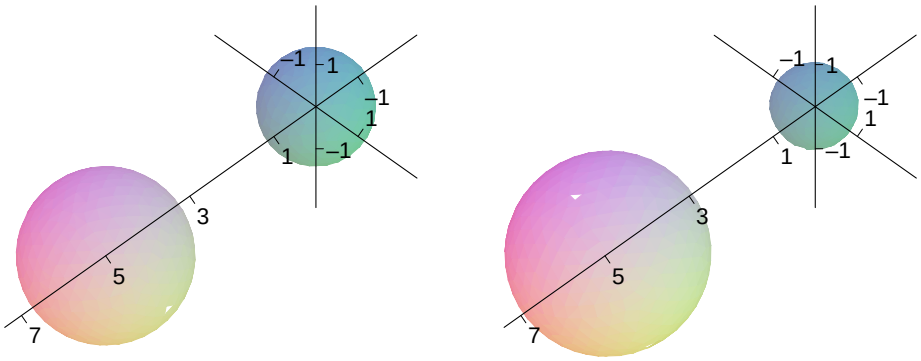

0 Iterations

3000 Iterations

The smaller sphere shrinks and the larger sphere grows.

5.1.3 Two Spheres of Slightly Unequal Radii

A small perturbation goes a long way. One unit sphere is changed to an ellipsoid with $a = 1.1, b = 1, c = 1$, and instead of equilibrium we have the following. The first surface is

www.manaraa.com

at 0 iterations and the second is after 5000 iterations with $\Delta t = 0.0004$.

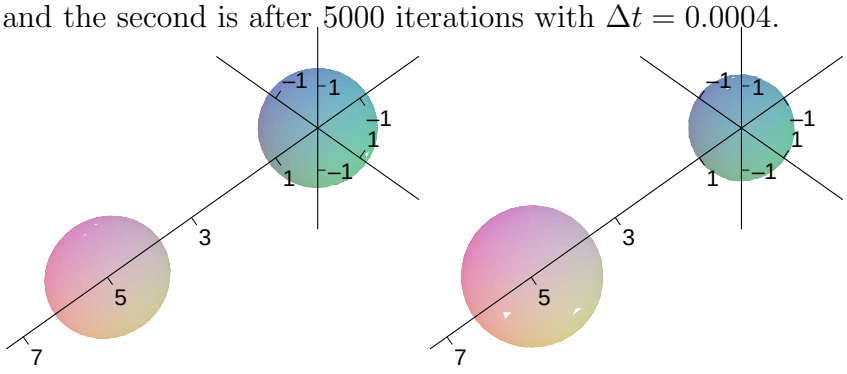

Below is a chart of the radii. Here the radius is the average distance of the nodes from the centroid.

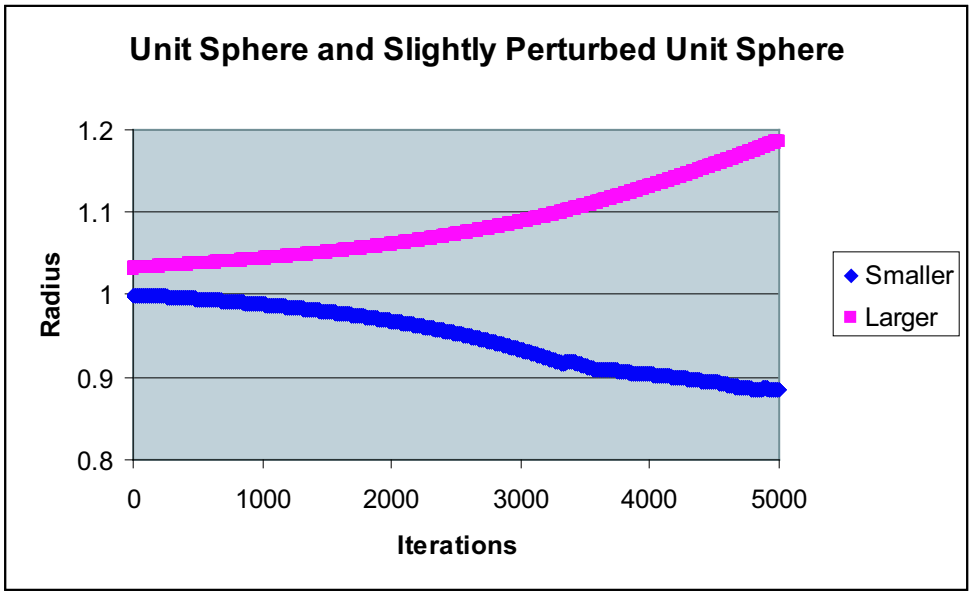

This demonstrates that the Mullins-Sekerka problem is ill-conditioned: a small perturbation in $\Gamma(0)$ can completely change the nature of the solution.

5.1.4 Three Spheres of Unequal Radii

Two of the spheres have a radius of 1, and shrink at the approximately same rate. The larger sphere has radius 2. We use $\Delta t = 0.0004$. Below are shown the initial surface and the surface after 1500 iterations.

www.manaraa.com

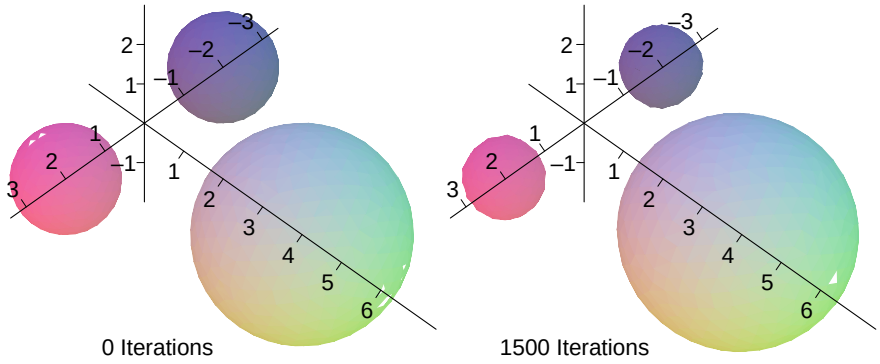

The smaller spheres shrink and the larger spheres grow.

www.manaraa.com

Chapter 6

Conclusion

We review the strengths of our scheme and give areas where further work remains to be done.

6.1 Strengths

The strengths of the numerical scheme presented in this dissertation include utilizing a reformulation of the Mullins-Sekerka problem so that computations are performed with regard to a surface instead of $\mathbb{R}^3$. A discretization of the sphere based on an icosahedron has nearly equally spaced nodes, which is an important ingredient when discretizing surfaces. The scheme is semi-implicit to increase stability with respect to time step size. Redistribution of nodes for the torus significantly extends the time interval for which the scheme is valid. We also deal with the topology change the torus undergoes as its shape tends toward that of a sphere. We presented a distorted torus that showed the tendency to pinch off.

6.2 Further Work

Improvements can be made to the scheme, such as further reducing runtime and resolving node spacing issues adaptively as surfaces evolve. Questions about Mullins-Sekerka flow have yet to be answered, specifically with regard to stiffness and convexity preservation in three dimensions.

www.manaraa.com

6.2.1 Convexity

In two dimensions, Mullins-Sekerka flow has been shown both numerically [5] and theoretically [29] to not preserve convexity. However, there are no results for the three-dimensional case. Numerically, a promising surface candidate for showing loss of convexity is a long, hot dog shaped tube.

6.2.2 Node Enrichment and Refinement

When evolving multiple particles other than spheres of equal radii, larger particles grow and smaller particles shrink. This leads to very large mesh size in the larger particles and bunching problems in the smaller particles, effecting the validity of our results. For example, the three spheres with initial radii 1,1, and 2 show this phenomenon. The left plot is the original surfaces and the right is after 1000 iterations.

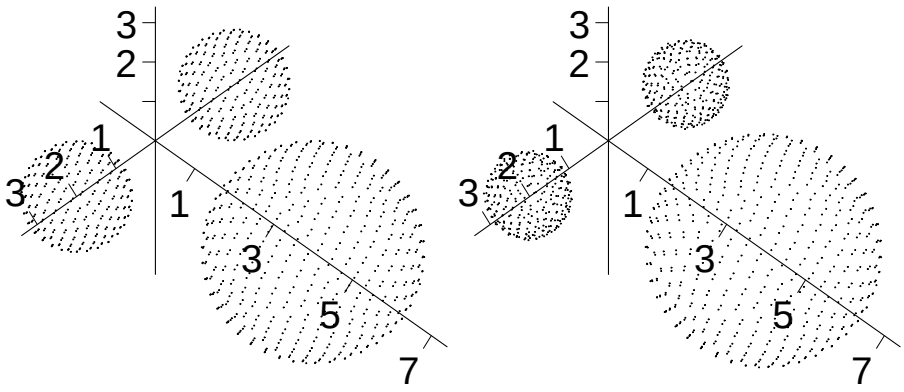

A solution to this would be a node enrichment and refinement scheme that added or removed nodes as necessary. Ultimately particles sufficiently tiny would be removed altogether.

6.2.3 Convergence of Surface Estimate Scheme

A very important part of our numerical scheme involves the estimation of mean curvature and the normal at a node. We do this by using the iterative method found in [45] to find a surface of the form $z = Ax + By + Cx^2 + Dxy + Ey^2$ that best fits the node and its eight nearest neighbors. The method supposes that such a surface with the z-axis corresponding

www.manaraa.com

to the normal to the surface is the best fit surface and hence gives the best estimate of mean curvature.

Several things need to be proved. First is that the iterative process does indeed yield a surface that minimizes error, i.e., we need to show that the weighted error of the j^{th} iteration

$$F_j(A,B,C,D,E) = \sum_{i=1}^{8} \frac{(Ax_i + By_i + Cx_i^2 + Dx_iy_i + Ey_i^2 - z_i)^2}{x_i^2 + y_i^2 + z_i^2}$$

is bounded above by a sequence converging to 0. Note that F_j is bounded below by 0.

The iterative process involves a change of coordinate system at each step. This results in a product of change of basis matrices. We need to show that these change of basis matrices approach the identity and also that their product approaches the identity. For the change of basis matrices to approach the identity, it is necessary that A_j and B_j approach 0. This is equivalent to the normal to the surface approaching the z-axis. Numerical implementation of the iterative scheme show that the matrices and their products do indeed converge as desired provided nodes are reasonably equally spaced, but this needs to be proved rigorously.

Finally it remains to rigorously show that the mean curvature and normal are independent of the initial choice of coordinate system, as this is largely arbitrary.

6.2.4 Stiffness

Our problem shows indications of being stiff. The first is that the time step is necessarily constrained to be quite small or we lose validity. Secondly, when the explicit Euler's Method is used, it performs better than both the Center Difference Method and Adams-Bashforth Method, even though the latter two are both $\mathcal{O}(\Delta t^2)$ while Euler's Method is $\mathcal{O}(\Delta t)$. Euler's Method can be shown to be more suitable for stiff equations than the Center Difference and Adams-Bashforth Methods via analysis of a test equation [**?**]. On the other hand, the Implicit Trapezoid Method is A-Stable. Our adaptation of the Implicit Trapezoid Method works well for our problem.

Ascertaining whether the Mullins-Sekerka problem would be beneficial in explaining the behavior mentioned above. It would also help in deciding which numerical method should

www.manaraa.com

be used to advance the surface.

To verify that our problem is stiff, we need to show that the Jacobian matrix of $V(X)$ has eigenvalues with negative real part and the magnitude of these real parts differ widely [25].

6.2.5 Smoothness of V

In the theoretical derivation of the integral formulation, we require V to be continuous. We would like to relax this to $V \in L^2(\Gamma)$ or V measurable and bounded. If this is not possible, we would like to demonstrate why.

www.manaraa.com

Bibliography

[1] Alikakos, Nicholas D.; Bates, Peter W.; Chen, Xinfu *Convergence of the Cahn-Hilliard Equation to the Hele-Shaw Model*, Archive for Rational Mechanics and Analysis **128** (1994), 165–205.

[2] Alikakos, Nicholas D.; Bates, Peter W.; Chen, Xinfu; Fusco, Giorgio *Mullins-Sekerka Motion of Small Droplets on a Fixed Boundary*, The Jounal of Geometric Analysis **10** (2000), 575–596.

[3] Anderson, E. (Editor); Bischof, C.; Bai, Z.; Blackford, L. S.; *LAPACK Users' Guide*, SIAM, 1999.

[4] Atkinson, Kendall E. *The Numerical Solution of Integral Equations of the Second Kind*, Cambridge, Cambridge, 1997.

[5] Bates, Peter W.; Chen, Xinfu; Deng, Xinyu *A Numerical Scheme for the Two Phase Mullins-Sekerka Problem*, Electronic Journal of Differential Equations (1995), No. 11, 1–28.

[6] Bates, Peter W.; Lu, Kening; Xu, Daoyi *Differential Equations and Computational Simulations*, World Scientific Publishing Co. Pte. Ltd., Singapore, 2000.

[7] Boistelle, R.; Astier, J. P. *Crystallization Mechanisms in Solution*, Journal of Crystal Growth **90** (1988), 14-30.

[8] Brown, Sarah M. *The Mullins-Sekerka Problem in Three Dimensional Space* MS Thesis Brigham Young University 1999.

www.manaraa.com

[9] Burden, Richard L.; Faires, J. Douglas *Numerical Analysis* (7th ed.), Brooks/Cole, Pacific Grove, CA, 2001.

[10] Caginalp, G. *The Dynamics of a Conserved Phase Field System: Stefan-like, Hele-Shaw and Cahn-Hilliard Models as Asymptotic Limits*, IMA Journal of Applied Mathematics **34** (1990), 77–94.

[11] Cahn, John W.; Hilliard, John E. *Free Energy of a Nonuniform System. I. Interfacial Free Energy*, The Journal of Chemical Physics, **28** (1958), No. 2, 258–267.

[12] Cahn, John, W. *On Spinodal Decomposition*, Acta Metallurgica, **9** (1961), 795–801.

[13] Chen, Xinfu *The Hele-Shaw Problem and Area-Preserving Curve-Shortening Motions*, Archive for Rational Mechanics and Analysis **123** (1993), 117–151.

[14] Chen, Xinfu; Hong, Hiaxing; Yi,Fahuai *Existance, Uniqueness, and Regularity of Classical Solutions of the Mullins-Sekerka Problem*, Communications in Partial Differential Equations **21** (1996), No. 11&12, 1705–1727.

[15] Chen, Xinfu *Global Asymptotic Limit of Solutions of the Cahn-Hilliard Equation*, Journal of Differential Geometry **44** (1996), 262–311.

[16] Deng, Xinyu *A Numerical Analysis Approach for the Hele-Shaw Problem*, M. S. Thesis, Brigham Young University, April 1994.

[17] Escher, Joachim; Simonett, Gieri *A Center Manifold Analysis for the Mullins-Sekerka Model*, Journal of Differential Equations **143** (1998), 267–292.

[18] Escher, Joachim; Simonett, Gieri *Classical Solutions for Hele-Shaw Models with Surface Tension*, Advances in Differential Equations **2** (1997), No. 4, 619–642.

[19] Escher, Joachim; Simonett, Gieri *On Hele-Shaw Models with Surface Tension*, Mathematical Research Letters **3** (1996), 467–474.

www.manaraa.com

[20] Evans, Lawrence C. *Partial Differential Equations*, AMS, Providence, RI, 1998.

[21] Folland, Gerald. B. *Introduction to Partial Differential Equations* (2nd ed.), Princeton University Press, Princeton, NJ, 1995.

[22] Greenbaum, A.; Greengard, L.; McFadden, G. B. *Laplace's Equation and the Dirichlet-Neumann Map in Multiply Connected Domains*, Journal of Computational Physics **105** (1993), 267–278.

[23] Horn, Roger A.; Johnson, Charles R. *Martix Analysis*, Cambridge, Cambridge, 1985.

[24] Isaacson, Eugene *Analysis of Numerical Methods* John Wiley & Sons, Inc., New York. 1966

[25] Kincaid, David; Cheney, Ward *Numerical Analysis* (2nd ed.), Brooks/Cole, Pacific Grove, 1996.

[26] Larson, Roland E.; Hostetler, Robert P. *Algebra and Trigonometry* (4th ed.), Houghton Mifflin, Boston, 1997.

[27] Lindsay, Keith *A Three-Dimensional Cartesian Tree-Code and Applications to Vortex Sheet Roll-Up*, Ph.D. thesis (University of Michigan, Ann Arbor, MI. 1997).

[28] Lindsay, Keith; Kransy, Robert *A Particle Method and Adaptive Treecode for Vortex Sheet Motion in Three-Dimensional Flow*, Journal of Computational Physics **172** (2001), 879–907.

[29] Mayer, Uwe F. *Two-Sided Mullins-Sederda Flow Does Not Preserve Convexity*, Proceedings of the Third Mississippi State Conference of Difference [sic] Equations and Computational Simulations (1997), 171–179.

[30] Meyers, Norman; Serrin, James *The Exterior Dirichlet Problem for Second Order Elliptic Partial Differential Equations*, Journal of Mathematics and Mechanics, **9** No. 4 (1960), 513–538.

www.manaraa.com

[31] McFadden, G.B.; Voorhees, P.W.; Boisvert, R.F.; Meiron, D.I. *A Boundary Integral Methods for the Simulation of Two-Dimensionl Particle Coarsening*, Journal of Scientific Computing **1** No. 2 (1986) 117–144

[32] McOwen, Robert *Partial Differential Equations: Methods and Applications*, Prentice-Hall, Inc., Upper Saddle River, NJ, 1996

[33] Mikhlin, S. G. *An Advanced Course of Mathematical Physics*, American Elsevier Publishing Company, Inc., New York, NY, 1970.

[34] Milic, Natasa *On the Mullins-Sekerka Model for the Phase Transitions in Mixtures*, Quarterly of Applied Mathematics **49** No. 3 (1991), 437–445.

[35] Mitrovic, Dragisa; Zubrinic, Darko *Fundamentals of Applied Functional Analysis*, Addison Wesley Longman Limited, England, 1998

[36] Mullins, W. W.; Sekerka, R. F. *Morphological Stability of a Particle Growing by Diffusion and Heat Flow*, Journal of Applied Physics **34** (1963), No. 2, 323–329.

[37] Oprea, John *The Mathematics of Soap Films: Explorations with Maple*, AMS, Providence, RI, 2000.

[38] Pego, R. L. *Front Migration in the Nonlinear Cahn Hilliard Equation*, Proceedings of the Royal Society of London. Series A, Mathematical and Physical Sciences **422** No. 1863 (1989), 261–278.

[39] Protter, M. H.; Morrey, C. B. *A First Course in Real Analysis*, Springer-Verlag, New York, 1991.

[40] Smirnov, V.I. *Integral Equations and Partial Differential Equations*, Pergamon Press Ltd. 1964

[41] Stein, Sherman K. *Calculus and Analytic Geometry*, McGraw Hill, New York, 1987.

www.manaraa.com

[42] Stoth, Barbara E. E. *Convergence of the Cahn-Hilliard Equation to the Mullins-Sekerka Problem in Spherical Symmetry*, Journal of Differential Equations **125** (1996), 154–183.

[43] Sutton, Daud *Platonic & Archimedean Solids*, Walker & Company, New York, 2002.

[44] Voorhees, P.W.; McFadden, G.B.; Boisvert, R.F.; Meiron, D.I. *Numerical Simulation of Morphological Development During Ostwald Ripening*, Acta. Metall. **36**, No. 1 (1988), 207–222.

[45] Zinchenko, Alexander Z.; Rother, Michael A.; Davis, Robert H. *A Novel Boundary-Integral Algorithm for Viscous Interaction of Deformable Drops*, Physics of Fluids **9** (1996) No. 6, 1493–1511.

[46] Zhu, Jinhyi; Chen, Xinfu; and Hou, Thomas Y. *An Efficient Boundary Integral Method for the Mullins-Sekerka Problem*, Journal of Computational Physics **127** (1996), 246–267.

www.manaraa.com